Investigation of Two-Dimensional Incompressible Inviscid Axisymmetric Elliptical Vortices Using a Vortex-In-Cell Method

Munwwar Mansoor Chaudhary

A thesis submitted to the Faculty of Graduate and Postdoctoral Studies
in partial fulfilment of the requirements for the degree of

MASTER OF APPLIED SCIENCE

in Mechanical Engineering

Ottawa-Carleton Institute for Mechanical and Aerospace Engineering
University of Ottawa
Ottawa, Canada

April 2014

Abstract

A Vortex-In-Cell (VIC) scheme is implemented to study the evolution of two-dimensional elliptical vortices in a periodic domain. The mixed Eulerian-Lagrangian vortex-in-cell method adopted in this study is chosen because of its low dissipation errors and low computational cost. The goal of this thesis is to implemented this vortex-in-cell method and study how incompressible, inviscid elliptical vortices evolve. It is found that, through a process of filamentation, an initial vorticity profile evolves to a final axisymmetric configuration. It is found that the rate of axisymmetrization is controlled by the initial aspect ratio of the vortex.

This thesis provides a practical overview of the numerical solution of inviscid, incompressible two-dimensional flows using the vortex-in-cell method. The computational domain is enclosed by an Eulerian mesh and the vorticity field is discretized into a finite set of Lagrangian elements (vortex particles). A Poisson equation is solved on the mesh at each time instance to compute the velocity field. The $M_4^{'}$ interpolation scheme is used to exchange vorticity and velocity information between the Lagrangian particles and the Eulerian grid. Vortex-particle locations are integrated in time using a predictor-corrector time integration scheme.

Highly resolved solutions using a pseudo-spectral method are used as a benchmark to verify the vortex-in-cell implementation and to study solution convergence as a function of each parameter of the scheme. In addition, the vortex-in-cell method is validated by

comparing with other related numerical studies. Finally, the evolutions of several initially elliptical vortex distributions with different aspect ratios are studied.

Acknowledgements

First of all I would like to express my gratitude to my supervisor Dr. Roger Milane and co-supervisor Dr. James McDonald for their kind support, cooperation, encouragement and valuable advice which helped me a lot to complete my masters from one of the best universities in Canada. I greatly appreciate their patience and tolerance towards me during my masters. Their understanding nature and fatherly concern are worth mentioning and thanking. Since August 2013, Dr. Roger Milane was unavailable due to serious illness; therefore, my co-supervisor Dr. James McDonald has helped and guided me to complete this master's thesis.

I would also like thank my colleague and friends for their support. Also, I want to thank the people in academic of mechanical engineering department for their help.

Finally, I would like to thank my parents and family especially my elder brothers Mr. Masroor Mansoor and Mr. Masood Mansoor for providing financial support and helping me in all the difficult times and constantly praying for me. It is because of them that I am at this stage of my life. Their trust and belief in me has made it possible for me to achieve my life goals.

Table of Contents

Chapter 5. Verification Studies and Results

Chapter 6. Conclusions and Recommendations

List of Figures

List of Tables

Nomenclature

Roman Characters

a, b	Major and minor axes of the ellipse
d	Distance between vortices
h	Grid spacing
H	Length of the computational domain
M	Number of grid points in each direction
N_{v}	Number of vortices
t	Time
$\vec{u}$	Velocity vector
u, v	Velocity components
u_p, v_p	Velocity components of the vortices
$u_{(i,j)}, v_{(i,j)}$	Components of velocity at gird nodes
$x_{(i,j)}, y_{(i,j)}$	Cartesian coordinates along horizontal and vertical directions
x_p, y_p	Coordinates of the vortices
Δt	Time step
$\Delta x, \Delta y$	Grid sizes in x- and y-direction
$\vec{G}$	Green function of Laplace operator
J_{mn}	Vorticity moment

$\vec{k}$	Curl of Green's function

Greek Symbols

Γ	Circulation
Γ_i	Circulation of a vortex
ϕ	Any scalar quantity
υ	Kinematic viscosity
υ_4	Hyperviscosity
$\prod$	Interpolation kernel
ψ	Stream function
ξ	Vorticity vector
$\xi_{average}$	Average vorticity of the domain
λ	Aspect ratio
λ_{eff}	Effective aspect ratio
$*$	Convolution integral
$\vec{\alpha}$	Strength of vortex point

Subscripts

i, j	Notation indices in x and y directions
m, n	Notation indices in x and y directions for vorticity moment
p	Particle value
o	Initial value
n	Time step

Chapter 1

1.0 Introduction and Motivations

Vorticity is one of the main fluid properties and plays a vital role in understanding the nature of flow. It is the dominant effect in many situations, both engineered and natural. For example, weather phenomena, such as storms, tornadoes and hurricanes, are characterized by their vortical structures. Turbulent flows are also dominated by vortices. The majority of practical engineering flows are turbulent and flow behaviour and mixing are highly dependent on details of the vortices in the flow. In these situations, accurate numerical predictions depend on the availability schemes with low dissipation and a direct treatment of vorticity. Vortex methods are attractive in these cases, as they naturally maintain many physical properties of vortical flows, such as the conservation of vorticity. The direct treatment of vorticity offered by these methods is well suited for flow prediction in a wide range of practical vorticity-dominated flow situation.

In this thesis, a Lagrangian numerical scheme is implemented based on a vortex method for the direct simulation of a two-dimensional, incompressible, inviscid flow. Vortex methods belong to the family of particle methods. In these methods, the dynamics of the flow are determined

through the evolution of the vorticity field. The solution of the equation of motion is approximated through the use of discrete "vortex particles", which serve as carriers of circulation (Christiansen, 1973; Chang, 1994; and Ghoniem, Gagnon, 1987). They carry information about the vorticity field, which can be relatively easily analyzed, and vortex particles are simply convected with the local fluid velocity. The accuracy and efficiency of vortex methods can be comparable with the classic methods such as the finite-difference methods or spectral methods (Cottet *et al*. 2000, 2002). One attractive feature of the method is that the Navier-Stokes equation is used without the need for pressure terms. In this work, Vortex-In-Cell (VIC) and Pseudo-Spectral methods are implemented for two-dimensional, incompressible, inviscid flow.

The evolution of vortices with non-uniform initially elliptical vorticity distributions in two dimensions is studied in order to understand vortex filamentation and vortex axisymmetrization (the relaxation of elongated vortices towards axial symmetry). This process is the fundamental phenomenon of this situation (Melander *et al*. 1987, 1988). The ejection of filaments from vortices depends on the initial conditions (aspect ratio of the elongated vortex, vorticity distribution, etc.) and it occurs because a stagnation point of saddle type lies within the vortex, as shown by Melander *et al.* (1987, 1988) and Mariotti *et al.* (1994).

For incompressible, inviscid flow, the velocity and pressure fields can be obtained from the vorticity, as it contains all the dynamic information of the flow (Leonard, 1980). Helmholtz showed that in incompressible and inviscid flows vorticity can be understood as material lines that are convected with the local fluid velocity (Helmholtz, 1858). Hence, vortex methods are often attractive numerical methods for the solution of fluid-dynamic problems. In vortex-particle methods, regions which contain vorticity are discretized into a finite number of vortex elements

which are advected with the flow. The translation and deformation of these elements are solved in a Lagrangian frame. Furthermore, vortex methods can be used to obtain the complete detail of the flow field through the kinematics and dynamics of incompressible, inviscid flow.

In this thesis, a new implementation of a vortex-in-cell method for two-dimensional, incompressible, inviscid flow is created. Similar implementations have been used recently to study other phenomena, for example, Sadek (2012) used such a scheme to study three-dimensional mixing layers. Due to the two-dimensional nature of the current study, and the details of calculating the velocity field on a periodic domain, the creation of a new implementation is justified. The main purpose is to investigate the different algorithmic elements of a vortex method, and to gain insight into parameters necessary to solve complex flow problems accurately and reliably. The Navier-Stokes or Euler equation can be used to formulate the governing vorticity transport equation. As stated earlier, one of the advantages of this governing equation is that there is no pressure term present. The pressure only needs to be computed if calculating the surface forces is desired. Also, if the vorticity field has compact support, relatively small computational domains can be used without the solution being affected by artificial boundaries.

In direct vortex methods, which are a pure Lagrangian approach the Biot-Savart law is used to calculate the velocity field and the fluid conditions at infinity are satisfied automatically. The solution of the underlying Poisson equation by this law gives rise to N^2 operations at every time step, when N vortex particles exist in the solution domain (Leonard, 1985). The vortex-in-cell approach and fast multipole method were developed to deal with this high-computational-cost problem, as both have the potential to reduce the number of computations per time step to

$O(N \log N)$. The first method reduces the computational cost by using a numerical solution of the Poisson equation on a fixed grid to determine the particle velocity, whereas the second method approximates the effect of a cluster of particles at a certain distance by a finite series approximation (Cottet and Koumoutsakos, 2000), which also reduces the computational cost. Hence, the VIC methods can be much faster than direct method (Cottet and Poncet, 2003).

In VIC methods, the domain is first discretized using a fixed Eulerian mesh. The second step is to assign the location and strength of vortex particles. The velocity field is computed by solving a Poisson equation on the fixed grid. The convection of the vortex elements can be considered as the main core of vortex methods. An appropriate time-integration scheme and time-step size are selected for Lagrangian convection of the vortex particles. In this thesis, the technique used to solve the discrete Poisson equation for the instantaneous velocity, commutated on the grid, is by Jacobi iterative method and a predictor-corrector method is used for time integration of particle locations.

1.1 Aims and Objectives

The aim of this study is to create a new implementation of a vortex-in-cell method for two-dimensional, incompressible, inviscid flow in a periodic domain and to empirically determine values for the various parameters of the scheme needed to obtain reliable results. This is used to study the evolution of vortices which are initially elliptical with non-uniform vorticity distributions. The vortex-in-cell method is first validated by comparing with the related numerical studies. The evolution of several initially elliptical vorticity distributions with varying aspect ratios are then computed and analyzed.

The initially non-uniform vorticity distributions used in this present study are extensions of those previously employed by Melander, McWilliams and Zabusky (1986), hereafter referred to as MMZ, and Koumoutsakos (1997). In 1986, MMZ used a pseudo-spectral method and in 1997, Koumoutsakos used high resolution Lagrangian (vortex) method to simulate such non-uniform vorticity distributions. Their results are used for comparison in the current vortex-in-cell study. The code is limited to solve two-dimensional, incompressible, inviscid flow but can be used for different initial non-uniform vorticity distributions.

These goals of this thesis are summarized in the following objectives:

1. Implement a vortex-in-cell method for two-dimensional, incompressible, inviscid flow in a periodic domain.
2. Compute highly resolved solutions with a pseudo-spectral method to use as a benchmark to verify the vortex-in-cell implementation and empirically determine the parameters needed to obtain reliable, accurate results with the VIC method.
3. Validate the vortex-in-cell numerical code by comparing with the numerical results given by MMZ and Koumoutsakos.
4. Study elliptical vortex evolution and axisymmertization for a range of initial vorticity distributions.

1.2 Thesis Structure

The overall structure of this thesis is summarized here. First a detailed literature survey on different types of vortex methods is discussed in Chapter 2. The Navier-Stokes equation is used to derive the governing differential vorticity equation for two-dimensional, incompressible,

inviscid flows in Chapter 3. A detailed description of vortex-in-cell and pseudo-spectral methods is given in Chapter 4. In Chapter 5, a study of the axisymmetrization of elliptical vortices with initially non-uniform vorticity profiles is shown. The vortex-in-cell method is first validated by comparing with related numerical studies. Solution-method parameters are varied in order to ensure that reliable converged solutions are obtained. In addition, the evolution of several initial vorticity distributions are computed and studied. In Chapter 6, conclusions are given and recommendations for future research directions are proposed.

Chapter 2

Literature Survey

Numerical solution accuracy varies over a wide range of approximations and different numerical techniques are available to find the solution of flow problems. The main advantage of vortex methods is that the particles carry the vorticity, thus its value can be easily conserved. These methods are therefore very applicable to any problem involving complex vortex dynamics, such as simulation of high Reynolds number turbulent flows. In Section 2.1 of this chapter, details of literature related to vortex methods that have been developed and applied to different flow situations and the main features of vortex methods are reviewed. The relevant literature of the specific techniques used in this work for simulating a two-dimensional, incompressible, inviscid flow with given initial vorticity distributions is reviewed in Section 2.2.

2.1 Vortex Methods

In fluid dynamics, numerical techniques can be classified as either Eulerian or Lagrangian approaches. In Eulerian approaches the fluid flow quantities are defined as functions of position in space, $\vec{x}$, and time, t. In Lagrangian approaches, fluid material elements are specified by

position, $\vec{x}_0$, at some initial time, t_0, and tracked as time proceeds. Consequently, the dynamical history of the fluid element can be directly obtained by Lagrangian methods (Batchelor, 1979).

Vortex methods are Lagragian methods and can be used to approximate either the Navier-Stokes equations or Euler equations. Instead of a velocity-pressure formulation of the fluid motion, the vorticity form of the governing equations is discretizated, as discussed in many reviews such as Chorin, (1996), Winckelmans (2004), Leonard (1980,1985) and Puckett (1993). In an early example of the technique Rosenhead (1932) used a vortex method to simulate the evolution of two dimensional vortex sheets by point-vortex approximation using hand calculations. In 1962, again a point-vortex method was applied to simulate vortex sheets by Abernathy and Kronauer. In 1973, Chorin used a particle (vortex blob) method to simulate the flow around a two dimensional cylinder at high Reynolds number by using a finite vortex core for the discretization of the vorticity field. This advancement removes the velocity singularity present in point vortices. Later, Zabuky introduced a contour dynamics method, which can accurately simulate the evolution of piecewise constant distributions of vorticity in 1979. Leonard also used a vortex method in three-dimensions to simulate both aircraft-trailing vortices and two-dimensional mixing layers in 1980. Dritschel introduced contour surgery (CS) methods in 1989. In this technique some of the difficulties of contour dynamics are removed, as a constant piecewise structure of the vorticity field is maintained by truncating the small-scale structures, which allowed the extensions of the simulations to more complex inviscid flows. This is done by removing vortex particles of a size that is less than a given threshold. In 1997, Koumoutsakos implemented a high resolution Lagrangian (vortex) method to simulate the inviscid evolution of elliptical, non-uniform vorticity distributions. Such initially elliptical vortices are the focus of the present work.

Although details of each of these techniques and studies vary, they all rely on several general common ideas. The following can be considered the three main features of vortex methods:

- A vorticity field is discretized instead of a velocity field. This is done through the definition of vortex particles, or elements.
- The velocity field is estimated from the discretized vorticity field through the solution of a Poisson equation.
- The vorticity field evolves through the convection of vortex particles according to the computed velocity field.

Two-dimensional vortex methods comprise a wide range of solution techniques that have been proposed and implemented. Two advantages of the vortex methods are the absence of the pressure term in the governing equations and the automatic satisfaction of the continuity equation. A vortex method is characterized by both the use of the Navier-Stokes (or Euler) equations in vorticity-velocity form, and by a Lagrangian discretization of the vorticity. Vortex methods can be faster than Eulerian finite-difference methods by up to an order of magnitude, even when the domain is completely filled with vorticity (Ould-Salihi *et al*. 2000).

2.2 Vortex-In-Cell (VIC)

In the published literature, both Vortex-In-Cell (VIC) and Particle-In-Cell (PIC) names are used to identify these methods. An integral part of vortex-in-cell methods is to calculate the velocity field on a fixed Eulerian grid. These vortex-in-cell methods have lower computational cost, reducing the order from $O(N^2)$ to $O(N \log N)$, for N vortex particles in the flow field. VIC is a pure particle-mesh (PM) algorithm, as proposed by Christiansen (1973), which is an extension of

the Cloud-In-Cell (CIC) algorithm. The Cloud-In-Cell method was introduced by Birdsall and Fuss (1969) for the numerical treatment of plasma particle flows. The governing equations for these flows are very similar to those of the stream function equations for fluid velocities.

The first particle-in-cell method was used for hydrodynamic problems by Harlow (1956), he did not use a Poisson equation but used the zero-size particle and nearest-grid-point method (ZSP-NGP) to simulate the problem. It was Christiansen (1973) who first proposed to determine the velocity field by covering the solution domain with an Eulerian mesh in his study of the Kelvin-Helmholtz instability in two-dimensions. He used the stream function approach, where the stream function is computed through the solution of a Poission equation on the Eulerian grid. In VIC, the Lagrangian particles are moved and tracked while information is exchanged between the Lagrangian particles and the Eulerian grid. The VIC method has been used successfully in two-dimensional flow cases, where typically the vorticity-stream function formulation is most convenient. This method has been implemented by many authors, some of whom are, Aref and Siggia (1980) for shear layer flow and Chang and Chern (1991) for flow around a circular cylinder. Couet *et al*. (1981) simulated a periodic mixing layer for inviscid flow in three-dimensions. Micheal *et al.* (2000) used this method for viscous flow to simulate the diffusion of a line vortex and propagation of a vortex ring. A vortex flow in unbounded domain was simulated using VIC by Lui and Doorly (2000). In 2003, Cottet and Poncet used it to simulate their work in three-dimensional flows over a finite length cylinder and Chatelain *et al*. in 2008, used this method to simulate an aircraft wake at different Reynolds number with a large parallel distributed memory-implementation.

The common distinctive feature that separates these VIC methods from “pure” vortex methods is the computation of the velocity field on a grid. The initial vorticity field is discretized into a finite

set of particles, each of which is defined by its position and strength (circulation). The velocity field is computed by solving a Poisson equation on this fixed grid. The vorticity is then advected explicitly by the moving particles. In comparison to pure Lagrangian methods, the grid serves to both compute the velocity field and smooth the vorticity over a region of a dimension that depends on the interpolation scheme and grid spacing. In VIC methods the efficient and accurate exchange of information between the particle and mesh is important as finite grid size produces a loss of information related to wavelengths that are shorter than the grid spacing. Longer wavelength variations can be recovered accurately through the use of efficient interpolation schemes. The simplest interpolation scheme is a piecewise constant kernel; it simply assigns the particle variable to the nearest grid point. The second possible interpolation scheme is piecewise linear. This result in area weighing in two dimensions and volume weighing in three-dimensional flows and was used by many researchers such as Lui and Doorly (2000), Lui (2002) and Milane and Abdolhoseini (2004). This interpolation and smoothing formula interpolates the particle values to the nearest four grid points in two-dimension according to their distance from the particle. Monaghan (1985) proposed a one-dimensional moment-conserving B-spline interpolation formula that increases the accuracy of the interpolation without affecting smoothness properties. It is known as $M_4^{'}$ scheme and it was later extended to two- and three-dimensional vortex methods (Cottet and Koumoutsakos, 2000). This method is now widely used in the literature because of its accuracy and smoothness characteristics, see for example Cottet and Poncet (2003), Giovannini and Gagnon (2006) and Van Rees *et al*. (2011). The $M_4^{'}$ scheme is also adopted in this work.

Chapter 3

Governing Equations

Physical problems involving incompressible flow are governed by the continuity and momentum equations of fluid mechanics. For these situations, given a vorticity distribution, the velocity field can be determined through the solution of a Poisson equation. Vorticity is materially conserved in two-dimensional, inviscid, incompressible flow. In this chapter, details of the derivation of the governing differential equations for two-dimensional inviscid, incompressible flow are presented.

3.1 Vorticity Equation

The Navier-Strokes momentum equation, in terms of the velocity vector, $\vec{u}(\vec{x},t)$, and pressure, $p(\vec{x},t)$, for incompressible Newtonian viscous fluids with constant viscosity may be written, in the absence of body forces, as

$$\frac{\partial \vec{u}}{\partial t} + \left(\vec{u} \bullet \nabla\right) \vec{u} = -\frac{1}{\rho}\nabla p + \upsilon \nabla^2 \vec{u} \quad . \qquad (3.1)$$

In Equation (3.1), υ and ρ denote the kinematic viscosity and the density of the fluid respectively and ∇ is a vector operator given by $\left[\frac{\partial}{\partial x}\vec{e}_x + \frac{\partial}{\partial y}\vec{e}_y + \frac{\partial}{\partial z}\vec{e}_z\right]$.

Vorticity is a measure of the local spin of fluid element; hence vorticity, $\vec{\zeta}$, of a flow field with a velocity distribution, $\vec{u}$, is defined as the curl of the velocity field,

$$\vec{\zeta} = \nabla \times \vec{u} \ . \tag{3.2}$$

Thus, if the flow is two-dimensional, the vorticity will be a vector in the direction perpendicular to the flow.

Equation (3.1) can be rewritten in terms of vorticity. To do this, the following vector-calculus identities are used,

$$\frac{1}{2}\nabla(\vec{u} \bullet \vec{u}) = (\vec{u} \bullet \nabla)\ \vec{u} + \vec{u} \times (\nabla \times \vec{u}), \tag{3.3}$$

$$\nabla \times \nabla \varphi = 0 \ , \tag{3.4}$$

and,

$$\nabla \times (\vec{u} \times \vec{\zeta}) = (\vec{\zeta} \bullet \nabla)\ \vec{u} - (\vec{u} \bullet \nabla)\,\vec{\zeta} + \vec{u}\nabla \bullet \vec{\zeta} - \vec{\zeta}\nabla \bullet \vec{u} \ . \tag{3.5}$$

Where φ is any scalar quantity and the last two terms of right-hand side of Equation (3.5) vanish in this situation because the divergence of curl of any quantity is zero, $\nabla \bullet \vec{\zeta} = \nabla \bullet (\nabla \times \vec{u}) = 0$, and $\nabla \bullet \vec{u} = 0$ due to the incompressibility condition. Using Equation (3.1) and substituting the value of $(\vec{u} \bullet \nabla)\,\vec{u}$ from Equation (3.3) one obtains,

$$\frac{\partial \vec{u}}{\partial t} + \frac{1}{2}\nabla(\vec{u} \bullet \vec{u}) - \vec{u} \times (\nabla \times \vec{u}) = -\frac{1}{\rho}\nabla p + \upsilon \nabla^2 \vec{u}\,, \qquad (3.6)$$

$$\frac{\partial \vec{u}}{\partial t} + \frac{1}{2}\nabla(\vec{u} \bullet \vec{u}) - \vec{u} \times \vec{\zeta} = -\frac{1}{\rho}\nabla p + \upsilon \nabla^2 \vec{u}\ . \qquad (3.7)$$

In some fluid applications, it is more convenient to cast the above equation in term of vorticity. This is done by taking the curl of Equation (3.7). The pressure term and the second term on the left-hand side vanish (because of Equation (3.4)). The result is

$$\frac{\partial}{\partial t}(\nabla \times \vec{u}) + \frac{1}{2}\nabla \times \nabla(\vec{u} \bullet \vec{u}) - \nabla \times (\vec{u} \times \vec{\zeta}) = -\frac{1}{\rho}\nabla \times \nabla p + \upsilon\ \nabla^2(\nabla \times \vec{u})\ , \quad (3.8)$$

$$\frac{\partial \vec{\zeta}}{\partial t} - (\vec{\zeta} \bullet \nabla)\vec{u} + (\vec{u} \bullet \nabla)\vec{\zeta} = \upsilon\ \nabla^2 \vec{\zeta}, \qquad (3.9)$$

$$\frac{\partial \vec{\zeta}}{\partial t} + (\vec{u} \bullet \nabla)\vec{\zeta} = (\vec{\zeta} \bullet \nabla)\vec{u} + \upsilon\ \nabla^2 \vec{\zeta}. \qquad (3.10)$$

Equation (3.10) is the vorticity transport equation; the left-hand side of the equation treats the convection of vorticity. The first and second terms on the right-hand side are the stretching term, $(\vec{\zeta} \bullet \nabla)\vec{u}$, and the diffusion term, $\upsilon\ \nabla^2 \vec{\zeta}$, respectively. The stretching term is the rate of deformation of vortex lines and the diffusion term is the rate of viscous diffusion of vorticity. For two-dimensional flows, the vortex-stretching term is absent since $\vec{u} = u\ (x, y)\vec{e}_x + v\ (x, y)\vec{e}_y$ and $\vec{\zeta} = \zeta_z(x, y)\vec{e}_z$, therefore, $(\vec{\zeta} \bullet \nabla)\vec{u} = 0$. Hence, there is no vortex stretching in planar flows and the vorticity of a fluid element will change due to viscous effects alone.

Since the rate of change of the vorticity of material particles is defined by $\frac{D\vec{\zeta}}{Dt} = \frac{\partial \vec{\zeta}}{\partial t} + (u \bullet \nabla)\vec{\zeta}$, the above equation (3.10) can be written as,

$$\frac{D\vec{\zeta}}{Dt} = \upsilon \nabla^2 \vec{\zeta}. \qquad (3.11)$$

For two-dimensional, incompressible, inviscid flows, the viscous term vanishes and the vorticity-transport equation is,

$$\frac{D\zeta_z}{Dt} = 0. \qquad (3.12)$$

Equation (3.12) is the foundation for the Kelvin and Helmholtz Theorems, which state that infinitesimal packets of vorticity convect at the local velocity like material elements (Batchelor, 1967). In two-dimensional, inviscid, incompressible flow, vorticity is conserved. Furthermore, specification of the vorticity field completely determines the flow field.

The incompressibility condition can be used to define a stream function, ψ, from which the velocity components u and v in the x and y directions can be found as,

$$u = \frac{\partial \psi}{\partial y}, \quad \text{and} \quad v = -\frac{\partial \psi}{\partial x}. \qquad (3.13)$$

The z component of vorticity is then given by

$$\zeta_z = \frac{\partial v}{\partial x} - \frac{\partial u}{\partial y}. \qquad (3.14)$$

Substituting the value of u and v from equation (3.13) into equation (3.14) gives the vorticity in term of the stream function as a Poisson equation,

$$\zeta_z = -\nabla^2 \psi. \qquad (3.15)$$

Given a vorticity field, Equation (3.15) can be solved for the stream function and the velocity field can then be obtained through Equation (3.13).

Chapter 4

Numerical Methods

4.1 Vortex-In-Cell (VIC) Methods

The current numerical method is based on the discretization of Equations (3.12) and (3.15) using a mixed Eulerian-Lagrangian vortex-in-cell method. The main concern of this work is the solution of the vorticity transport Equation (3.12). Computationally calculating the velocity field is one of the most important parts of vortex methods and is done through the solution of Equation (3.15). The technique by which the flow field is discretized into vortex particles is discussed in Section 4.2. Interpolation techniques are used to transfer velocity from nodes of the Eulerian grid to the vortex particles and vorticity is transferred from particles to nodes, as described in Wang and Milane (2006). In this work the $M_4^{'}$ interpolation scheme is implemented because it has low dissipation error and maintains high accuracy and smoothness. Detailed discussion regarding interpolation techniques is covered in Section 4.3. The convection step that describes the convection of the interacting vortices involves the solution of the vorticity transport equation, Equation (3.12), for two-dimensional flows,

$$\frac{\partial \zeta_z}{\partial t} + u\frac{\partial \zeta_z}{\partial x} + v\frac{\partial \zeta_z}{\partial y} = 0. \qquad (4.1)$$

This transport equation describes the motion of the vortex particles. The fluid velocity is calculated at the nodes by solving the Poisson Equation (3.15). Following this, the velocity components at the nodes are transferred to the location of each vortex particle. Again, the $M_4^{'}$ interpolation technique is used. Next, the vortex particles are simply convected using the equation of motion of a material point. These steps are discussed in Sections 4.4 and 4.5. A second scheme that transfers vorticity from nodes to particles while performing remeshing is discussed in Section 4.6. The specific flow problems to be studied in this work, including initialization and boundary conditions are shown in Section 4.7. An overall summary of the VIC method is shown in Section 4.8. Finally, the outline of a pseudo-spectral method that is used for verification is discussed in Section 4.9.

4.2 Vortex Particles

Circulation, Γ, around the boundary of the small region of constant vorticity can be defined as the vorticity of the fluid times the area, *A*, of the small region. In a Lagrangian representation, the fluid volume is discretized into a finite set of material particles and Equation (4.1) is used to describe the motion of each particle as they interact with each other. In vortex methods, the vorticity field is discretized into a finite number of N_P point vortex elements each with different circulations, Γ_p. If point vortices are used, the total vorticity field can be given as

$$\zeta(\vec{x}) = \sum_{p=1}^{N_P} \Gamma_p \delta(\vec{x} - \vec{x}_p) \qquad (4.2)$$

where $\delta(\vec{x})$ is the Dirac delta function, $\vec{x}$ represents the coordinates at which the vorticity is calculated and $\vec{x}_p$ is the position coordinate of each vortex element. Cottet and Koumoutsakos (2000) show mathematical justification for this particle approximation along with its error estimates. The Biot-Savart law, i.e., the Green's function, has a singularity at the origin. When the distance between two vortices tends to zero, that is, $(x - x_p) \to 0$, this creates large velocities in its neighbourhood, which causes numerical and theoretical difficulties. To remove this singularity, finite core-size vortices may also be used (Chorin, 1973).

In vortex methods, the velocity field is recovered from the vorticity field using a Poisson equation. For "pure" vortex methods (without an Eulerian grid) a Biot-Savart law is used to solve the Poisson equation for unbounded domains. Denoting the Green's function of Laplace operator by $\vec{G}(\vec{x})$, the velocity field can be recovered using the Biot-Savart formula (Cottet and Koumoutsakos, 2000),

$$\vec{u}(\vec{x}) = \int_{-\infty}^{\infty} \left[\nabla \times \vec{G}(\vec{x} - \vec{x}')\right] \times \zeta(\vec{x}')dV(\vec{x}') = \int_{-\infty}^{\infty} \vec{k}(\vec{x} - \vec{x}') \times \zeta(\vec{x}')dV(\vec{x}') = \vec{k}(\vec{x}) * \zeta(\vec{x}) \quad (4.3)$$

where * corresponds the convolution integral and $\vec{k}$ represents the rotational part of $\vec{G}$ i.e. $\vec{k} = \nabla \times \vec{G}$. When the vorticity field is discretized into a finite number of particles, the integral in Equation (4.3) is replaced by a summation, as

$$\vec{u}_i(\vec{x}_i) = \sum_{j \neq 1} \vec{k}(\vec{x}_i - \vec{x}_j) \times \vec{\alpha}_j \quad (4.4)$$

where $\vec{\alpha} = \int \vec{\zeta} dV$ is the strength of the point vortex. Equation (4.4) shows that in the computational domain, at any point vortex, *i*, the velocity is the accumulative effect of the

induced velocity of all other vortex particles. The determination of the velocity of all particles through the Biot-Savart integral solution of the Poisson equation, therefore, gives rise to N^2 operations at every time step when N vortex particles exist in the solution domain (Leonard, 1985). In order to accelerate the computation of the velocity, two remedies have been developed to reduce the number of computations per time step to $O(N \log N)$, the first is the fast multipole expansion, proposed by Greengrad and Rokhlin (1987), and the second is the vortex-in-cell (VIC) method, originally derived from plasma physics by Christiansen (1973).

In the mixed Eulerian-Lagrangian vortex-in-cell method adopted by this study, the grid serves as a mollification mechanism that removes the singularity of the vorticity representation in Equation (4.2). This creates some errors but is effective for removing the singularities from the flow field. The vortex-in-cell approach is adopted in this work, which replaces the Biot-Savart integral on Lagrangian points by solution of Poisson equation on an Eulerian mesh.

4.3 Interpolation Scheme

The main difference between "pure" vortex methods and VIC is the solution of the Poisson equation on a fixed Eulerian mesh. Before this is done, the vorticity field must be interpolated from the vortex particles to the mesh. After, the computed velocity field must be interpolated back to the particles. The interpolation techniques which are used in this work to transfer velocity from nodes to vortex particles and vorticity from particles to nodes, are summarized in Wang and Milane (2006). Cartesian tensor products of one dimensional interpolation rules can be used for two and three-dimensional flows. Mathematically, the two dimensional interpolation schemes on uniform meshes are expressed in terms of grid spacing, $h = \Delta x = \Delta y$, as

$$\zeta_{(i,j)} = \frac{1}{h^2}\sum_{p=1}^{N_p}\Gamma_p \prod\left(\frac{x_p - x_{(i,j)}}{h}\right) \prod\left(\frac{y_p - y_{(i,j)}}{h}\right) \tag{4.5}$$

where $\prod$, is the interpolation kernel and subscripts, p and (i,j), indicate the particle and grid locations respectively. A Cartesian tensor product of 1D kernels is built for the 2D or 3D interpolations. Two families of interpolation kernels are commonly used in VIC schemes, referred to as, the "Λ" and the "M" families. By defining, $u = \frac{|x_p - x_i|}{h}$, lower-order members of these one-dimensional interpolation kernels can be expressed as,

$$\prod(u) = \Lambda_0(u) = \begin{cases} 1 & if \quad 0 \le u \le \frac{1}{2}, \\ 0 & otherwise, \end{cases} \tag{4.6}$$

$$\prod(u) = \Lambda_1(u) = \begin{cases} 1-u & if \quad 0 \le u \le 1, \\ 0 & otherwise, \end{cases} \tag{4.7}$$

$$\prod(u) = \Lambda_2(u) = \begin{cases} 1-u^2 & if \quad 0 \le u \le \frac{1}{2}, \\ \frac{1}{2}(1-u)\ (2-u) & if \quad \frac{1}{2} \le u \le \frac{3}{2}, \\ 0 & otherwise, \end{cases} \tag{4.8}$$

$$\prod(u) = \Lambda_3(u) = \begin{cases} \frac{1}{2}(1-u^2)\ (2-u) & \text{if} \quad 0 \le u \le 1, \\ \frac{1}{6}(1-u)\ (2-u)\ (3-u) & \text{if} \quad 1 \le u \le 2, \\ 0 & \text{otherwise}, \end{cases} \tag{4.9}$$

$$\prod(u) = M_3(u) = \begin{cases} \frac{1}{2}(\frac{3}{2}+u)^2 \ -\frac{3}{2}(u+\frac{1}{2})^2 & \text{if} \quad 0 \le u \le \frac{1}{2}, \\ \frac{1}{2}(\frac{3}{2}+u)^2 & \text{if} \quad \frac{1}{2} \le u \le \frac{3}{2}, \\ 0 & \text{otherwise}, \end{cases} \tag{4.10}$$

$$\prod(u) = M_4(u) = \begin{cases} \frac{1}{6}(2-u)^3 \ -\frac{4}{6}(1-u)^3 & \text{if} \quad 0 \le u \le 1, \\ \frac{1}{6}(2-u)^3 & \text{if} \quad 1 \le u \le 2, \\ 0 & \text{otherwise}, \end{cases} \tag{4.11}$$

$$\prod(u) = M_4^{'}(u) = \begin{cases} 1-\frac{5}{2}u^2 \ +\frac{3}{2}u^3 & \text{if} \quad 0 \le u \le 1, \\ \frac{1}{2}(1-u)\ (2-u)^2 & \text{if} \quad 1 \le u \le 2, \\ 0 & \text{otherwise}, \end{cases} \tag{4.12}$$

The first interpolation formula, Λ_0 kernel, gives a first-order scheme and can exactly approximate only constant functions. It is equivalent to nearest grid point (NGP) interpolation and is identical to the M_1 kernel (omitted). Only the total circulation (zeroth vorticity moment) is conserved when this interpolation is used. The second interpolation formula, Λ_1 kernel, gives a

second-order accurate scheme and can approximate exactly only linear functions, it is equivalent to the M_2 kernel (omitted) and is often called the "tent-function". The total circulation and linear impulse (first moment of vorticity) of the problem is conserved when this interpolation is used within a vortex method. The stencil for this kernel comprising of 2^d nodes, where d is the number of dimensions in the problem. The third-order kernel is Λ_2, which correspond to quadratic interpolation. It conserves zeroth, first, and second moments of vorticity, and requires a stencil comprising of 3^d nodes. Lack of smoothness and continuity between adjacent cells are the main disadvantages of this interpolation scheme. The kernel Λ_3, is known as Everett's fourth-order formula, which is a piecewise-cubic and continuous kernel that requires a stencil of 4^d nodes. Up to the third moment of vorticity can be conserved by using this interpolation scheme. Indeed, the Λ family of kernels is constructed precisely by specifying that increasing moments of vorticity be conserved.

The "M" family of interpolation kernels is derived from splines; by being more regular than the Λ family, this interpolation scheme often preferred. The first member of the central B-spline kernels that is different from the Λ kernels is the M_3 kernel which has continuous first derivatives. The second distinct interpolation kernel is the M_4 kernel. Both of these schemes are second-order accurate. A higher-order accuracy kernel (third order) was introduced in J. J. Monaghan (1985), which is a one-dimensional moment-conserving B-spline interpolation formula that increases the accuracy without affecting the smoothness properties. When this kernel is used, the total circulation, linear impulse, and angular impulse are conserved within a vortex method. To ensure highly accurate results one can use this M_4' kernel. It was later extended to

two- and three-dimensional vortex methods (Cottet and Koumoutsakos, 2000). This scheme is more accurate than the Λ_2 scheme, as was shown in Cottet, Ould Salihi, and El Hamraoui (1999). Though, both have the same formal order of accuracy and stencil.

The $M_4^{'}$ scheme is used because of its low computational dissipated error. The $M_4^{'}$ one-dimensional kernel is given by Equation (4.12). The total circulations, first and second moments are conserved. To understand the implementation of the $M_4^{'}$ scheme, let us consider an example of a one dimensional situation. If a particle is located at a point, x_p at a distance of u = 0.3 to the right of a grid point, x_i, as shown in Figure 4.1. Using the $M_4^{'}$ scheme, this particle will contribute to the vorticity of the grid points x_{i-1}, x_i, x_{i+1}, x_{i+2}, in the following proportions, -0.0735, 0.8155, 0.2895, -0.0315, respectively.

In a two-dimensional coordinate system, the vorticity of a particle at point, $\vec{x}_p$, within a cell, will be distributed to the closest 16 mesh points by the two dimensional filter built from the tensorial product of the one dimensional kernel, as illustrated in Figure 4.2.

4.4 Numerical Approximation for Poisson's Equation

The evolution of vorticity is governed by Equation (4.1), which corresponds to the evolution of vorticity for an incompressible, inviscid and axisymmetric fluid flow. The velocity on the grid is required to convect the particle in the flow domain and velocity can be determine by solving Equation (3.15) after vorticity is interpolated to the grid. Poisson's equation, Equation (3.15) with periodic boundary conditions is singular or under-determined in general (McBryan, 2014). To be

solvable, restrictions must be placed on the right-hand side, ζ_z. Specifically, there is no solution unless vorticity, ζ_z, integrates to zero over the domain. When this is true, there are infinitely many solutions differing by only a constant. This constant is unimportant as it will vanish when derivatives of the stream function are taken to determine the velocity. In this work, to ensure solvability of the Poisson equation one should add a constant which is the average vorticity, $\zeta_{avergae}$, over the whole domain. In the discrete setting, this average is equal to the sum of all the vorticity at the nodes divided by total number of nodes of the domain. Once this correction has been added, the sum of the right-hand side of the discrete Poisson equation is equal to zero and the system is solvable. The discrete version of Equation (3.15), is obtained, for a Cartesian grid, by approximating the derivatives using a second-order central finite-difference scheme, such that

$$\frac{\psi_{(i+1,j)} - 2\psi_{(i,j)} + \psi_{(i-1,j)}}{(\Delta x)^2} + \frac{\psi_{(i,j+1)} - 2\psi_{(i,j)} + \psi_{(i,j-1)}}{(\Delta y)^2} = -\zeta_{(i,j)} + \zeta_{average}. \tag{4.13}$$

Where Δx and Δy are the grid spacing in the x and y directions, respectively, and i and j are indices indicating nodes ordering along the x and y directions, respectively. By rearranging Equation (4.14) and solving for $\psi_{(i,j)}$, it becomes

$$\psi_{(i,j)} = \left[\frac{\left(\psi_{(i+1,j)} + \psi_{(i-1,j)}\right)(\Delta y)^2 + \left(\psi_{(i,j+1)} + \psi_{(i,j-1)}\right)(\Delta x)^2 + (\zeta_{(i,j)} - \zeta_{average})(\Delta x)^2(\Delta y)^2}{2(\Delta x)^2 + 2(\Delta y)} \right]. \tag{4.14}$$

In this work, the size of grid spacing in the x and y directions are equal, i.e. $h = \Delta x = \Delta y$. Thus Equation (4.14) becomes

$$\psi_{(i,j)} = \frac{\psi_{(i+1,j)} + \psi_{(i-1,j)} + \psi_{(i,j+1)} + \psi_{(i,j-1)} + (\zeta_{(i,j)} - \zeta_{average})(\Delta x)^2}{4} \quad . \qquad (4.15)$$

Given a vorticity distribution, one can solve this linear system of equations to get $\psi_{(i,j)}$ at each node (i, j) of the computational domain. In this work, the Jacobi iterative method is used to solve the resulting linear system. Following this, using Equation (3.13), the components of the velocity field at the nodes are approximated using central difference approximations for the first derivative as

$$u_{(i,j)} = \frac{\psi_{(i,j+1)} - \psi_{(i,j-1)}}{2(\Delta y)} \text{ , and } v_{(i,j)} = -\frac{\psi_{(i+1,j)} - \psi_{(i-1,j)}}{2(\Delta x)} \quad . \qquad (4.16)$$

These velocity $u_{(i,j)}$ and $v_{(i,j)}$ are interpolated back to the particles again using $M_4^{'}$ interpolation scheme. This velocity is then used to convect the vortices.

4.5 The Convection Step

In this thesis a vortex-in-cell method is used and an initial vorticity field is discretized into a set of vortex particles. Once the Poisson equation is solved and the velocity on the mesh is known, the components of the particle velocity, $\vec{u}_p = (u_p, v_p)$, acting on the center of a vortex blob can be calculated, again using the $M_4^{'}$ interpolation technique as

$$u_p = \sum_{(i,j)}^{16} u_{(i,j)} \ \prod \left\{ \frac{x_p - x_{(i,j)}}{h} \right\} \ \prod \left\{ \frac{y_p - y_{(i,j)}}{h} \right\}, \tag{4.17a}$$

$$v_p = \sum_{(i,j)}^{16} v_{(i,j)} \ \prod \left\{ \frac{x_p - x_{(i,j)}}{h} \right\} \ \prod \left\{ \frac{y_p - y_{(i,j)}}{h} \right\}. \tag{4.17b}$$

These summations $\sum_{(i,j)}^{16}$, are over the 16 nodes that affect each particle. The convection step of the vorticity transport equation involves integrating the equation of motion of a material point, describing the motion of each vortex particle,

$$\frac{d\vec{x}_p}{dt} = \vec{u}(\vec{x}_p, t). \tag{4.18}$$

using a predictor-corrector method, where the predictor step is

$$\vec{x}_p^*(t + \Delta t) = \vec{x}_p(t) + u_p \Delta t, \tag{4.19a}$$

$$\vec{y}_p^*(t + \Delta t) = \vec{y}_p(t) + v_p \Delta t. \tag{4.19b}$$

Here Δt is the time-step and $\vec{u}_p$ is the particle velocity. This is only one half step of the time marching scheme. Following this, the procedure outlined in subsection 4.2-4.5 is repeated to calculate a corrector approximation to the particle velocity, $\vec{u}_p^*$. The final particle positions are calculated as

$$x_p(t + \Delta t) = x_p(t) + \left[\frac{u_p(t) + u_p^*(t + \Delta t)}{2} \right] \Delta t \tag{4.20a}$$

$$y_p(t+\Delta t) = y_p(t) + \left[\frac{v_p(t) + v_p^*(t+\Delta t)}{2}\right]\Delta t \qquad (4.20b)$$

4.6 Remeshing Schemes

Remeshing is performed to avoid clustering of particles in one location. In this simulation a remeshing (regridding) technique has been implemented in which the set of particles is simply placed back to the centre of each grid cell within the computation after every few time steps, as shown in Figure 4.3. The vorticity of vortex elements is reinitialized by interpolating the vorticity from the nodes of the Eulerian mesh to the vortex elements, again using $M_4^{'}$ interpolation scheme. If remeshing is not performed in vortex-in-cell methods, clustering of particles will take place in many places, which can cause oscillations in the flow, as shown in Figure 4.4. Also, when regions of the domain without vortex particles develop; flow can no longer be modelled in these regions. This is why remeshing is so important in vortex-in-cell method.

Today in vortex methods, as well as vortex-in-cell methods remeshing is necessary for many situations. In addition, in smooth particle hydrodynamics (SPH) methods it is also used. In fact, this is where originally it was introduced. From a research point of view, remeshing schemes are still an active area in vortex-method development.

4.7 Initialization and Boundary Conditions

The problems to be simulated in this present work are the evolution of various initially elliptical vortices. The computational domain used to solve the two-dimensional flow consists of a square

region covered by a uniform Cartesian mesh with the same grid spacing in each direction (*i.e.* $\Delta x = \Delta y$). The computational domain is from -3 to 3 in non-dimensional length units in both directions. Periodic boundary conditions are applied in each direction and the number of grid points in each direction is equal to *M.* A vortex particle is initially placed at the center of each cell. The location of each vortex particles in the computational domain is identified and circulation ($\Gamma_p = \zeta_p h^2$) of each vortex particles is calculated from the initial conditions. As a uniform grid is used in this thesis, the space associated with each particle is h^2. The vortex particles are therefore equidistant, and are separated by a distance, $d = H / N_v$, where N_v is the number of vortices in each directions and $H = \Delta x\ (M - 1)$ is the length of the computational domain. During a simulation, if a vortex particle exits the domain, it is reintroduced at the opposite boundary due to the periodic boundary condition.

For all problems considered in this work, the initial vorticity field is one used by Melander, McWilliams and Zabusky (1986) and Koumoutsakos (1997) as well as extension thereon. A vorticity field function is defined as,

$$\zeta(r) = \Omega \begin{Bmatrix} 1 - f_q(r / R_0), & if, & r \le R_0, \\ 0, & & Otherwise \end{Bmatrix} \qquad (4.21)$$

where $f_q(z) = \exp\{-(q/z) \times \exp(1/(z-1))\}$ and the values of constants used by MMZ are $q = 2.56085$, $\Omega = 20$, $R_0 = 0.8$ and $z = r / R_0$. The value, *r*, is defined as $r = \sqrt{a^2 x^2 + b^2 y^2}$, leading to lines of constant vorticity that are ellipses of aspect ratio, $\lambda = \frac{a}{b}$.

4.8 Outline of VIC Method

The vorticity transport equation is solved using the VIC algorithm for each time step. The solution procedure is summarized in the following steps, in addition a flowchart representation is provided in Appendix A.1.

a) Add vortex particles to the center of each cell and calculate the vorticity at particle locations based on the initial conditions.

Predictor step

b) Transfer the vorticity from the particles to the nodes using the $M_4^{'}$, interpolation scheme Equation (4.5).

c) Solve the Poisson's equations using the Jacobi iterative method with a left-to-right sweep of the nodes and bottom-to-top sweep of the lines using Equation (4.15). Iteration convergence is obtained when the sum of the absolute value of the difference between consecutive ψ vectors is less than 0.1.

d) Compute the velocities $u_{(i,j)}(t)$ and $v_{(i,j)}(t)$ at the nodes using Equation (4.16).

e) Transfer the computed velocities to the location of each vortex using the M_4' interpolation scheme, Equation (4.17a) and (4.17b).

f) Update the coordinates of the vortices, while keeping their circulation constant, Equation (4.19a) and (4.19b).

g) Given (x^*, y^*, ζ) stored at every particle in the domain, reinitialize each node with zero vorticity.

Corrector step

h) The corrector step starts by transferring the new vorticity field from the new locations of the vortices to the nodes by repeating step (b). Then the Poisson equation is again solved by using the Jacobi iterative method.

i) Compute the new velocities at the nodes $u_i^*(t+\Delta t)$ and $v_i^*(t+\Delta t)$ using Equation (4.16).

j) Transfer the velocities to the location of each vortex using the $M_4^{'}$ interpolation scheme, Equation (4.17a) and (4.17b), to find the velocity $u_p^*(t+\Delta t)$ and $v_p*(t+\Delta t)$ at the location of each vortex particle.

k) Update the co-ordinates of the vortices, while again keeping the circulation constant using Equation (4.20a) and (4.20b).

l) End the corrector step by storing the position values, $\vec{x}_p(t+\Delta t)$, of the particle and reinitializing each node to zero vorticity.

Time advancement

m) March in time by repeating the calculations from step b) through l) until the required time is reached. The remeshing is carried periodically after a prescribed number of time steps.

4.9 Outline of Pseudo-Spectral Method

The pseudo-spectral method is easy to implement and has high accuracy when compared to finite-difference and finite-element methods. A pseudo-spectral method is used to verify our VIC implementation. In addition, this method is implemented because of the following reasons:

- It has very high accuracy.
- Available libraries make implementation relatively easy.

- Issues related to the singularity of the Poisson problem on a periodic domain are automatically handled by projecting the vorticity field onto the Fourier modes.
- After applying the Fourier transform, differential operators become algebraic. They are, therefore, much easier to handle numerically.

The pseudo-spectral method has more limitations compared to other approaches; one of them is that in finite domains the problem has to be periodic. If the problem is not naturally periodic, it has to be reformulated to a periodic setting. The pseudo-spectral method works well and can save up to several orders of magnitude in computer memory and computation time.

For details regarding these methods, the reader is referred to important works by Kreiss and Oliger (1972). The additional basic theory related to this method can also be found, for example, in Orszag (1972), Fornberg (1975), and Gottlieb and Orszag (1977). In many important situations pseudo-spectral methods perform far better than other numerical methods, therefore it is a leading technique in several fields, such as, turbulence in fluid dynamics, nonlinear wave dynamics, weather forecasting, etc. Hence, the pseudo-spectral method is the best choice to verify the current VIC implementation, as our problem is two-dimensional, with uniform grid and has periodic boundary condition.

4.9.1 Fourier Transform and Discrete Fourier Transform

For completeness, details of the method are outlined here. The Fourier transform of a function $\zeta(x),\ x \in \Re$ is the function $\hat{\zeta}(k)$ defined by

$$\hat{\zeta}\ (k)\ =\ \int_{-\infty}^{\infty} e^{-ikx}\zeta(x)\ dx, \qquad k\ \in\ \Re. \tag{4.22}$$

The function $\hat{\zeta}\ (k)$ can be interpreted as the amplitude density of ζ at wavenumber, *k*, and this process of decomposing a function into its constituent waves is called Fourier analysis, where *i* is the base imaginary number, $i = \sqrt{-1}$. Conversely, one can reconstruct ζ from $\hat{\zeta}$ using the inverse Fourier transform:

$$\zeta(x)\ =\ \frac{1}{2\pi}\int_{-\infty}^{\infty} e^{-ikx}\hat{\zeta}\ (k)\ dk, \qquad x\ \in\ \Re. \tag{4.23}$$

This is Fourier synthesis. The variable *x* is the physical variable, and *k* is the Fourier variable or wavenumber.

The Discrete Fourier Transform (DFT) is the standard tool for numerically studying problems in frequency space using a finite number of discrete frequencies. In practice, the discrete Fourier transforms are usually computed by a Fast Fourier Transform (FFT) algorithm. This reduces the computational time, as the order of computation decreases from an O(N^2), needed for a full discrete Fourier transform, to one that is only O(Nlog$N$), as discovered in 1965 by Cooley and Tukey. The following is a brief review of the technique.

Let us consider a basic periodic grid which will be a subset of the interval [0; 2π] with *N*, equally spaced grid node at locations, x_j, each separated by a distance, $h = \frac{2\pi}{N}$:

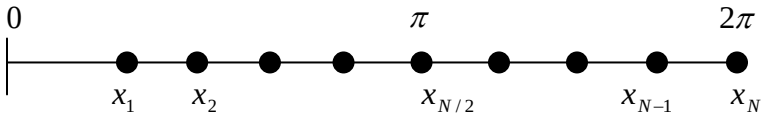

(Intervals of length other than 2π are easily handled through a linear mapping to this domain.)

The formula for the discrete Fourier transform (DFT) of the function evaluated at each grid point, $\zeta = [\zeta_0, \zeta_1, \zeta_2, ...\zeta_{N-1}]$, is another vector whose k^{th} component is

$$\hat{\zeta}_k = \sum_{j=0}^{N-1} e^{-i(2\pi/N)kj} \cdot \zeta_j, \qquad k = 0, ...N-1 \quad (4.24)$$

and the inverse discrete Fourier transform of the vector $\hat{\zeta} = [\hat{\zeta}_0, \hat{\zeta}_1, \hat{\zeta}_2, ...\hat{\zeta}_{N-1}]$ is another vector whose j^{th} component is given by

$$\zeta_j = \frac{1}{N} \sum_{k=0}^{N-1} e^{i(2\pi/N)kj} \cdot \hat{\zeta}_k, \qquad j = 0, 1, ...N-1 \qquad (4.25)$$

In Equation (4.24) and (4.25), the wavenumber *k*, like the spatial index *j*, takes only integer values. Due to periodicity, the customary domain of *k* actually computed is *[-N/2+1, N/2]*. This is always the case when the DFT is implemented via the Fast Fourier transform algorithm. Other common domains are *[-N/2, N/2-1]* (*N* even) and *[-(N-1)/2, (N-1)/2]* (*N* odd).

Fourier transform is a linear operation; it can be applied direction-by-direction for multiple dimensions. For two-dimension, ζ is now an $Nx \times Ny$ matrix containing function values at grid nodes, with components $\zeta_{(j_x, j_y)}$, $0 \le j_x \le Nx-1$ and $0 \le j_y \le Ny-1$. The formula for the two dimensional discrete Fourier transforms of the matrix, ζ, is another matrix of the same dimension whose (k_x, k_y) component is,

$$\hat{\zeta}_{(k_x, k_y)} = \sum_{j_y=0}^{Ny-1} \sum_{j_x=0}^{Nx-1} e^{-i\left[(2\pi/Nx)k_x\, j_x + (2\pi/Ny)k_y\, j_y\right]} \cdot \zeta_{(j_x, j_y)}, \qquad (4.26)$$

and the inverse discrete Fourier transform is given by

$$\zeta_{(j_x, j_y)} = \frac{1}{Nx\ Ny} \sum_{k_y=0}^{Ny-1} \sum_{k_x=0}^{Nx-1} e^{-i\left[(2\pi/Nx)k_x\, j_x + (2\pi/Ny)k_y\, j_y\right]} \cdot \hat{\zeta}_{(k_x, k_y)}. \qquad (4.27)$$

The pseudo-spectral code solves the following modified vorticity-transport equation, (McWilliams, 1984),

$$\frac{\partial \zeta_z}{\partial t} + u\frac{\partial \zeta_z}{\partial x} + v\frac{\partial \zeta_z}{\partial y} = \left[-\upsilon_4 \Delta^2\right]\zeta_z. \qquad (4.28)$$

where *u* and *v* velocities can be related to derivatives of the stream function as shown in Equation (3.13) and $\upsilon_4 \Delta^2 \zeta$ is a hyperviscosity term, which is used to stabilize the numerical technique. Equation (4.28) can be rewritten as

$$\frac{\partial \zeta_z}{\partial t} + \frac{\partial \psi}{\partial y}\frac{\partial \zeta_z}{\partial x} - \frac{\partial \psi}{\partial x}\frac{\partial \zeta_z}{\partial y} + \upsilon_4 \Delta^2 \zeta_z = 0. \qquad (4.29)$$

The stream function is found through the solution of the Poisson equation, Equation (3.15). The numerical solution procedure of the pseudo-spectral method to solve Equation (4.29) is as follows:

1. Choose a resolution *N*×*N* where *N* is the number of grid nodes in real space and number of modes in Fourier space per direction. The computational domain is from -3 to 3 in non-dimensional length (*L*) units in the *x* and *y* directions and has periodic boundary conditions in both directions.
2. The initial vorticity field is computed at the nodes using Equation (4.21).
3. The vorticity at each node is transformed, $\zeta_{(j_x, j_y)} \Rightarrow \hat{\zeta}_{(k_x, k_y)}$, to Fourier space by using an FFT, which returns the two-dimensional discrete Fourier transform of ζ.
4. The stream function is computed in Fourier space by solving the Fourier transform of the Poisson equation, Equation (3.15). The Fourier transform of this equation is algebraic,

$$-\nabla^2 \psi = \zeta \Rightarrow -\left[(k_x)^2 + (k_y)^2\right]\hat{\psi} = \hat{\zeta}, \qquad \text{or} \qquad \hat{\psi} = -\frac{\hat{\zeta}_{(i,j)}}{(k_x)^2 + (k_y)^2}.$$

5. The discrete Fourier transform of the velocity components can be determined in a similar manner, by using Equation (3.13),

$$u = \frac{\partial \psi}{\partial y} \Rightarrow \hat{u} = ik_y \, \hat{\psi}$$

$$v = -\frac{\partial \psi}{\partial y} \Rightarrow \hat{v} = ik_x \, \hat{\psi}$$

6. The derivatives of the discrete vorticity field in physical space can be also be related to algebraic functions in Fourier space,

$$\frac{\partial \zeta}{\partial x} \Rightarrow ik_x \, \hat{\zeta} \quad \text{and} \quad \frac{\partial \zeta}{\partial y} \Rightarrow ik_y \, \hat{\zeta} \, .$$

7. The discrete Fourier transform of the hypervicosity term in Equation (4.29) can be found as,

$$\Delta^2 \zeta_z \Rightarrow \left[(k_x)^2 + (k_y)^2 \right]^2 \hat{\zeta}$$

8. Traditionally, the hypervicosity, υ_4, is calculated as, $\upsilon_4 = \frac{\alpha}{\kappa^2 \Delta t}$, where α is the damping coefficient, Δt is the timestep and κ^2 is equal to $\left[\left(\frac{\pi}{\Delta x} \right)^2 + \left(\frac{\pi}{\Delta y} \right)^2 \right]^2$. For this work, a value of $\alpha = 5.0$ is used.

9. The inverse discrete Fourier transform of the terms computed in steps 4, 5, 6 and 7 can be computed and their values can be inserted directly into the discrete version of Equation (4.29),

$$\frac{\partial \zeta_{(j_x, j_y)}}{\partial t} + \frac{\partial \psi_{(j_x, j_y)}}{\partial y} \frac{\partial \zeta_{(j_x, j_y)}}{\partial x} - \frac{\partial \psi_{(j_x, j_y)}}{\partial x} \frac{\partial \zeta_{(j_x, j_y)}}{\partial y} + \upsilon_4 \Delta^2 \zeta_{(j_x, j_y)} = 0. \qquad (4.30)$$

10. Equation (4.30) now represents a system of ordinary differential equations that can be advanced in time by any standard time-integration techniques. 4^{th} order Runge-Kutta was used for time marching.

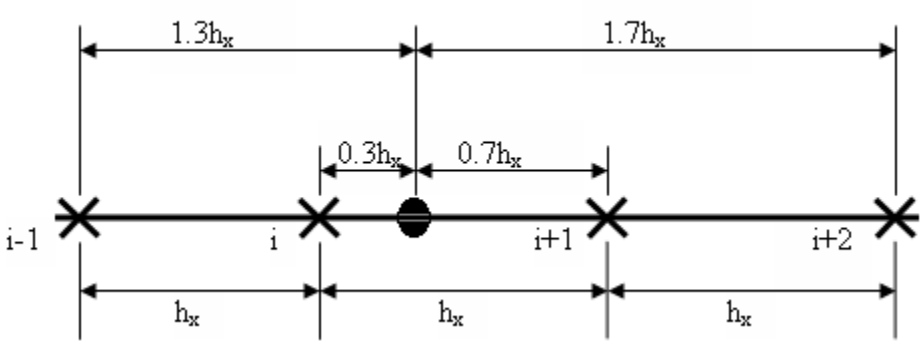

$$\zeta_{(x_i-1=1.3)} = \frac{1}{2}(1-1.3)\times(2-1.3)^2 = -0.0735. \qquad \zeta_{(x_i=0.3)} = 1-\frac{5}{2}(0.3)^2+\frac{3}{2}(0.3)^3 = 0.8155.$$

$$\zeta_{(x_{i+1}=0.7)} = 1-\frac{5}{2}(0.7)^2+\frac{3}{2}(0.7)^3 = 0.2895. \quad \zeta_{(x_i+2=1.7)} = \frac{1}{2}(1-1.7)\times(2-1.7)^2 = -0.0315.$$

Figure 4.1 One dimensional example of $M_4^{'}$ interpolation scheme.

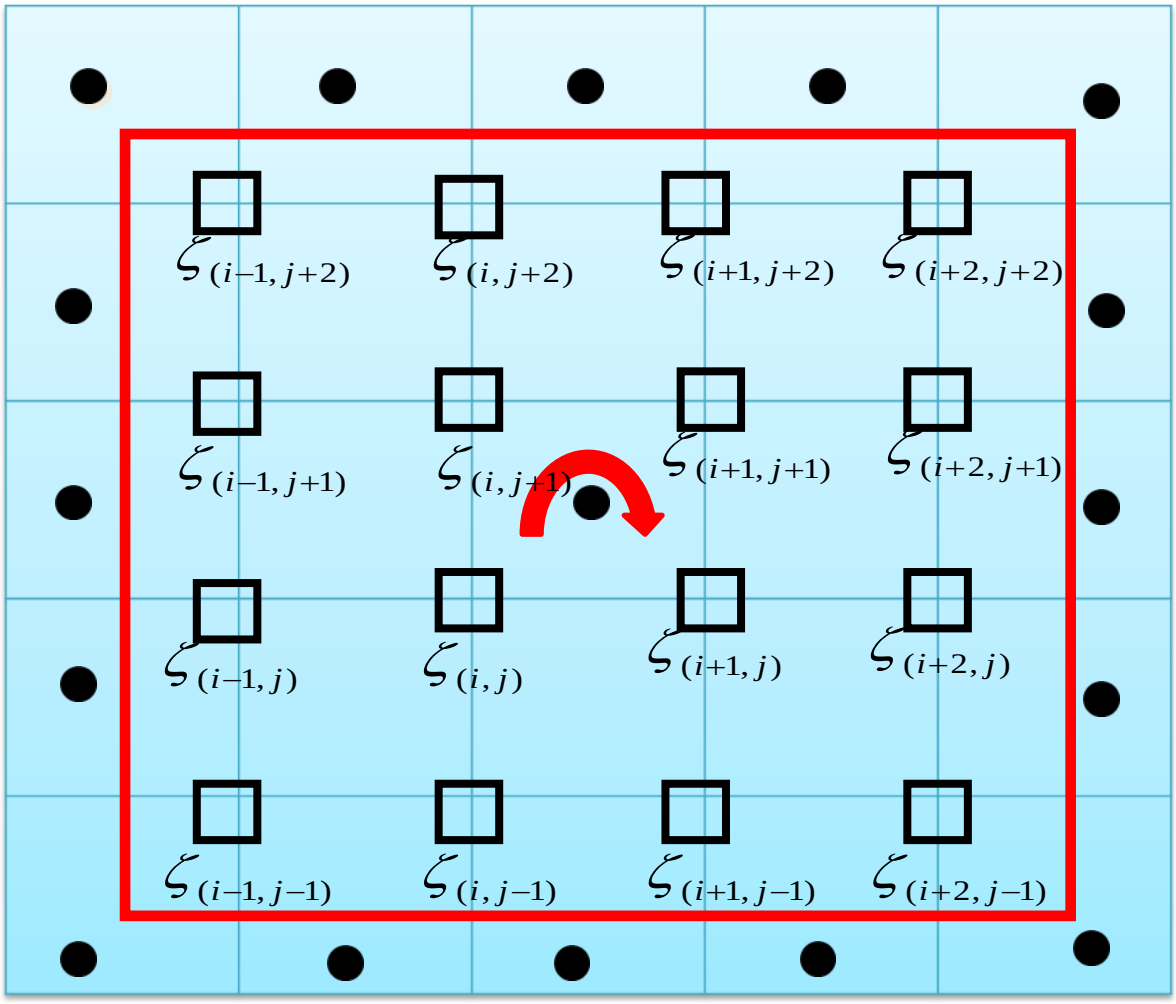

Figure 4.2 Illustration of nodes affected by the M_4' interpolation scheme.

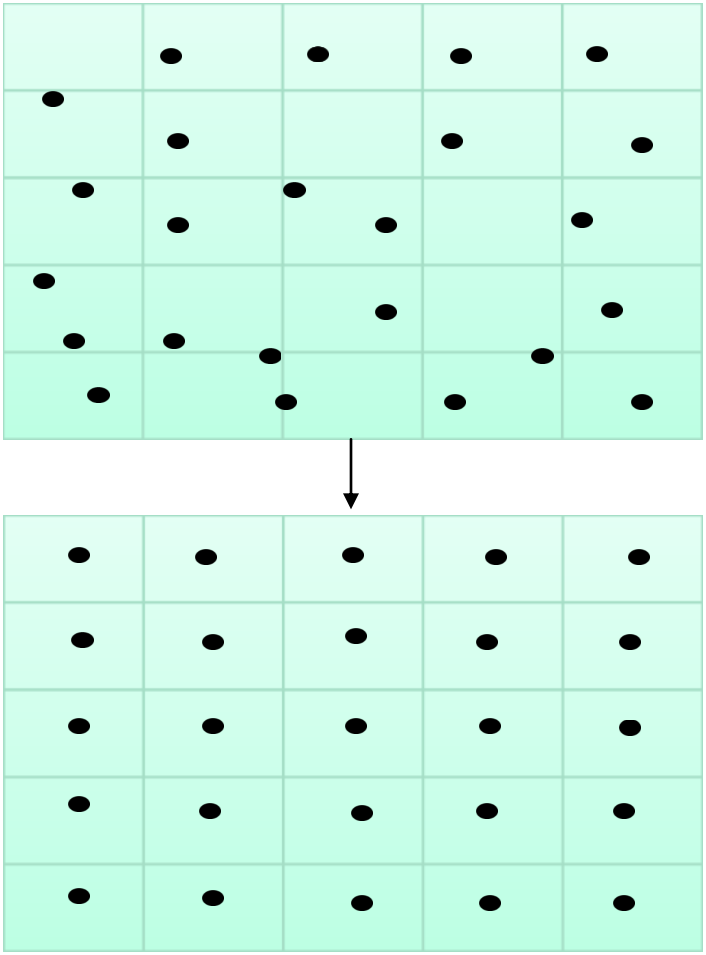

Figure 4.3 Illustration of the remeshing scheme adopted in this work. A non-uniform distribution of particle locations is reinitialized to avoid excessive stretching or clustering.

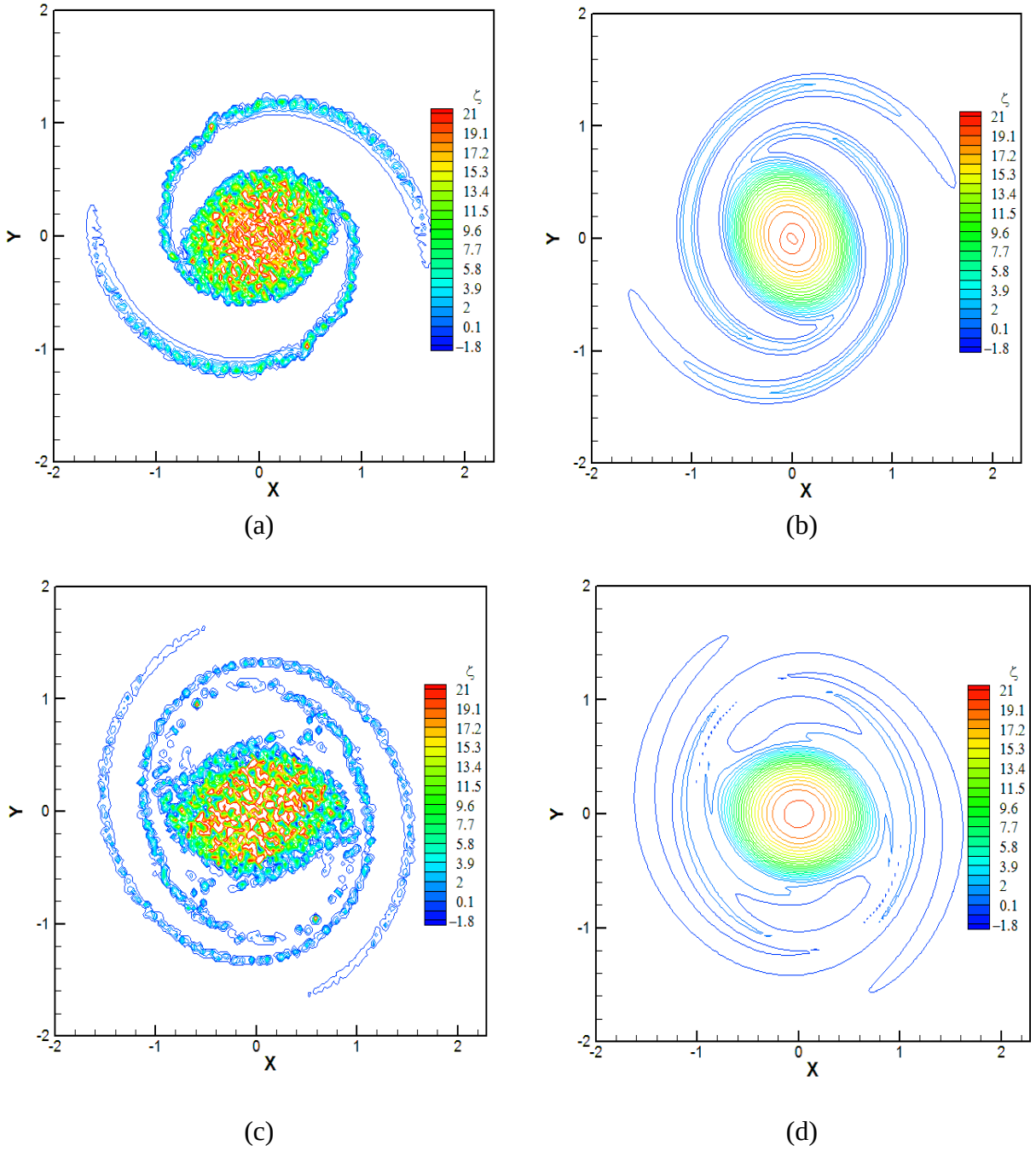

Figure 4.4 Comparison of vorticity contours for the evolution of an initially elliptical vortex with aspect ratio = 2.86, 200x200 grid, $\Delta x = \Delta y = 0.03$, with $\Delta t = 3.0 \times 10^{-3}$, using VIC method at times, (a) $T = 2.0$ (without remeshing), (b) $T = 2.0$ (with remeshing, $N_{rem} = 5$), (c) $T = 4.0$ (without remeshing), and (d) $T = 4.0$ (with remeshing, $N_{rem} = 5$).

Chapter 5

Verification Studies and Results

5.1 Introduction

Axisymmetrization and filamentation of elliptical vortices is a complicated process. Previously studies by Melander *et al*. (1987, 1988); Polvani *et al.* (1989); and Mariotti *et al.* (1994) have shown how this process is initiated. Basically, the root cause of this effect can be studied by examining the initial velocity field of an elliptical vortex in a frame of reference that is rotating with the average angular velocity of the flow. In this frame, the bulk of the fluid rotates in one direction; however, small parcels of fluid at the extremes of the major axis of the ellipse rotate in the other direction. This causes a fluid strain, as these parcels are stretched and elongated away from the core flow. The vortices eject filaments in amounts that depend on the initial conditions (vorticity distribution, aspect ratio of the vortex, etc.). The vortex breaks into filamentary structures when the strain field is strong enough and the filaments mix themselves within the ambient flow. In some literature this phenomenon is termed as "stripping" (Dritschel, 1989) and

is highly relevant to the dynamics of geophysical vortices, for example, the polar stratospheric vortex, blocking anticyclones and oceanic eddies (Dritschel, 1989).

The evolutions of single, unsteady vortices have been investigated in many studies by numerical simulations and much work has been done in the past decades. In this work, filamentation and axisymmerization of initially elliptical vortices are examined. A thorough study of this process using a VIC method does not seem to be present in the literature.

Before studying the evolution of a range of initially elliptical vorticity distributions, the current implementation is first verified to ensure its correctness. This verification comprises evolution prediction for a given vorticity field, a study of the effect of grid resolution, tests of the remeshing frequency, and a study of the effect of time-step size on the accuracy of the method are conducted. The method is also verified by comparing to results obtained using a new two-dimensional pseudo-spectral implementation and also with the numerical data of Melander, McWilliams and Zabusky (1986) and Koumoutsakos (1997).

Following this verification, the influence that the aspect ratio of initial vorticity distributions has on the evolution and eventual axisymmetrization of various vorticies is studied. Flow features to be considered are the development of the vorticity field, stream function, vorticity profile along the *x* and y axis during axisymmertization and effective aspect ratio. The complete numerical results of all computed simulations using the VIC and pseudo-spectral methods are tabulated in Table A2.1 which is provided in Appendix A2.

5.2 Convergence Study Results for the VIC Method

Extensive numerical work has been done on the convergence analysis of inviscid vortex methods. In theory, vortex methods are free from numerical dissipation errors for the vorticity of vortex particles. However, due to interpolation and remeshing schemes, they do introduce some numerical dissipation in practice. All problems in this study can be considered non-dimensional. The problem defined in Section 4.7 is solved with $a = 1.26$ and $b = 0.44$, the results for these cases are discussed in details in the next subsections.

5.2.1 The Effect of Grid Resolution

The sensitivity of the results to the grid size is tested by comparing results obtained on a series of meshes covering an initial box of dimensions [-3, 3] x [-3, 3]. The series of meshes used consists of (1) a 50x50 grid with grid size $\Delta x = \Delta y = 0.12$ and the number of vortex elements = 2500, (2) a 100x100 grid with grid size $\Delta x = \Delta y = 0.06$ and the number of vortex elements = 10,000, (3) a 200x200 grid with grid size $\Delta x = \Delta y = 0.03$ and the number of vortex elements = 40,000, (4) a 300x300 grid with grid size $\Delta x = \Delta y = 0.02$ and the number of vortex elements = 90,000, and (4) a 400x400 grid with grid size $\Delta x = \Delta y = 0.015$ and the number of vortex elements = 160,000. Results with $\Delta t = 0.1 \times \Delta x$ and the number of time steps between remeshing, $N_{rem} = 5$, are computed at non-dimensional time, T = 1.0, and are shown in Figure 5.1. It can be observed that increasing the grid refinement produces smoother and more refined vorticity contours. As maximum vorticity should be preserved, errors related to grid size may be directly observed in the non-conservation of the maximum vorticity, as shown in Figure 5.2. The errors obtained with different grids at time, T = 1.0, is also shown in Table 5.1. It can be noted that maximum vorticity

error decreases with increasing of number of grid points. In addition, the maximum vorticity error initially reduces quickly but for the last three meshes the error is less than one percent, therefore in this work, a grid of 200x200 cells is chosen as a good balance of accuracy and cost.

Table 5.1: Summary of errors for maximum vorticity for varying grid resolutions for cases shown in Figure 5.2.

Grid System	Time (T)	Exact ζ_{max}	ζ_{max}	% Error ζ_{max}
50x50	1.00	20.00	22.277	11.385
100x100	1.00	20.00	20.354	1.77
200x200	1.00	20.00	20.199	0.995
300x300	1.00	20.00	20.145	0.725
400x400	1.00	20.00	20.092	0.46

One could study the effect of changing the grid resolution and number of vortices independently. However, the logic to do this is not implemented in the present study. For example one could coarsen the grid while increasing the number of vortices and study the change in accuracy and computation time.

5.2.2 The Effect of Remeshing Frequency

In this simulation a remeshing (regridding) technique has been implemented in which, the set of particles is placed back to the centre of each grid cell within the computation every few time steps. This is done to avoid clustering of particles in one location. The vorticity of the new vortex elements is obtained by transferring the vorticity from the grid nodes to vortex elements using the $M_4^{'}$ interpolation scheme, which introduces some numerical dissipation. The effect of remeshing is tested by comparing the results obtained when using different number of time steps between

remeshing, N_{rem} = 5, 10, 15 and 25, for a computational domain covered by a 200x200 grid with grid size $\Delta x = \Delta y = 0.03$ and number of vortex elements, $N_V = 40{,}000$ vortices. Results with $\Delta t = 0.1 \times \Delta x = 3 \times 10^{-3}$ computed for time, T = 4.0, are shown in Figure 5.3. The error related to number of time steps between remeshing, N_{rem}, can be observed in the lack of conservation of the maximum vorticity as shown in Figure 5.4. These results are also tabulated in Table 5.2. It is also noticed that when number of time steps between remeshing is equal to 5 and 10, the result generates smoother vorticity contours, whereas when the number of time steps between remeshing is equal to 15 and 25, the result generates similar vorticity contours with much more noise. This is easily observed in Figure 5.3. Therefore, the results indicate that smaller number of time steps between remeshing produce less noise as compare to larger number of time steps between remeshing for the evolution of the initial elliptical vortex. Hence in this work, a number of time steps between remeshing, $N_{rem} = 5$, is chosen to obtain smooth, reliable results.

Table 5.2: Summary of errors for maximum vorticity for different number of time steps between remeshing for cases shown in Figure 5.3.

N_{rem}	Time (T)	Exact $\zeta_{\max}$	$\zeta_{\max}$	% Error $\zeta_{\max}$
5	4.00	20.00	20.195	0.975
10	4.00	20.00	20.206	1.03
15	4.00	20.00	20.322	1.61
25	4.00	20.00	20.484	2.42

5.2.3 The Effect of Time Step

A concise analysis of the effect of time-step size is presented here. As shown in Section 4.5, a second-order-accurate predictor-corrector time-marching method is used to integrate vortex particle positions. For this study, time steps 3.0×10^{-3}, 4.5×10^{-3}, 6.0×10^{-3}, 12.0×10^{-3} and 16.5×10^{-3} are tested by comparing the results obtained using a computational domain comprising 200x200 cells and number of time steps between remeshing, N_{rem} = 5. Results are shown at time, T = 4.0, in Figure 5.5. The relationship between errors in conservation of maximum vorticity as a function of the time step is shown in Figure 5.6. These results are also tabulated in Table 5.3. It can be noted that for $\Delta t = 16.50\times10^{-3}$ the maximum vorticity error at time, T = 4.0 is small as compare to others Δt results. However, it generates more noise in the flow, as observed in Figure 5.5.

Table 5.3: Summary of errors for maximum vorticity for different time steps for cases shown in Figure 5.6.

Δt (10^{-3})	Time *(T)*	Exact ζ_{max}	ζ_{max}	% Error ζ_{max}
3.00	4.00	20.00	20.195	0.975
4.50	4.00	20.00	20.160	0.8
6.00	4.00	20.00	20.106	0.53
12.00	4.00	20.00	20.055	0.275
16.50	4.00	20.00	19.984	-0.08

Examination of the numerical experiments presented in this section permits the following observation. From the calculations presented in Table 5.3, $\Delta t = 16.50\times10^{-3}$ seems best, however, Figure 5.5 shows that this time step generates more noise and oscillation in the flow.

This effect is probably caused by the increase in the time between remeshing, which happens every five timesteps. Hence, results from Figure 5.5, indicate that a choice of $\Delta t = 3\times10^{-3}$ is best and still maintains a maximum vorticity error that is less than 1%. This time step did indeed give good results in the case shown in Figure 5.6.

5.3 Convergence-Study Results for Pseudo-Spectral Method

With the parameters necessary to obtain reliable solutions with the VIC method known, a comparison with results from a pseudo-spectral method is undertaken to further verify the implementation. In this section, a convergence study of the pseudo-spectral code is undertaken before a direct comparison with VIC results is made.

5.3.1 The Effect of Number of Fourier Modes

The sensitivity of the results to the grid size is tested by comparing results obtained using a matrix of: (1) 50x50 modes with grid sizes $\Delta x = \Delta y = 0.12$, (2) 80x80 modes with grid sizes $\Delta x = \Delta y = 0.075$, (3) 100x100 modes with grid sizes $\Delta x = \Delta y = 0.06$, (4) 120x120 modes with grid sizes $\Delta x = \Delta y = 0.05$, (5) 150x150 mode with grid sizes $\Delta x = \Delta y = 0.04$, (6) 180x180 modes with grid sizes $\Delta x = \Delta y = 0.033$, (7) 200x200 modes with grid sizes $\Delta x = \Delta y = 0.03$ and (8) 220x220 modes with grid sizes $\Delta x = \Delta y = 0.027$. Results at time, $T = 1.0$, computed with $\Delta t = 0.1\times\Delta x$ are shown in Figure 5.7. It can be observed that increasing the number of modes produces smoother vorticity contours. Significant changes in the solution cease to be apparent in the four most refined results. Due to the efficiency of the pseudo-spectral method, parameters from the most refined simulation with 220x220 modes with grid sizes $\Delta x = \Delta y = 0.03$ and $\Delta t = 0.1\times\Delta x = 2.7\times10^{-3}$ are used for the VIC verification.

5.4 Comparison between VIC and Pseudo-Spectral Method

On the basis of above convergence study for both methods, one can now directly compare the results of the evolution of initially elliptical vorticity contours. For the VIC method, a number of time steps between remeshing, $N_{rem} = 5$, grid = 200x200 cells and $\Delta t = 3\times10^{-3}$, was used. For the pseudo-spectral method, 220x220 modes and $\Delta t = 2.7\times10^{-3}$ are used. Results are obtained at time, T = 0.0, 0.50, 1.0, 1.50, 2.0, 4.0, are shown in Figure 5.8. It can be observed that the results from both methods show good agreement and produce smooth vorticity contours for all time. When time is equal to 4.0, discrepancies begin to become apparent because the VIC method has slightly more dissipation error. However, the overall structure of the vortex remains the same for both methods.The errors in the conservation of maximum vorticity obtained with the different methods are shown in Table 5.4. As can be seen, the error in the maximum vorticity predicted by the VIC method remains near 1% through the whole computation.

This comparison gives further confidence that both the VIC method and pseudo-spectral method are implemented correctly and that the parameters chosen for the VIC method given acceptable results and is appropriate for the studies to follows.

Table 5.4: Summary of errors for maximum vorticity for VIC and Pseudo-Spectral methods as shown in Figure 5.8.

Time *(T)*	Exact ζ_{max}	ζ_{max} (VIC)	% Error ζ_{max} (VIC)	ζ_{max} (PS)	% Error ζ_{max} (PS)
0.0	20.00	20.003	0.015	20.000	0.00
0.50	20.00	20.258	1.29	20.008	0.04
1.00	20.00	20.199	0.995	20.013	0.065
1.50	20.00	20.165	0.825	20.019	0.095
2.00	20.00	20.163	0.815	20.018	0.09
4.00	20.00	20.195	0.975	20.029	0.145

5.5 Comparison between VIC and Other Numerical Results

The above two methods, used in this chapter, were able to produce good results and make very similar predictions for the evolution of the vorticity fields of an initially elliptical vortex in two-dimensions, incompressible, inviscid flow. A comparison between the present simulation results using VIC method and the results obtained from Koumoutsakos (1997) and Melander, McWilliams and Zabusky (1986) will be presented here. The comparison focuses on the results in relation to vorticity contours and the vorticity profile along the *x* and *y* axis for an elliptical vortex with an aspect ratio = 2.0 (*a=1.0* and *b=0.5*).

5.5.1 Comparison of Vorticity Contours

In Figure 5.9 and Figure 5.10, a contour of the vorticity field of a two-dimensional initially elliptical vortex is presented for different times. Figure 5.9 shows results of the calculation performed with the present vortex-in-cell method side-by-side to results obtained from

Koumoutsakos (1997), who used a high resolution vortex method. The same comparison is made to the simulation results of Melander, McWilliams and Zabusky (1986) in Figure 5.10. In this case a pseudo-spectral method was used for the same problem. One can see that the present method is in good agreement with the results of Koumoutsakos and Melander, McWilliams and Zabusky, in terms of the rotation angle of the structure and shape of vorticity contours. The vorticity decay in Figure 5.9 and 5.10 is qualitatively similar to the simulations of both studies, although there are slight differences. The difference in the results of the present simulation from those of Koumoutsakos (1997) and MMZ (1986) is probably due to the fact that initially using one vortex particle per grid cell is not enough and may be a source of excess numerical dissipation in the present calculations.

5.5.2 Comparison of Vorticity Profile along the *x* and *y* Axis

The vorticity profile along the *x* and *y* axis for the initially elliptical vortex are shown in Figure 5.11 using the present implementation with the fixed parameters determined above as compared with the simulation results of Koumoutsakos (1997), who used a high-resolution vortex method. The vorticity profile along *x* and *y* axis in Figure 5.11 shows that there is a slight difference in the bumps structure between the present simulation results and the numerical results of Koumoutsakos. However, there is very good agreement regarding the rate of axisymmetrization. The difference between the present simulation results and the results of Koumoutsakos may be due to the fact that remeshing is performed more often in the present calculations. Remeshing smoothes and stabilizes the calculation, however, it introduces numerical dissipation and may be the cause of the discrepancies.

5.6 Study of Different Aspect Ratio Results Using a VIC Method

In this section, the VIC method is applied to the study of vortices that are similar to those defined in Section 4.7, but with different aspect ratios. This is done to study the effect of initial aspect ratio on vortex evolution, which helps us to gain insight into the behaviour of vortical structures in general. Presently, the vortex-in-cell method with grid of 200x200, a number of time steps between remeshing, $N_{rem} = 5$, and $\Delta t = 3\times10^{-3}$, has been used to compute the evolution of several initially elliptical vortex profiles in two-dimensions. Results for these situations are computed to understand the effect of initial vortex shape on the process of filamentation and axisymmertization. Calculations were performed for initial aspect ratios of $\lambda = 1.416$ (a=1.26, b=0.89), 2.00 (a=1.26, b=0.63), 2.86 (a=1.26, b=0.44) and 4.06 (a=1.26, b=0.31) within a computational domain of [-3, 3] x [-3, 3]. From Figure 5.12 to Figure 5.15, one can observe that, in all cases, as the vortex structure rotates in the anti-clockwise direction, the spiral arms are ejected from the main structure and eventually reapproach, reattach, and merge with the main core as the vorticity aspect ratio reduces. Remaining filaments become narrow and are stretched such that the remaining vorticity dissipates towards zero. It is also noticed that, when the initial aspect ratio is increased the lengths of vortical arms that are ejected from the main structure also increase significantly. In addition, the decay time of an initially elliptical vortex profile increases with increasing initial aspect ratio. In the later stages of axisymmetrization, the vortical structure shows the vorticity is concentrated in a slightly elliptically deformed core of decreasing aspect ratio, while two vortical arms remain as a rotating object around the main core and both stretch and dissipate.

The evolution of an initially elliptical vortex for different initial aspect ratios reveals more clearly how the vorticity of the main core is quickly sheared, producing spiral arms and that this effect becomes more pronounced as the aspect ratio increases. These arms merge towards the core of the vortex and the overall vorticity aspect ratio slowly decays. As the structure begins to reach a steady state, the spiral arms mix and diffuse, leaving most of the vorticity concentrated in the core. In Figure 5.16 to Figure 5.19, the vorticity profile along the two axes is shown for all cases. One can observe the phenomena of spiral arms as bumps of decreasing amplitude in the profile along the edge of the core.

A non-monotonic vorticity profile can be observed for all aspect ratios along a location $x = 0$ at time, T = 1.0 as shown in Figure 5.16 to Figure 5.19. At time, T = 1.5, for all aspect ratios, one can observe the vortical waves on the surface of the vortex core caused by spiral arms. At the same time, on the vorticity profile along the two axes, shown in Figure 5.16 to Figure 5.19, one can notice the development of filaments by the formation of small parcels of vorticity on the axes. These parcels move outward from the core, while the core itself reduces in size and becomes axisymmetric. The aspect ratio of the main core quickly decreases from time, T = 2.0, to time, T = 4.0, as the vortical arms get wrapped around the main vortex core. Consequently, a reduction of the ellipticity is observed as the filaments eject from the main core.

In Figure 5.12 one can observe that the length of the filaments ejected from the main core are smaller due to the smaller initial aspect ratio of this case and vortical arms do not fully set wrapped around the main vortex core. In Figure 5.13 one can observe the length of the filament ejected from the main core is larger than the length of filament ejected for the lower aspect ratio case. The simulation shows at time, T = 4, the vorticity field is fully axisymmetrized and no further significant evolution of the elliptical vortex is expected. The vorticity profiles along the

axes for this aspect ratio are presented in Figure 5.17, and shows a smooth axisymmetric profile corresponding to the vorticity core. When the aspect ratio is equal to 4.06 the vorticity contours are shown in Figure 5.15. It is noticed that the length of the filament ejected from the main core are again much larger. The vortical arms get wrapped completely around the main vortex core, resulting in the thinning of the core-filament link and weak vorticity away from the core. Thus, resulting in axisymmetrization of the vortical structure, though this now takes place at a later time. Therefore, it can be concluded that initially elliptical vortex profiles will become axisymmetrized at different times for different aspect ratios. In addition, the filaments ejected from the main core have different length, which also depends upon the initial aspect ratio of the elliptical vortex profile.

The stream functions of an initially elliptical vortex evolution for different aspect ratio computed on the grid nodes are shown in Figure 5.20 to Figure 5.23. It can be noticed that the contours of stream functions are very similar for different times for each aspect ratio, which means the stream function of the problem does not change significantly during a computation.

5.6.1 Evolution of Effective Aspect Ratio

In an effort to quantify the rate of axisymmertrization of vortices of different initial aspect ratios, an effective aspect ratio, λ_{eff}, can be defined, as shown by Dritschel (1989). This parameter can be used as a measure of the aspect ratio of profiles that possess a largely elliptical shape, but are not strictly ellipses. This parameter is a function of vorticity moments, defined as

$$J_{mn} = \iint \vec{\zeta}(x,y) x^m y^n dx\ dy. \qquad (5.1)$$

During the post-processing of the previous results, the moments J_{11}, J_{02}, J_{20} are computed through numerical integration, using the grid nodes as quadrature points. Dritschel (1989) defines the effective aspect ratio for the vortical structures through the relation

$$\lambda_{eff}^2 = \frac{J+R}{J-R}, \tag{5.2}$$

where $R^2 = D^2 + 4J_{11}^2$, $D = J_{20} - J_{02}$ and $J = J_{20} + J_{02}$. This function will agree with the actual aspect ratio for the elliptical profile and gives a measure of the aspect ratio of general profiles.

The evolution of the effective aspect ratio computed for the vortices of different initial aspect ratios presented in Section 5.6 are shown in Figure 5.24. This figure shows that the effective aspect ratio of the various vortices decay towards a value of one very quickly. In fact, the decay rate for each situation seems to be roughly equal, with all vortices having an effective aspect ratio of nearly one at T = 1. This is contrast with the analysis of the previous section, when it was argued that vortices with larger initial aspect ratios become symmetric on longer time scales. This is because the effective aspect ratio used here does not effectively detect the long filaments in the vorticity distributions as structures that are not axisymmetric. This points to the difficulty of quantifying the degree of axial symmetry in a given profile. One must really examine the evolution of the vorticity profile carefully to make a judgement on the rate of axisymmertrization.

.

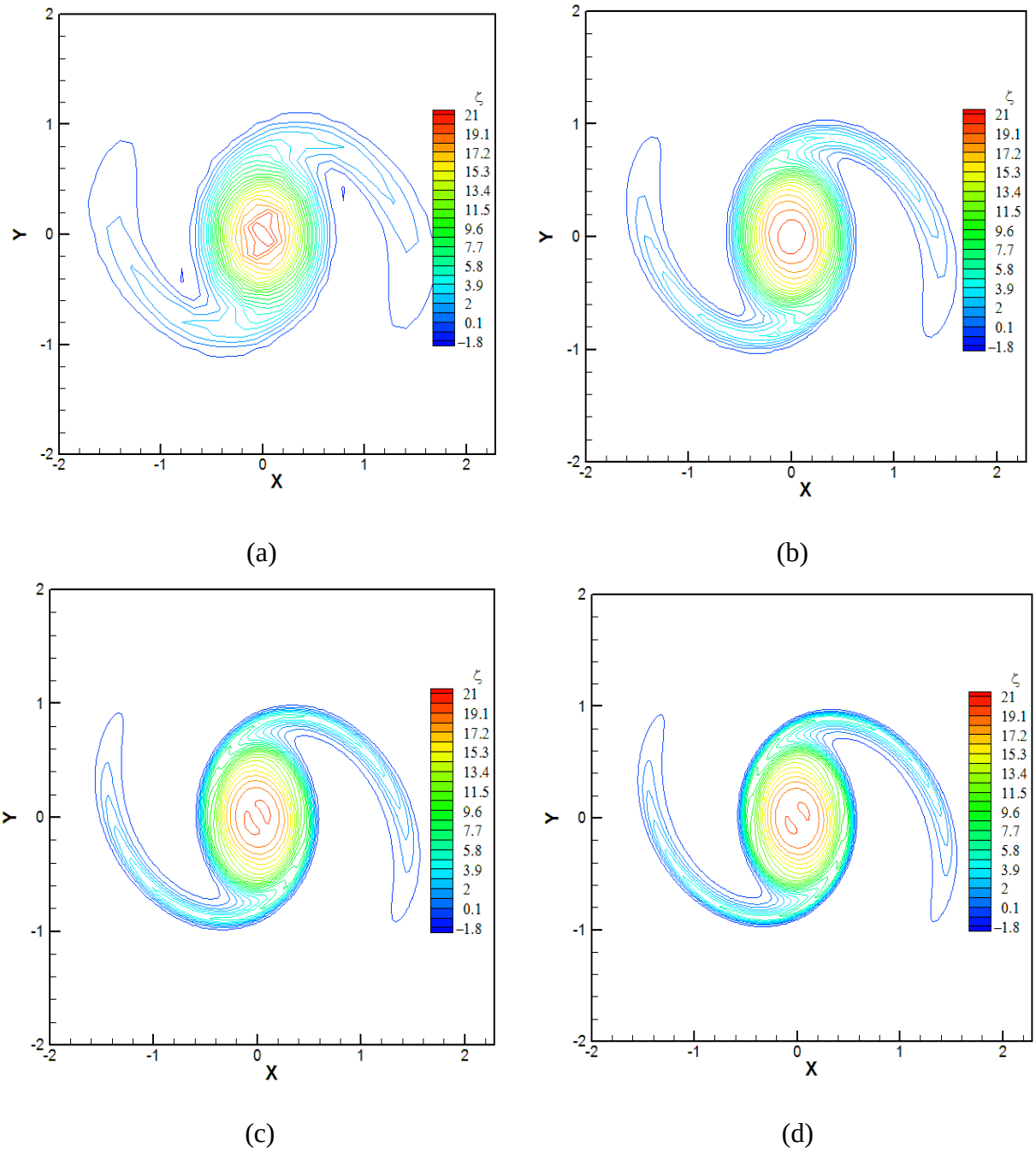

Figure 5.1 Vorticity contours for the evolution of an initially elliptical vortex with aspect ratio = 2.86, at varying grid resolutions (a) 50x50, $\Delta x = \Delta y = 0.12$, $\Delta t = 12.0 \times 10^{-3}$, (b) 100x100, $\Delta x = \Delta y = 0.06$, $\Delta t = 6.0 \times 10^{-3}$, (c) 200x200, $\Delta x = \Delta y = 0.03$, $\Delta t = 3.0 \times 10^{-3}$, (d) 300x300, $\Delta x = \Delta y = 0.02$, $\Delta t = 2.0 \times 10^{-3}$, and (e) 400x400, $\Delta x = \Delta y = 0.015$, $\Delta t = 1.5 \times 10^{-3}$, remeshing frequency, $N_{rem} = 5$. Solutions at time, $T = 1.0$ using VIC method.

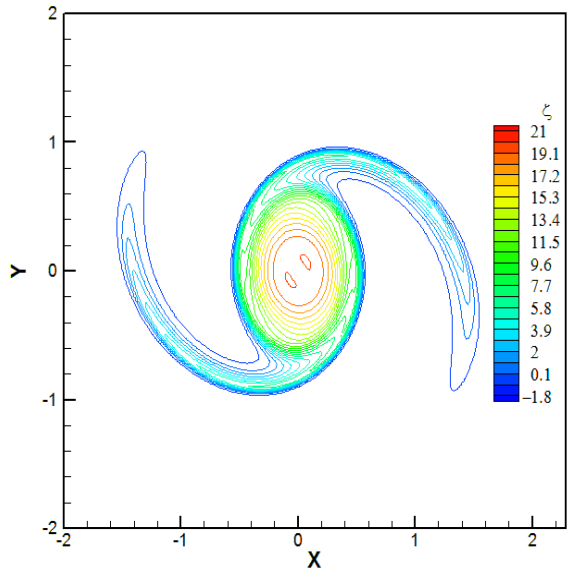

(e)

Figure 5.1- Continued

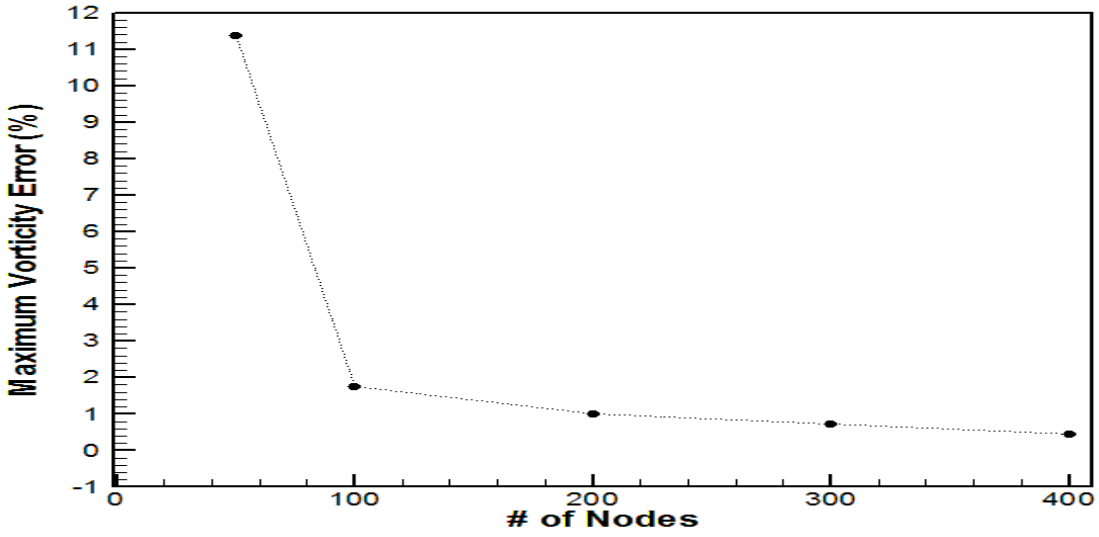

Figure 5.2 Relative errors in the conservation of maximum vorticity for cases illustrated in Figure 5.1.

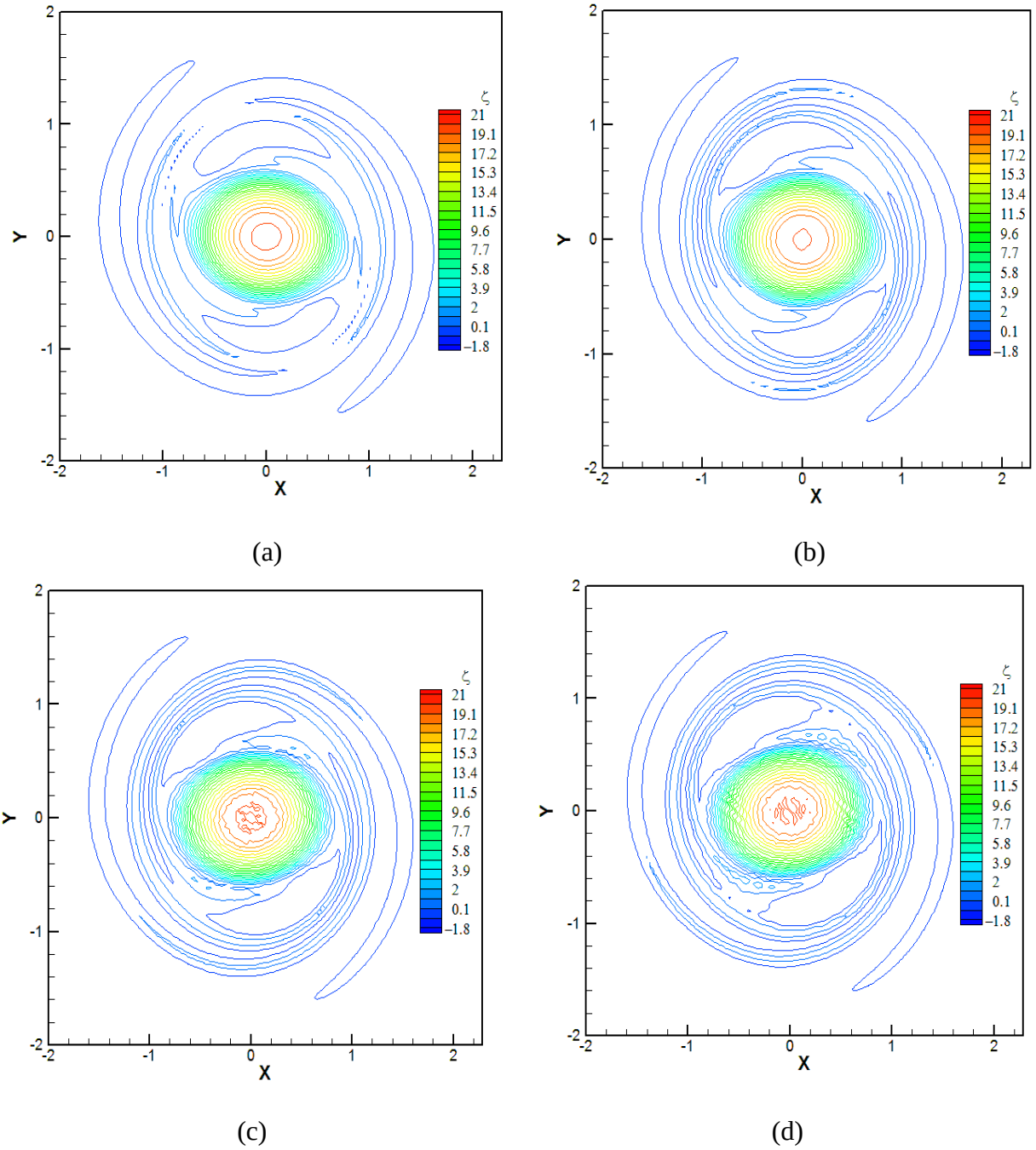

Figure 5.3 Vorticity contours for the evolution of an initially elliptical vortex with aspect ratio = 2.86, for varying remeshing frequency, N_{rem} (a) 5, (b) 10, (c) 15, (d) 25. All results computed with 200x200 grid, $\Delta x = \Delta y = 0.03$, $\Delta t = 3.0 \times 10^{-3}$, at time, $T = 4.0$ using VIC method.

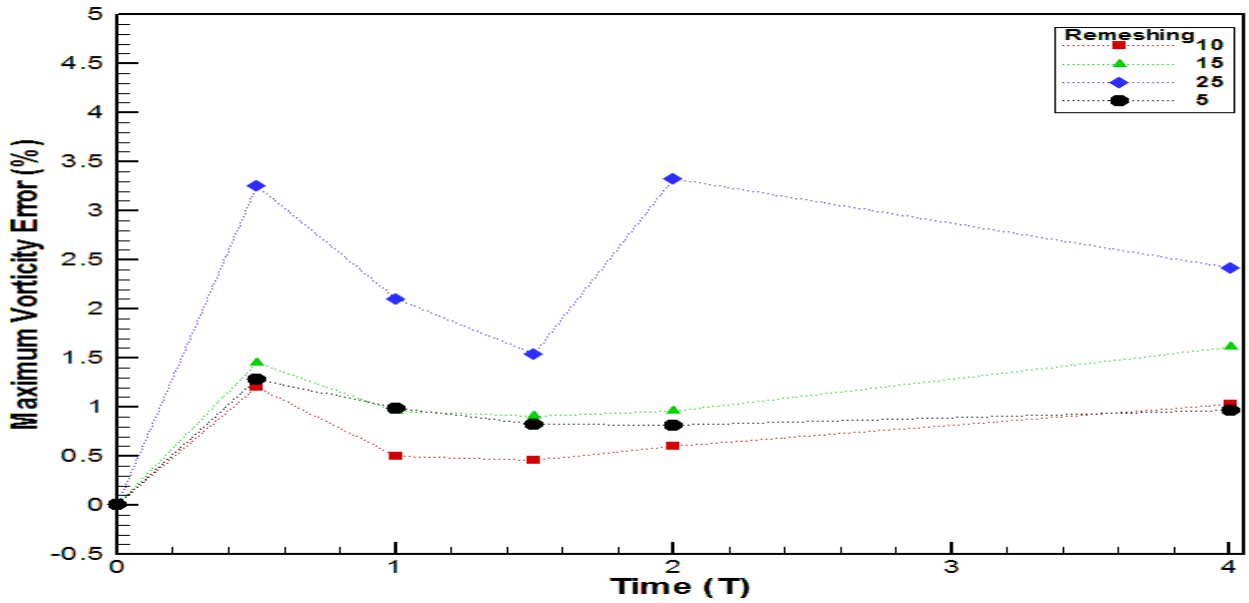

Figure 5.4 Relative errors in the conservation of maximum vorticity for different remeshing frequencies, shown in Figure 5.3, 200x200 grid, $\Delta x = \Delta y = 0.03$, $\Delta t = 3.0 \times 10^{-3}$, at times, $T = 0.5,\ 1.0,\ 1.5,\ 2.0$ and 4.0 using VIC method.

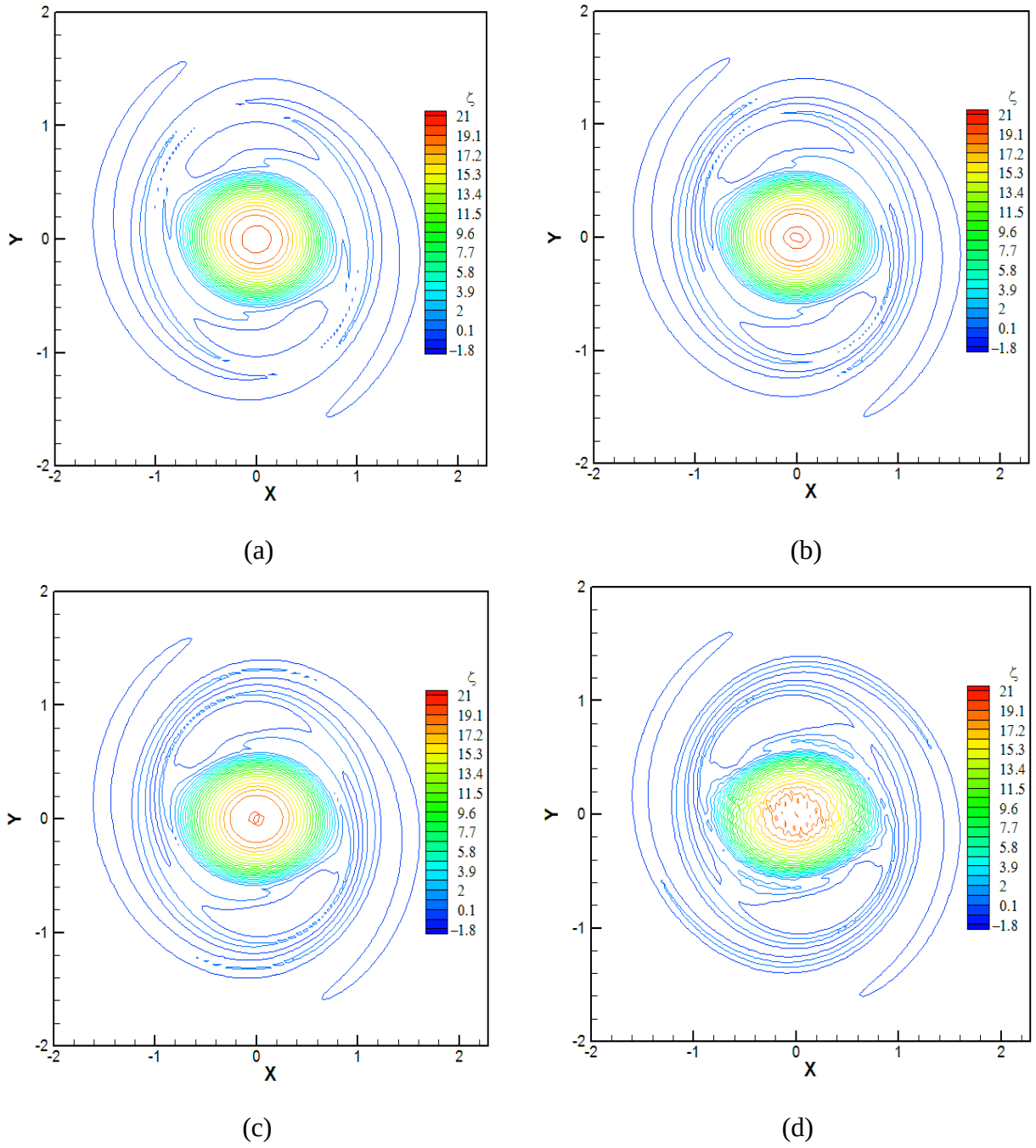

Figure 5.5 Vorticity contours for the evolution of an initially elliptical vortex with aspect ratio = 2.86, varying Δt, (a) 3.0×10^{-3}, (b) 4.5×10^{-3}, (c) 6.0×10^{-3}, (d) 12.0×10^{-3} and (e) 16.5×10^{-3}, for 200x200 grid, $\Delta x = \Delta y = 0.03$, remeshing frequency, $N_{rem} = 5$ at time, $T = 4.0$ using VIC method.

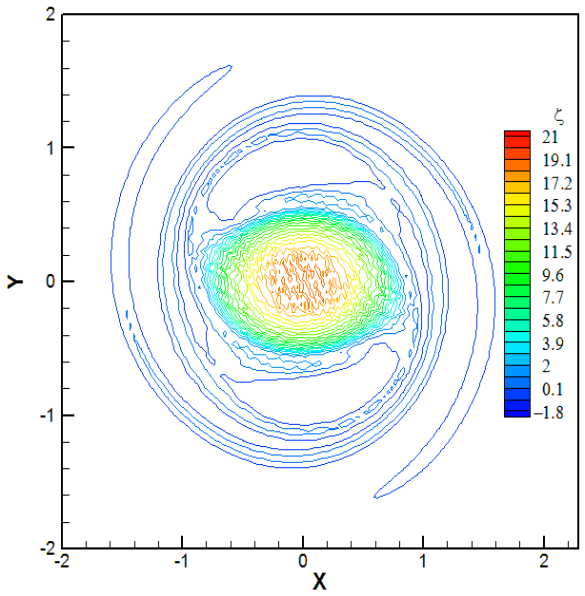

(e)

Figure 5.5 – Continued

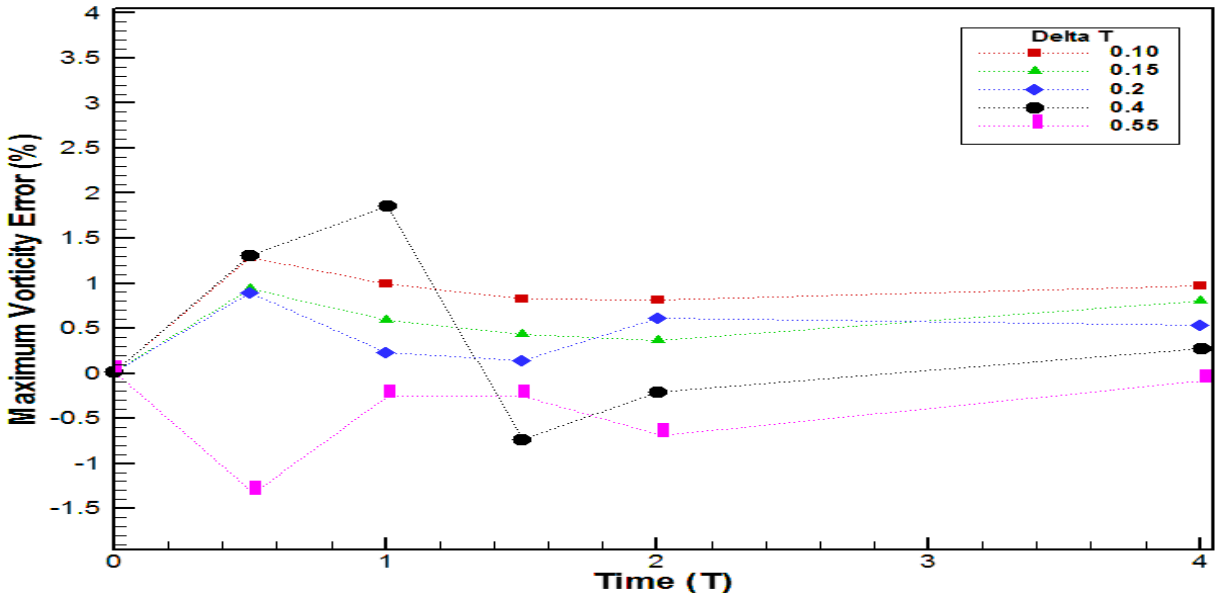

Figure 5.6 Relative errors in the conservation of maximum vorticity for varying Δt, as shown in Figure 5.5, for 200x200 grid, remeshing frequency, $N_{rem} = 5$ at time, $T = 0.5,\ 1.0,\ 1.5,\ 2.0$ *and* 4.0 using VIC method.

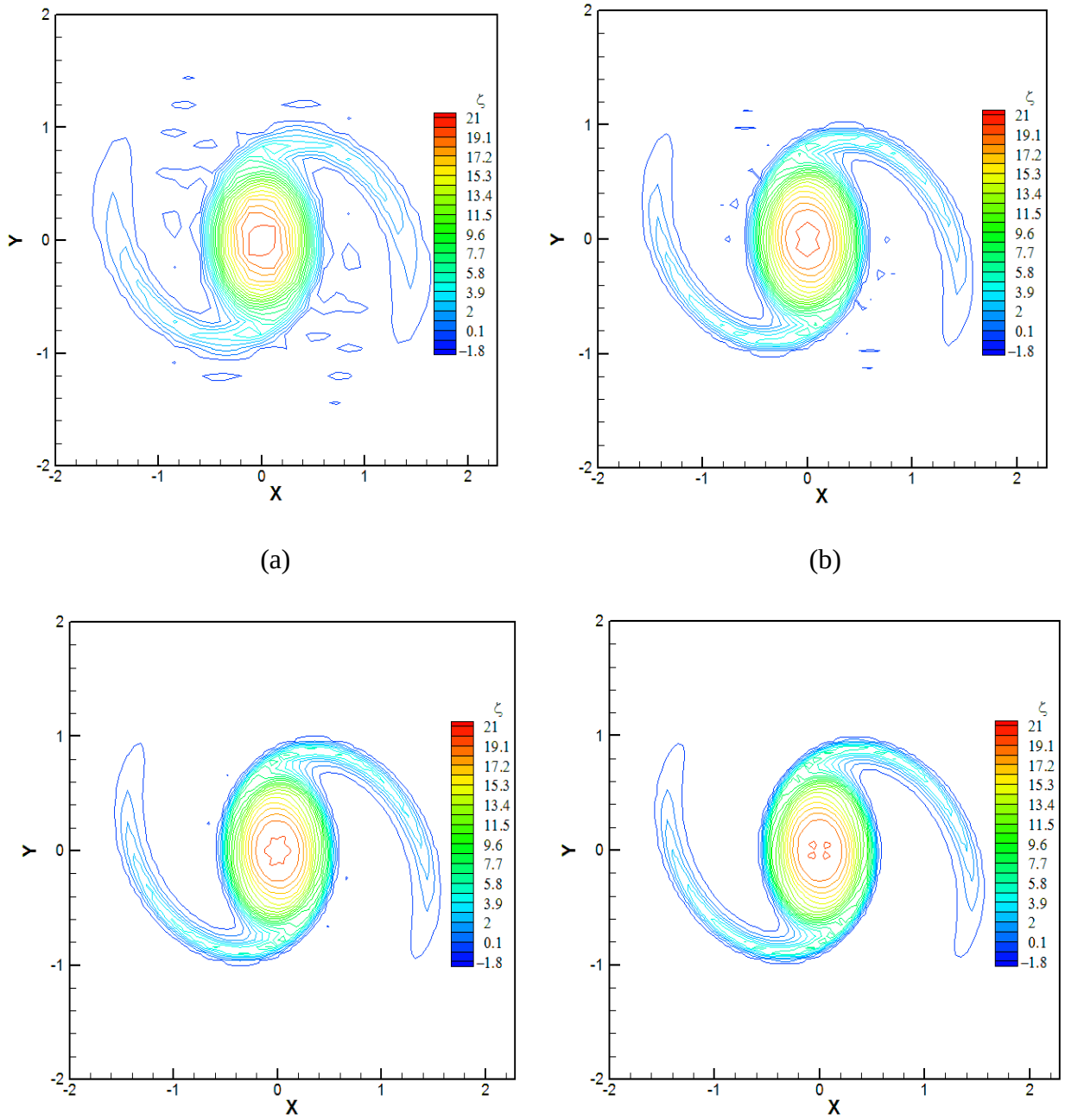

Figure 5.7 Vorticity contours for the evolution of an initially elliptical vortex with aspect ratio = 2.86 varying the number of modes in the spectral solution (a)50x50 modes, (b) 80x80 modes, (c)100x100 modes, (d)120x120 modes, (e)150x150 modes, (f)180x180 modes, (g)200x200 modes and (h)220x220 modes at time, T = 1.0 using pseudo-spectral method.

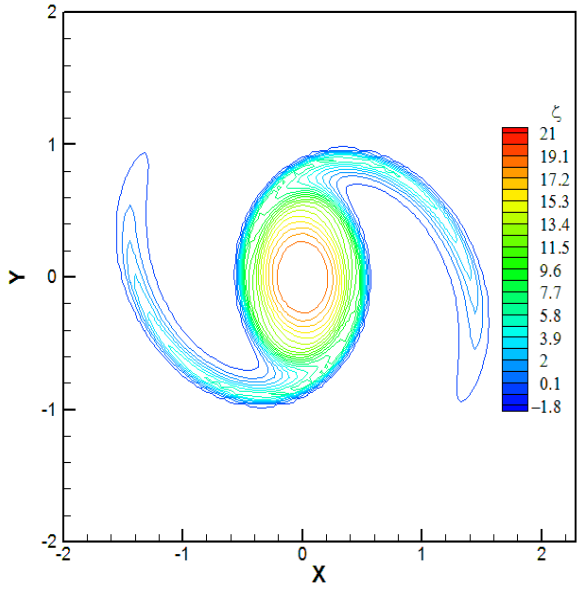

(e)

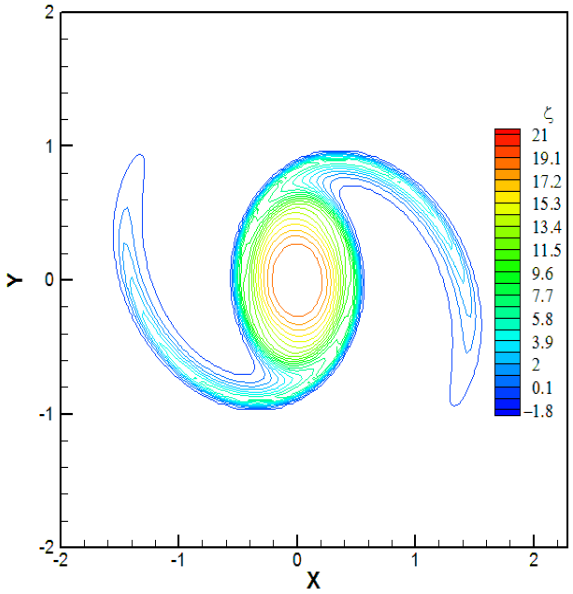

(f)

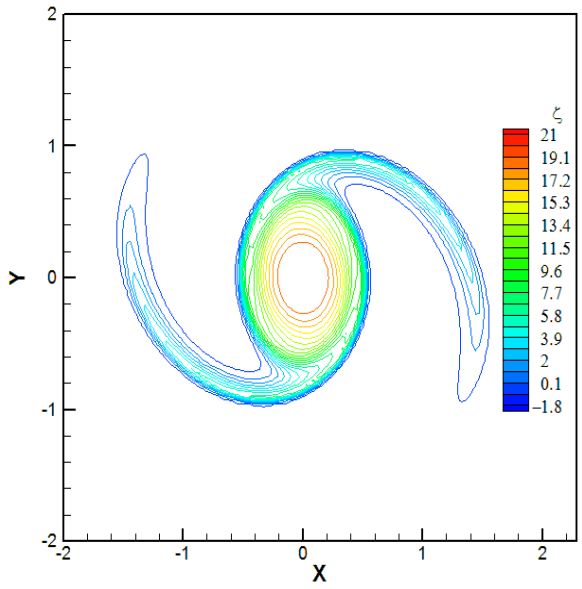

(g)

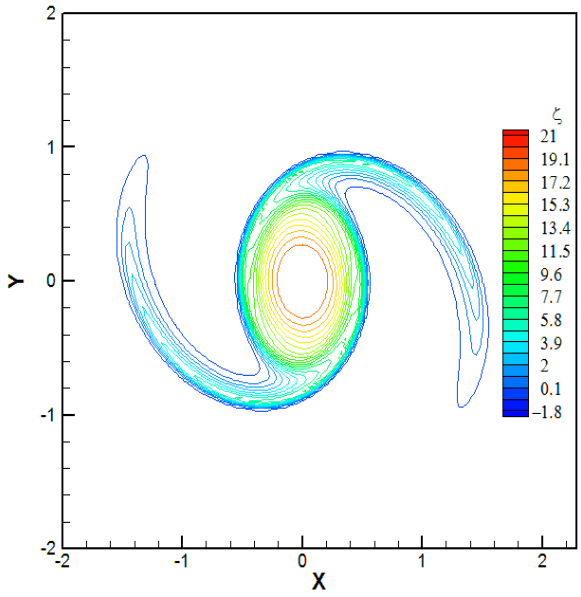

(h)

Figure 5.7- Continued

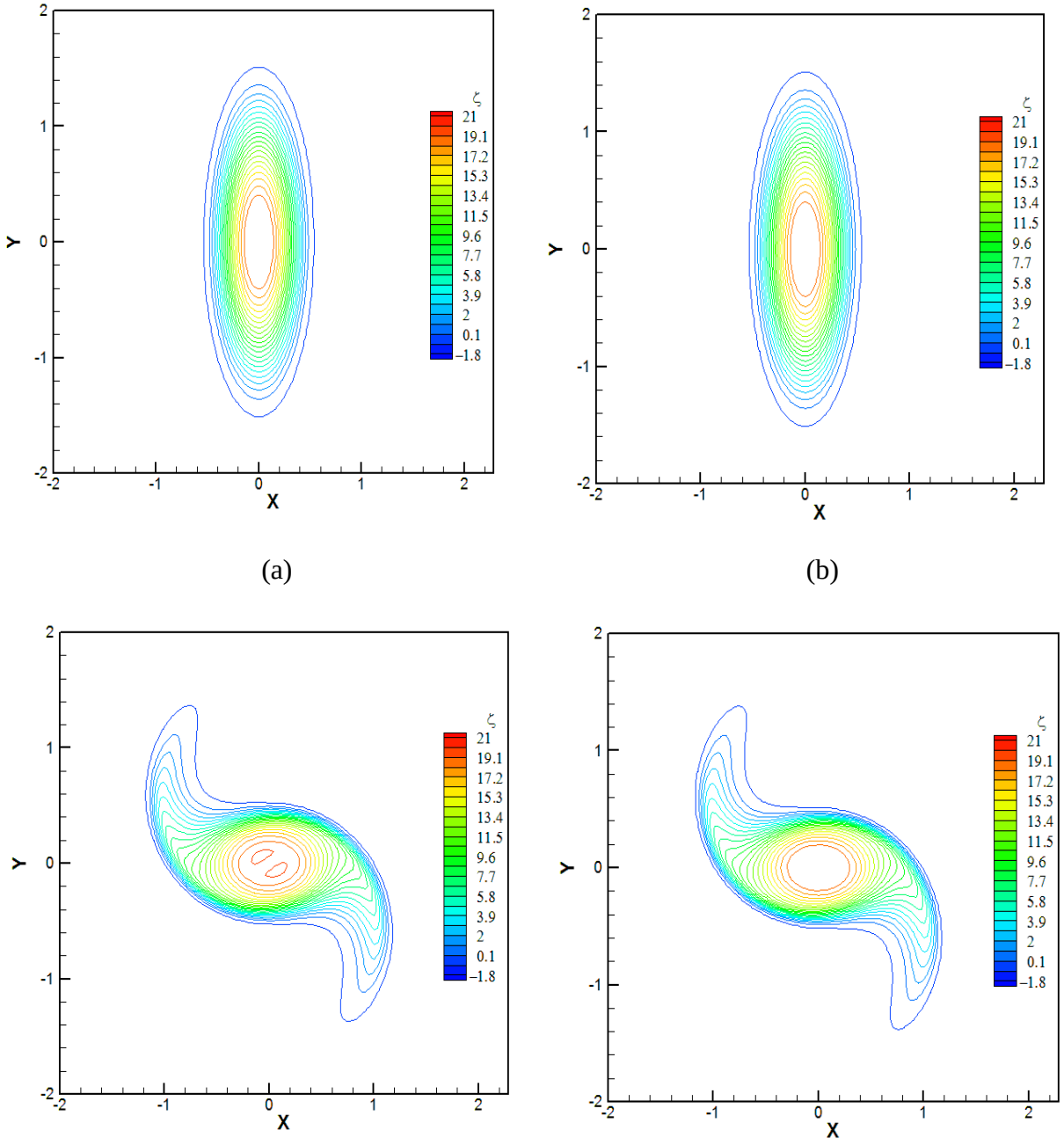

Figure 5.8 Comparison of vorticity contours for the evolution of an initially elliptical vortex with aspect ratio = 2.86, remeshing frequency, N_{rem}, 200x200 grid, $\Delta x = \Delta y = 0.03$ with $\Delta t = 3.0 \times 10^{-3}$, using VIC method (left) and with modes = 200x200 using Pseudo-Spectral method (right) at times, (a)-(b) T = 0.0, (c)-(d) T = 0.5, (e)-(f) T = 1.0, (g)-(h) T = 1.5, (i)-(j) T = 2.0 (k)-(l) T = 4.0.

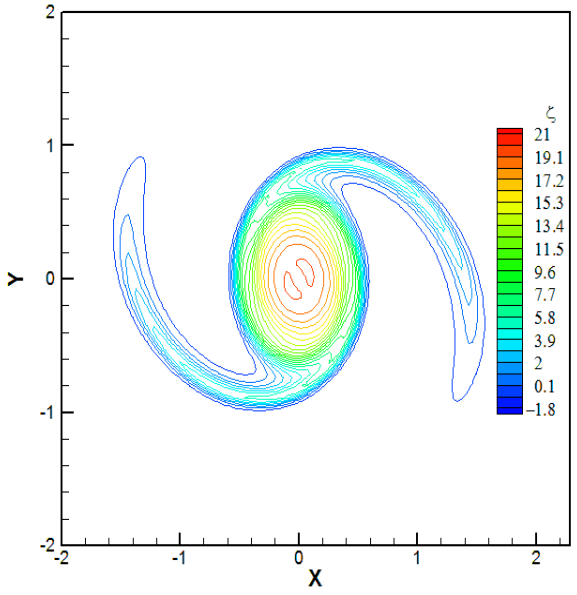

(e)

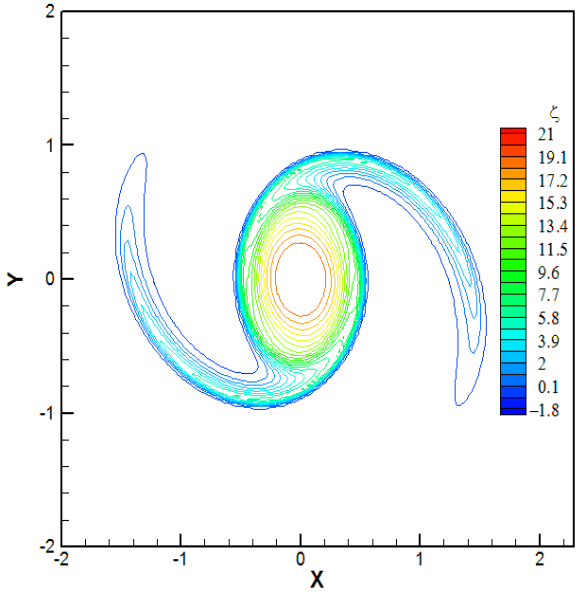

(f)

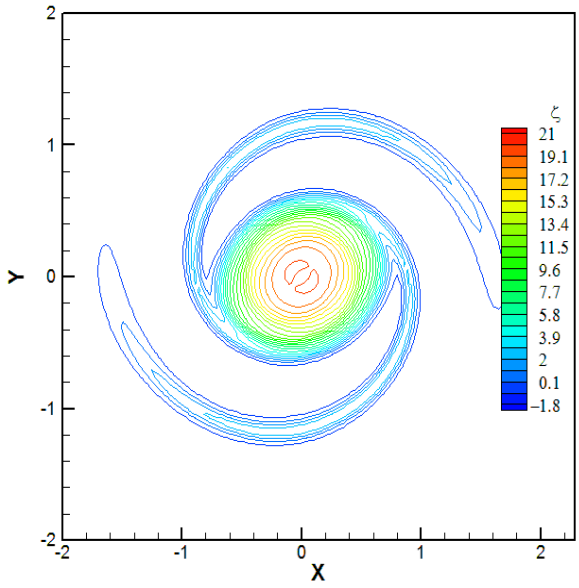

(g)

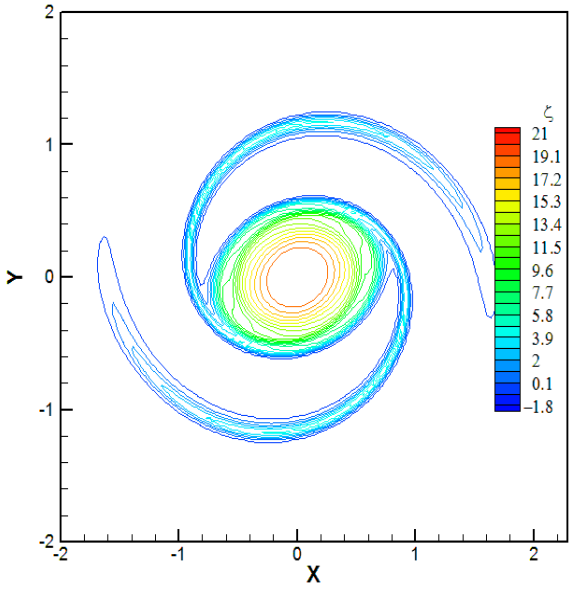

(h)

Figure 5.8- Continued

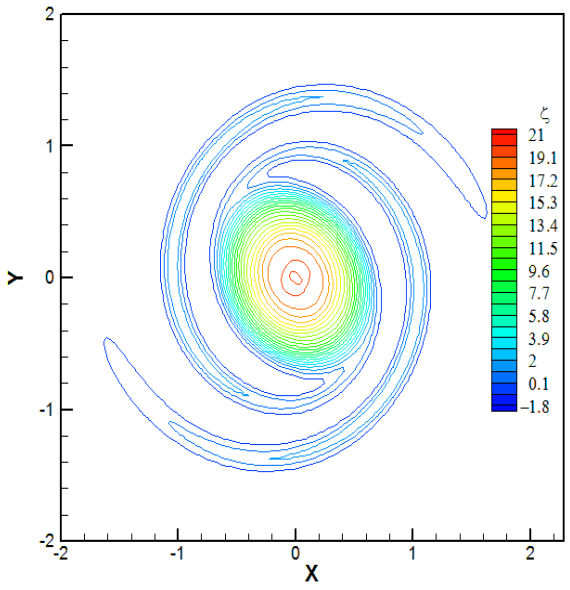

(i)

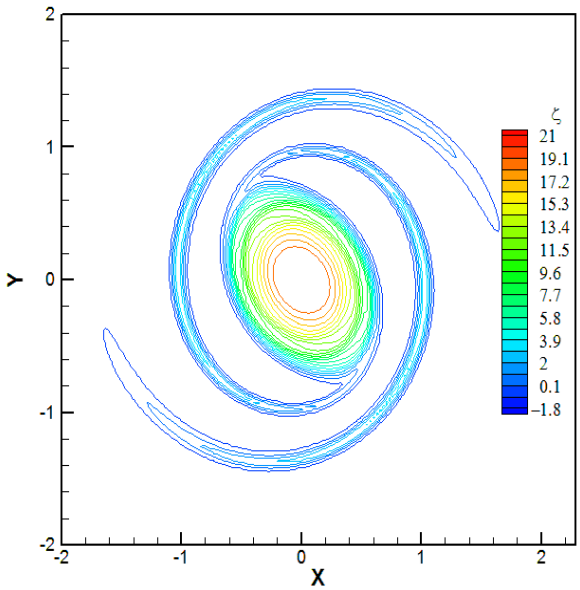

(j)

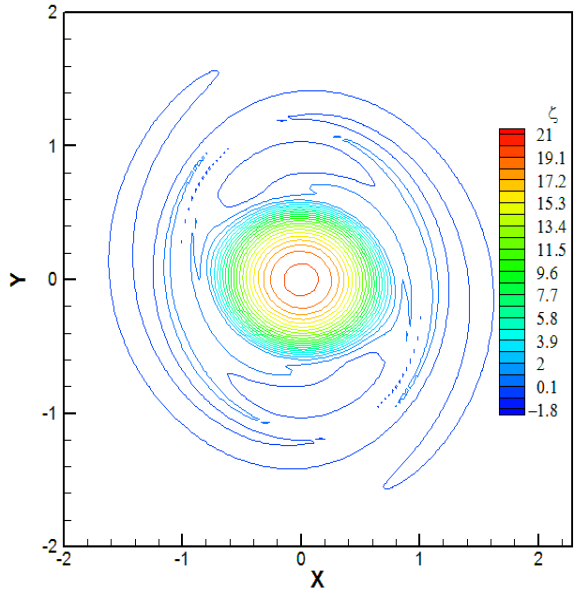

(k)

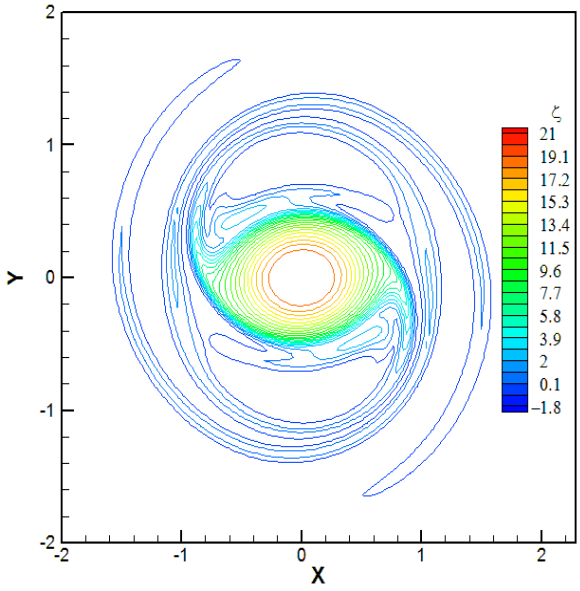

(l)

Figure 5.8- Continued

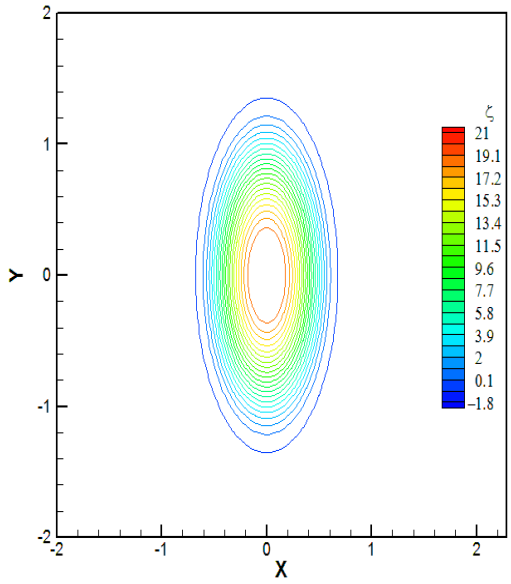

(a)

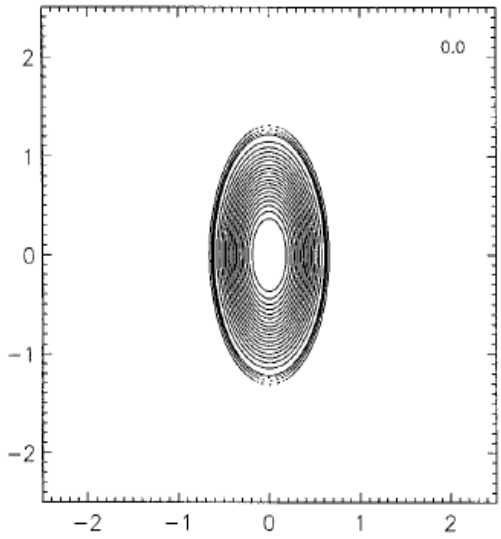

(b)

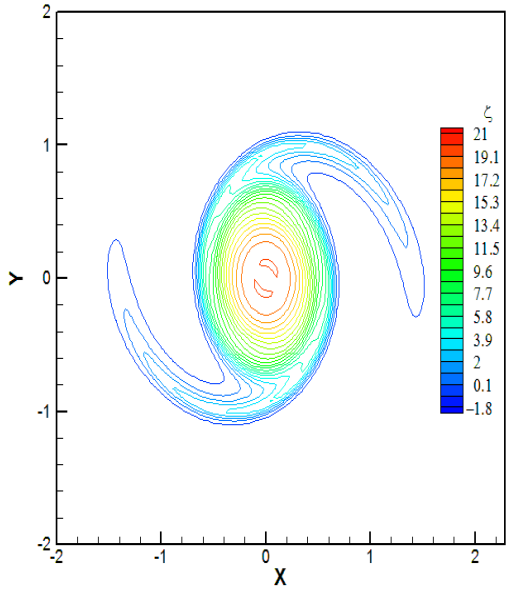

(c)

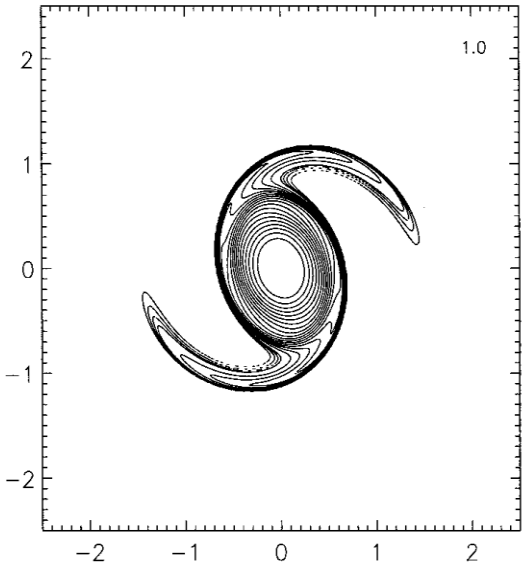

(d)

Figure 5.9 Comparison of vorticity contours for the evolution of an initially elliptical vortex with aspect ratio = 2.00, remeshing, $N_{rem} = 5$, 200x200 grid, $\Delta x = \Delta y = 0.03$ and $\Delta t = 3.0 \times 10^{-3}$ (left) with the results of Koumoutsakos (1997) (right) at times, (a)-(b) T = 0.0, (c)-(d) T = 1.0, (e)-(f) T = 1.5, (g)-(h) T = 4.0.

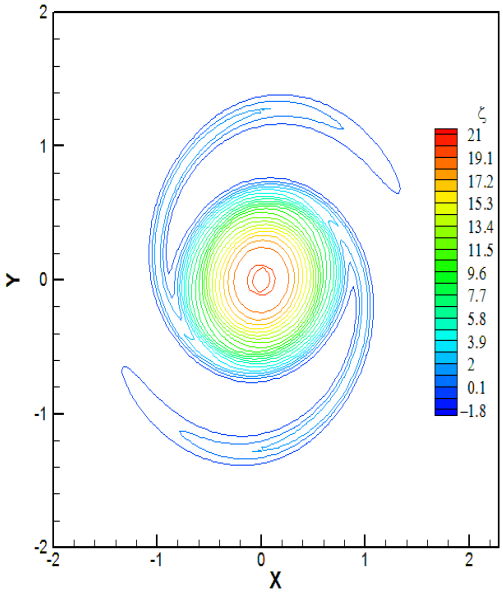

(e)

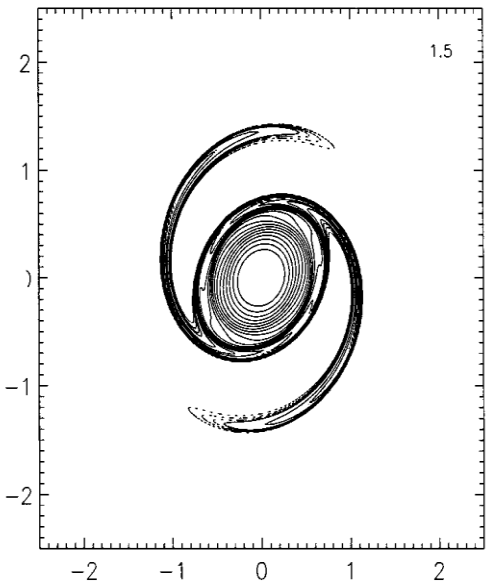

(f)

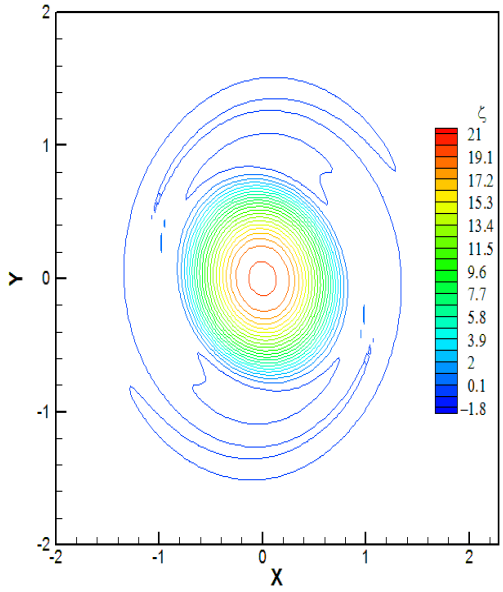

(g)

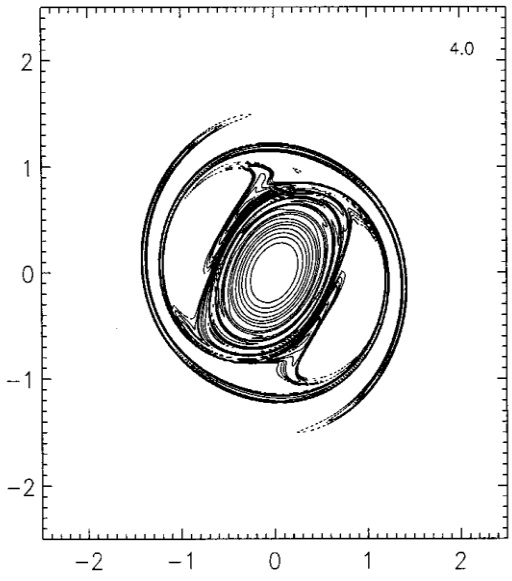

(h)

Figure 5.9- Continued

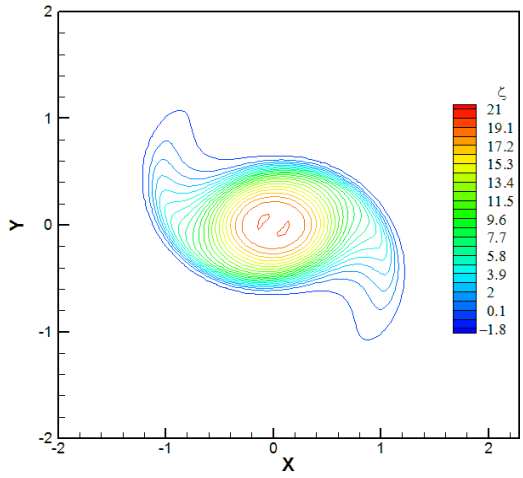

(a)

(b)

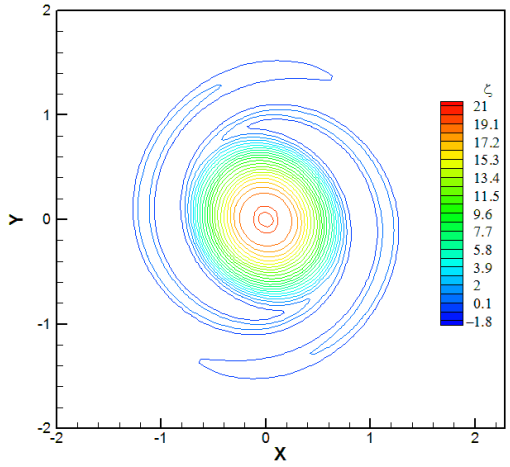

(c)

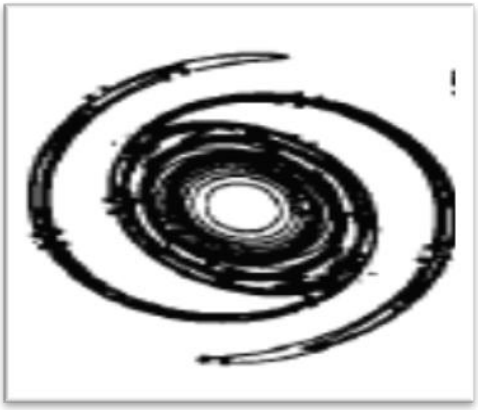

(d)

Figure 5.10 Comparison of vorticity contours for the evolution of an initially elliptical vortex with aspect ratio = 2.00, remeshing frequency, $N_{rem} = 5$, 200x200 grid, $\Delta x = \Delta y = 0.03$ and $\Delta t = 3.0 \times 10^{-3}$ (left) with the results of Melander, McWilliams and Zabusky (1986) (right) at times, (a)-(b) T = 0.5, (c)-(d) T = 2.0, (e)-(f) T = 4.0.

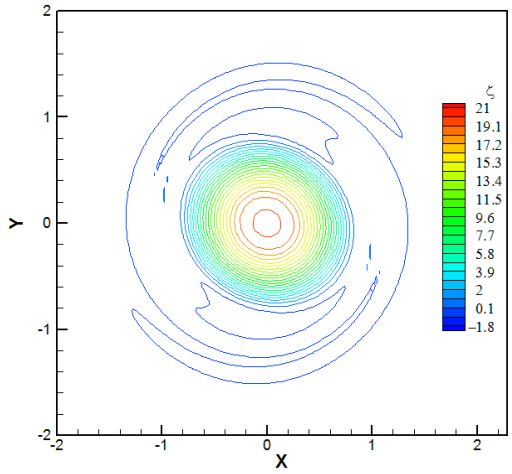

(e)

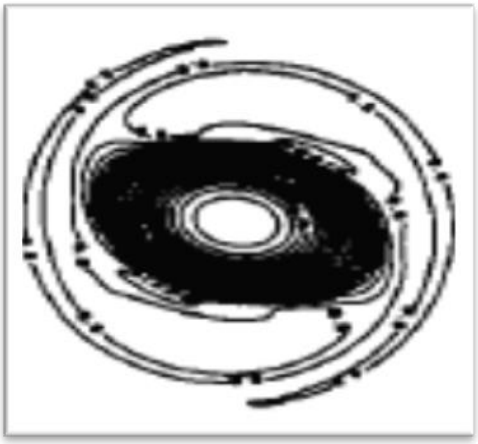

(f)

Figure 5.10- Continued

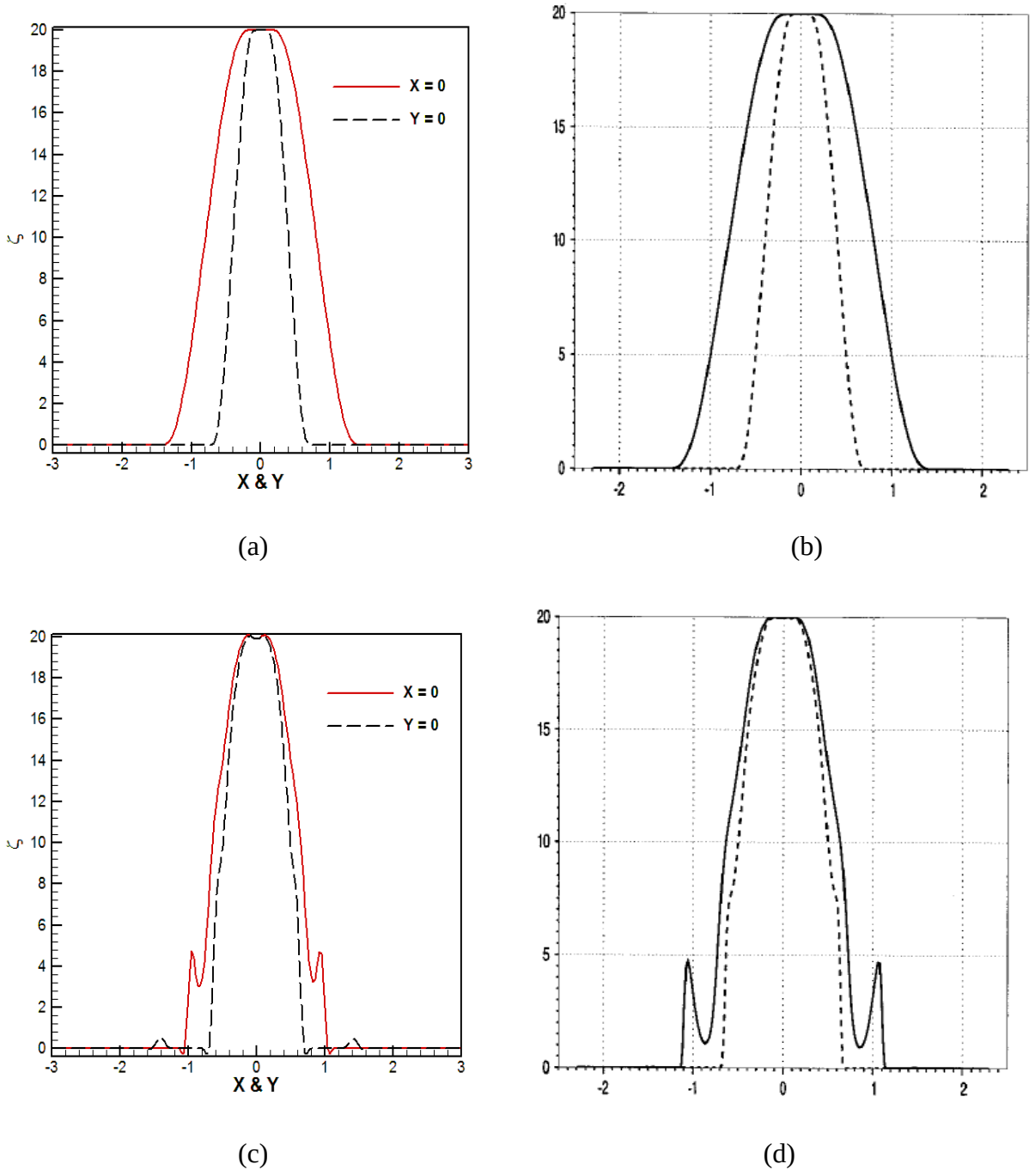

Figure 5.11 Comparison of vorticity along x and y axis for cases shown in Figure 5.9, computed using the present VIC implementation, remeshing frequency, $N_{rem} = 5$, 200x200 grid, $\Delta x = \Delta y = 0.03$ and $\Delta t = 3.0 \times 10^{-3}$ (left) with the results of Koumoutsakos (1997) (right) at times, (a)-(b) T = 0.0, (c)-(d) T = 1.0, (e)-(f) T = 1.5, (g)-(h) T = 4.0.

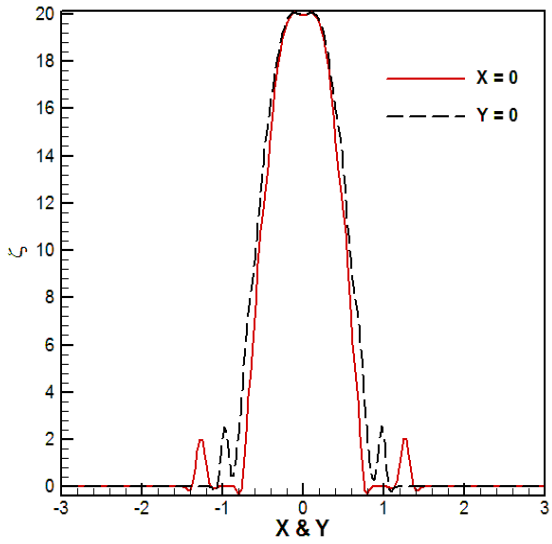

(e)

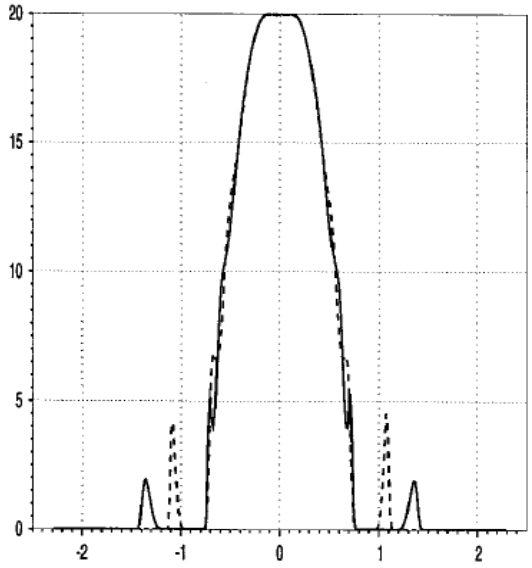

(f)

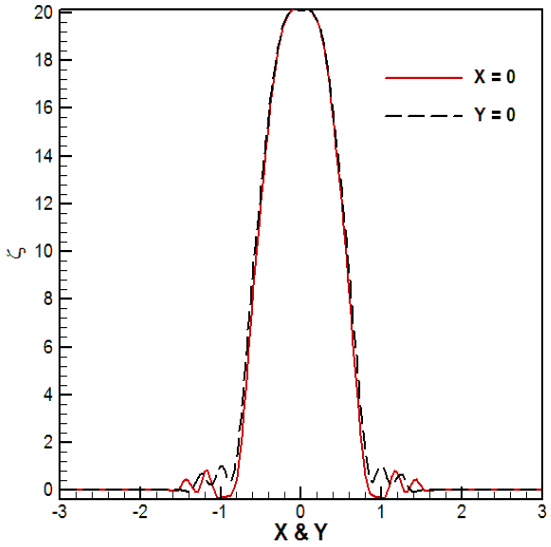

(g)

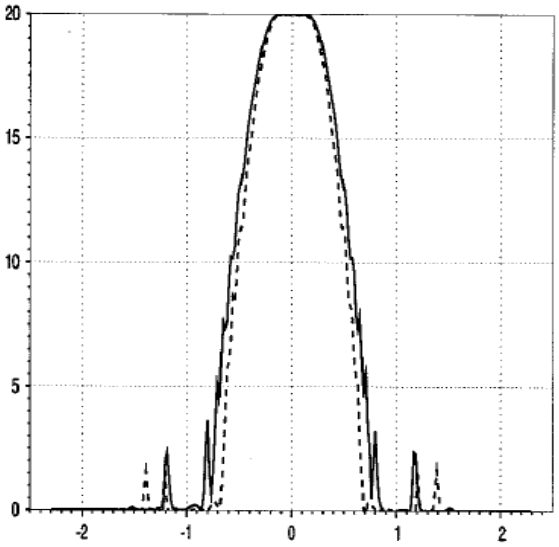

(h)

Figure 5.11- Continued

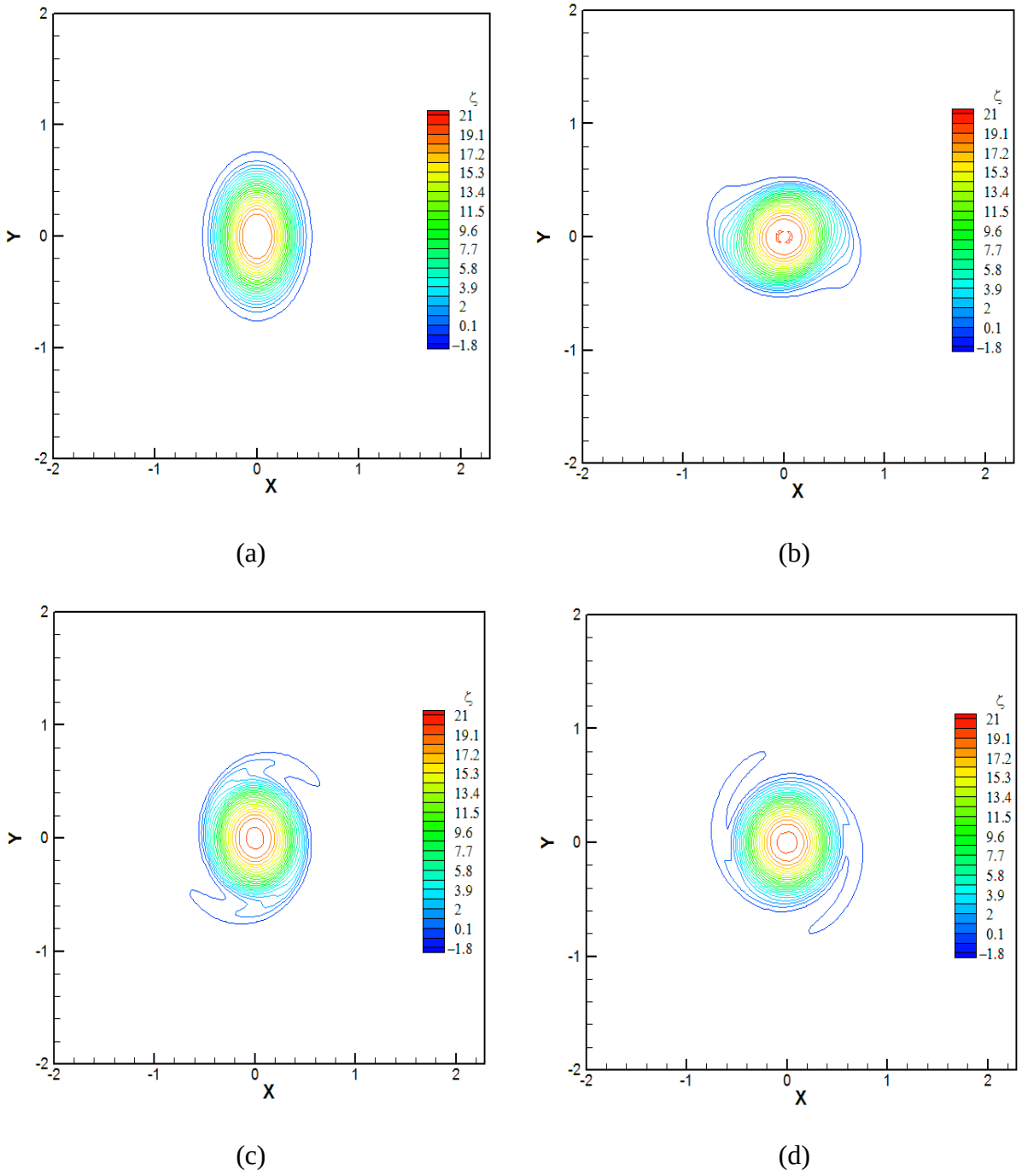

Figure 5.12 Vorticity contours for the evolution of an initially elliptical vortex with aspect ratio = 1.415, remeshing frequency, $N_{rem} = 5$, 200x200 grid, $\Delta x = \Delta y = 0.03$ and $\Delta t = 3.0 \times 10^{-3}$ at times, (a) T = 0.0, (b) T = 0.5, (c) T = 1.0, (d) T = 1.5, (e) T = 2.0 and (f) T = 4.0 using VIC method

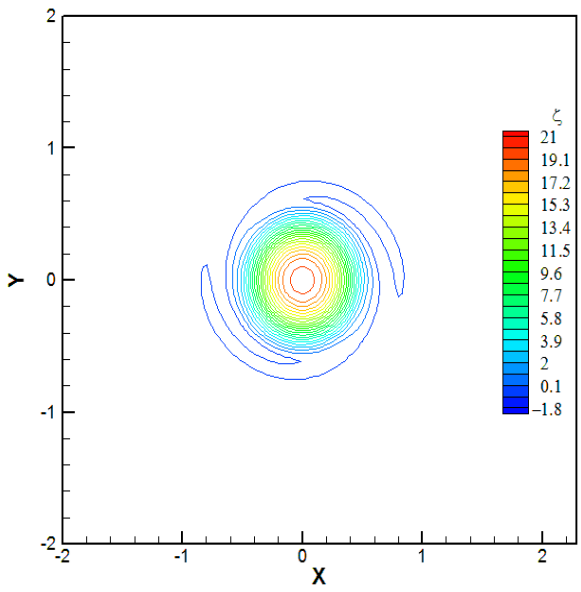

(e)

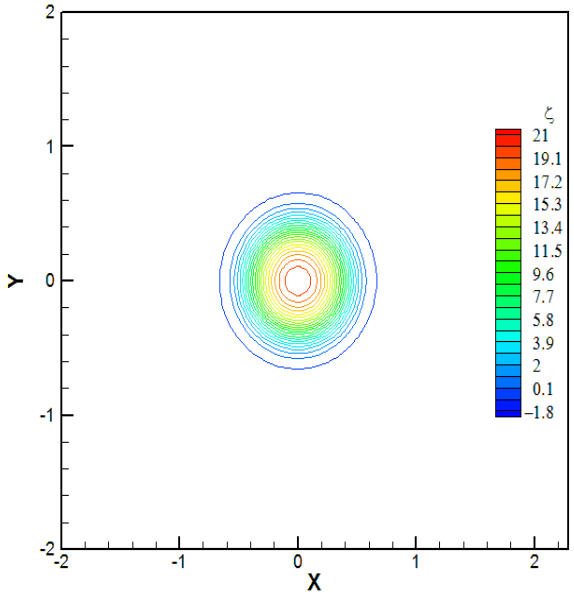

(f)

Figure 5.12- Continued

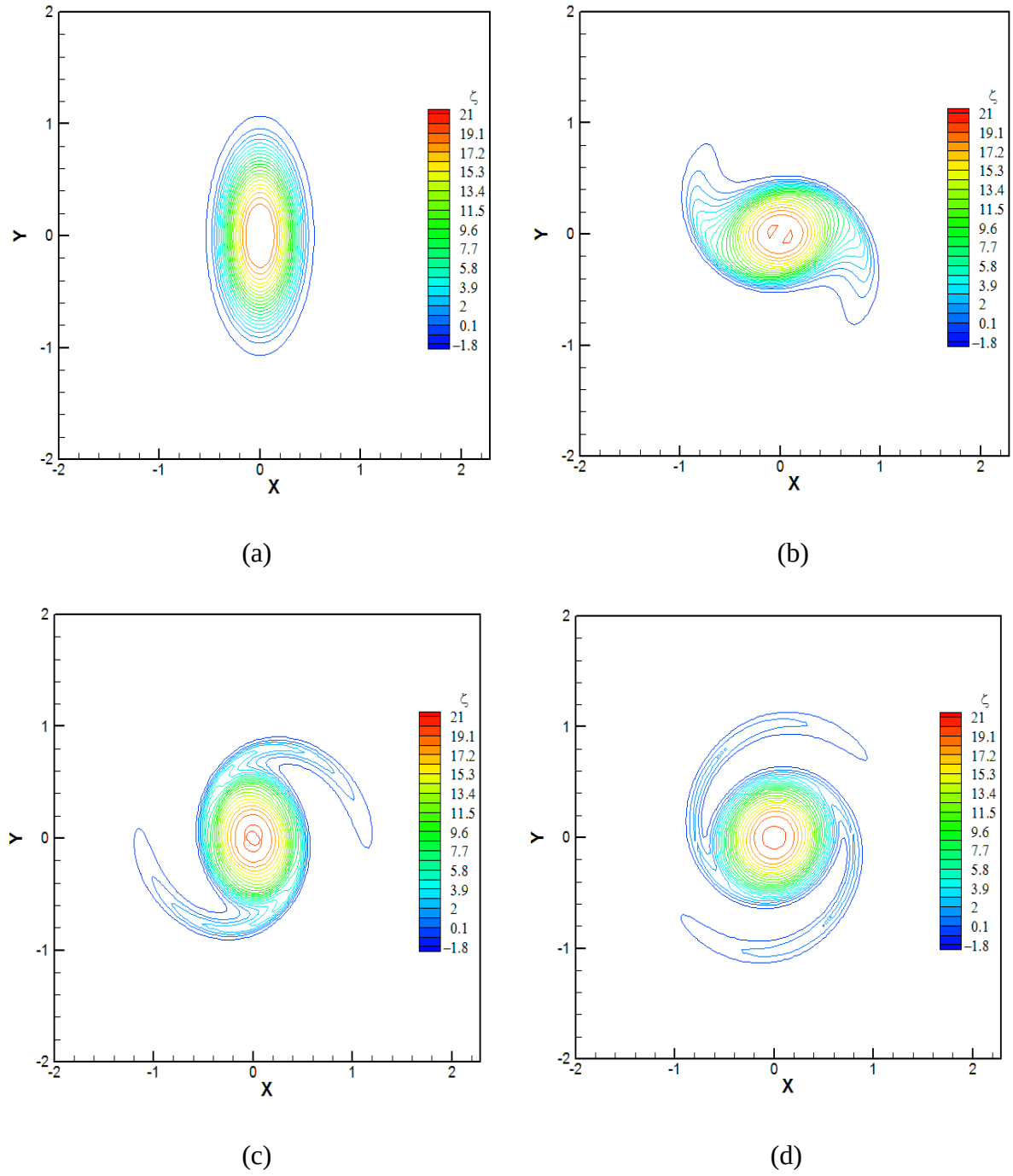

Figure 5.13 Vorticity contours for the evolution of an initially elliptical vortex with aspect ratio = 2.00, remeshing frequency, $N_{rem} = 5$, 200x200 grid, $\Delta x = \Delta y = 0.03$ and $\Delta t = 3.0 \times 10^{-3}$ at times, (a) T = 0.0, (b) T = 0.5, (c) T = 1.0, (d) T = 1.5, (e) T = 2.0 and (f) T = 4.0 using VIC method

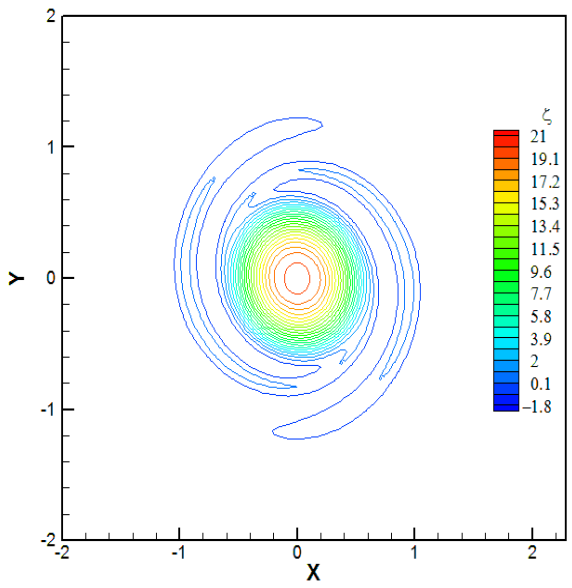

(e)

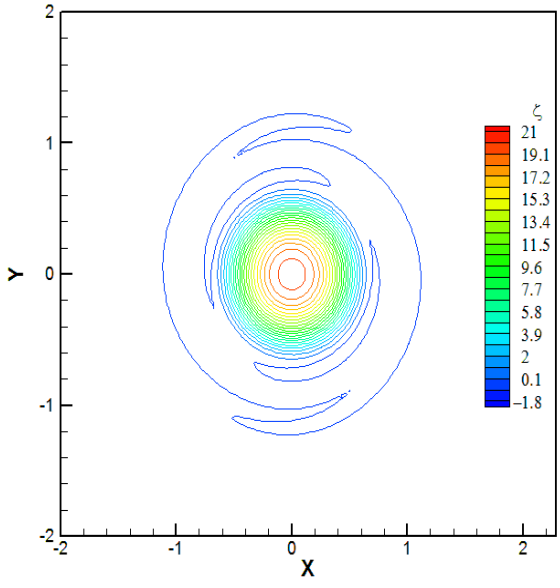

(f)

Figure 5.13.- Continued

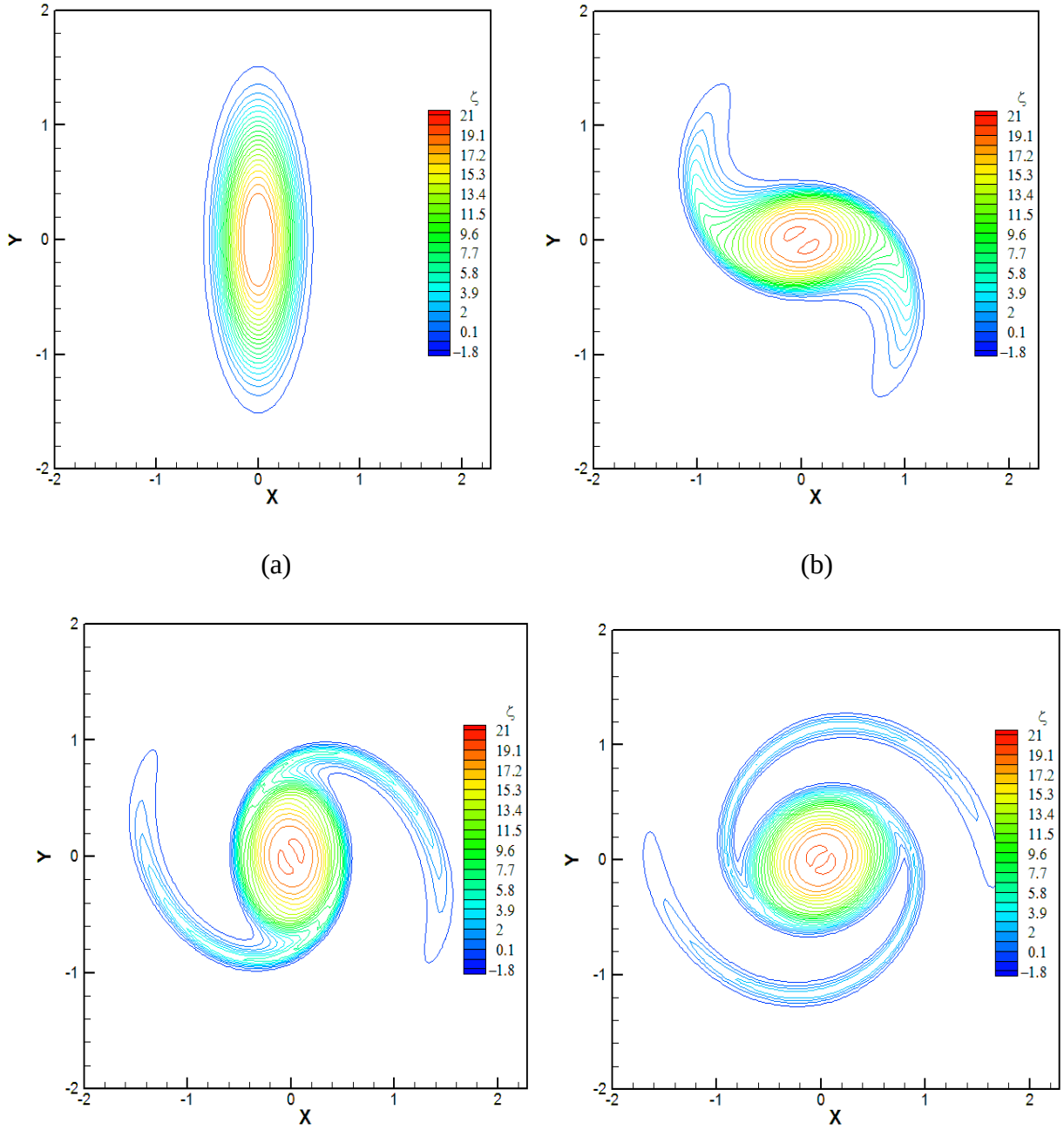

Figure 5.14 Vorticity contours for the evolution of an initially elliptical vortex with aspect ratio = 2.86, remeshing frequency, $N_{rem} = 5$, 200x200 grid, $\Delta x = \Delta y = 0.03$ and $\Delta t = 3.0 \times 10^{-3}$ at times, (a) T = 0.0, (b) T = 0.5, (c) T = 1.0, (d) T = 1.5, (e) T = 2.0 and (f) T = 4.0 using VIC method

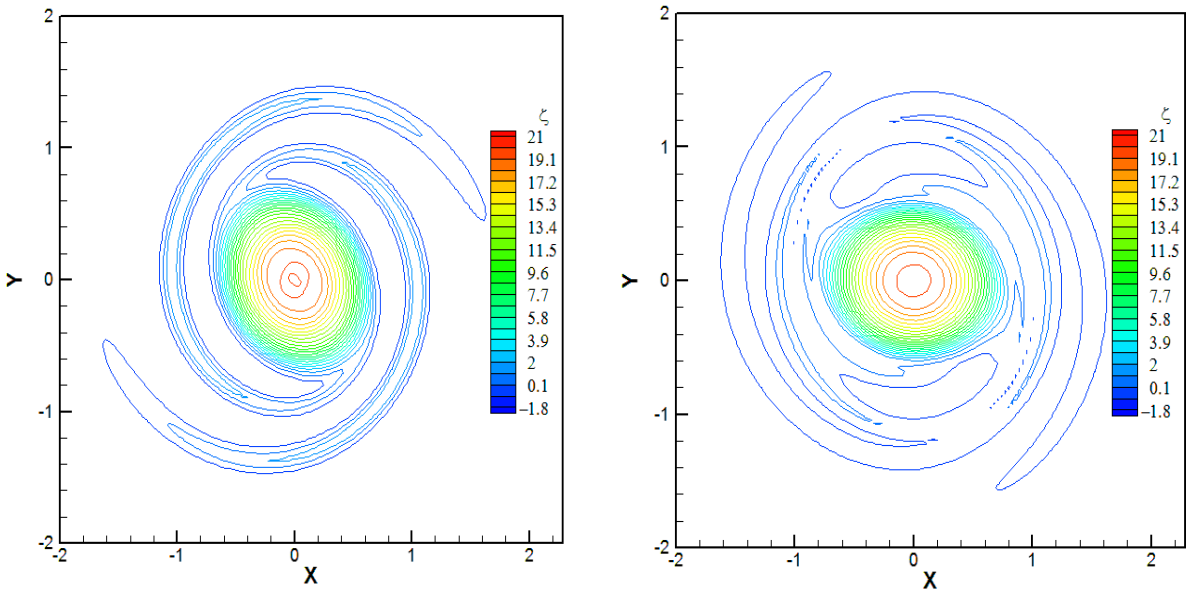

(e) (f)

Figure 5.14- Continued

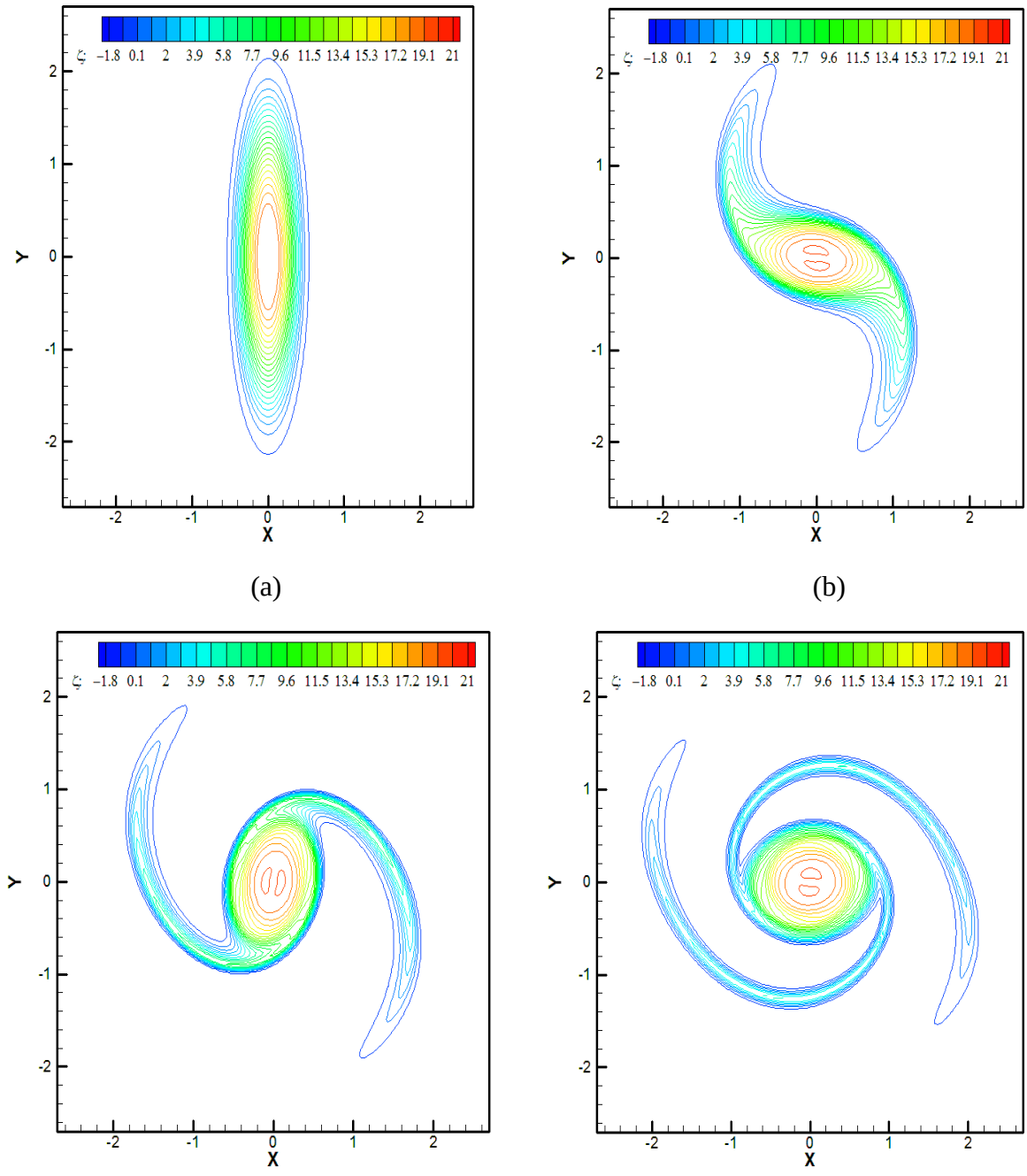

Figure 5.15 Vorticity contours for the evolution of an initially elliptical vortex with aspect ratio = 4.06, remeshing frequency, $N_{rem} = 5$, 200x200 grid, $\Delta x = \Delta y = 0.03$ and $\Delta t = 3.0 \times 10^{-3}$ at times, (a) T = 0.0, (b) T = 0.5, (c) T = 1.0, (d) T = 1.5, (e) T = 2.0 and (f) T = 4.0 using VIC method.

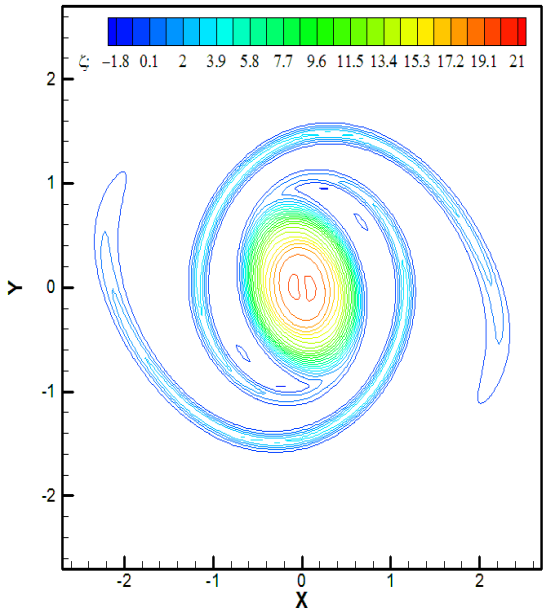

(e)

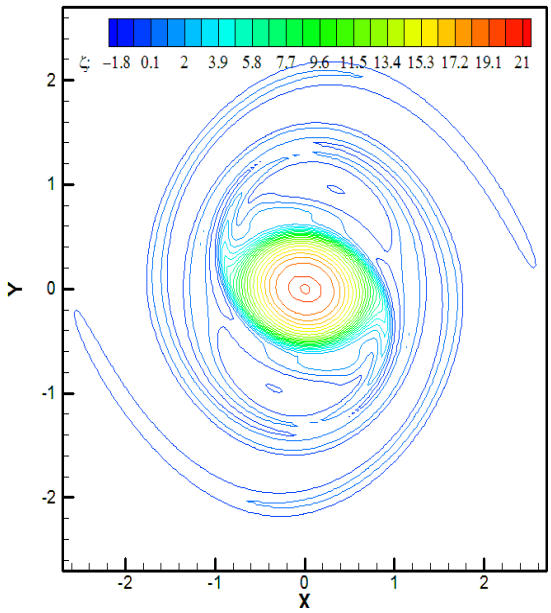

(f)

Figure 5.15.- Continued

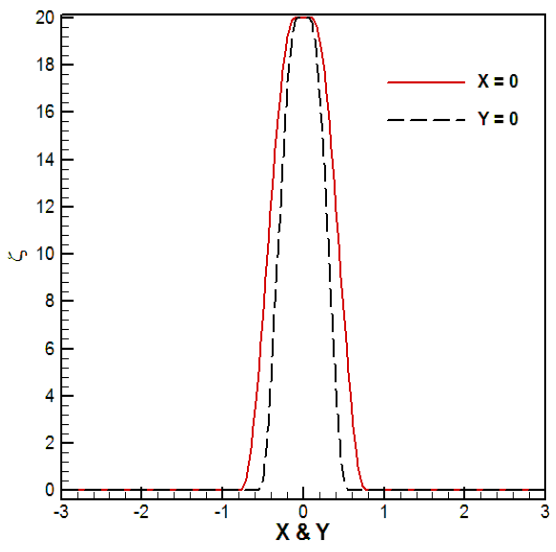

(a)

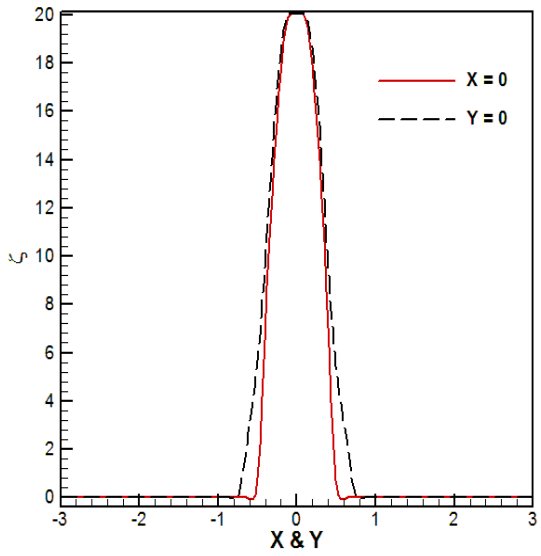

(b)

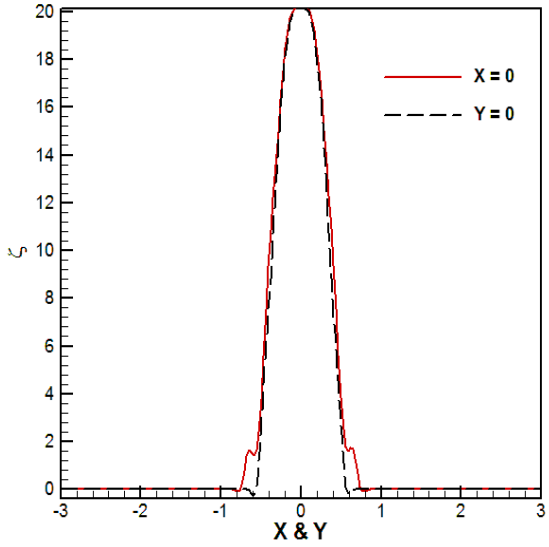

(c)

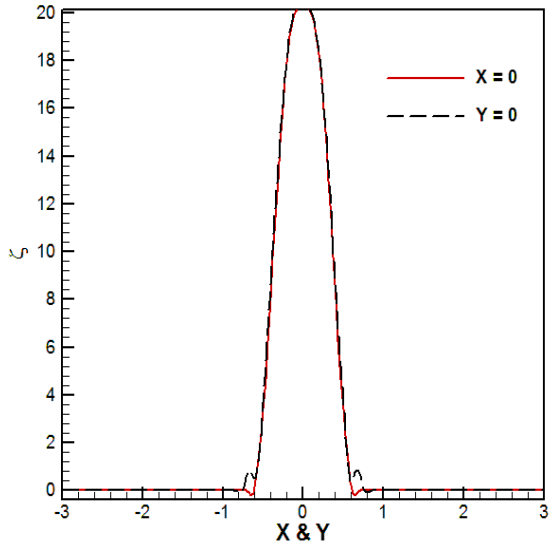

(d)

Figure 5.16 Vorticity along the x and y axis for the evolution of an initially elliptical vortex aspect ratio = 1.415, shown in Figure 5.12, remeshing frequency, $N_{rem} = 5$, 200x200 grid, $\Delta x = \Delta y = 0.03$ and $\Delta t = 3.0 \times 10^{-3}$ at times, (a) T = 0.0, (b) T = 0.5, (c) T = 1.0, (d) T = 1.5, (e) T = 2.0 and (f) T = 4.0 using VIC method.

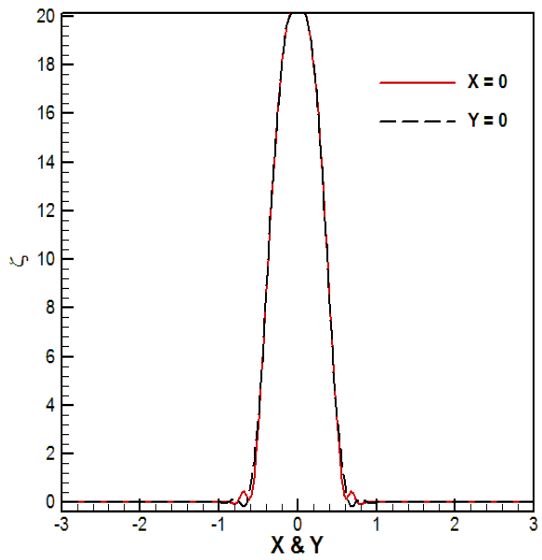

(e)

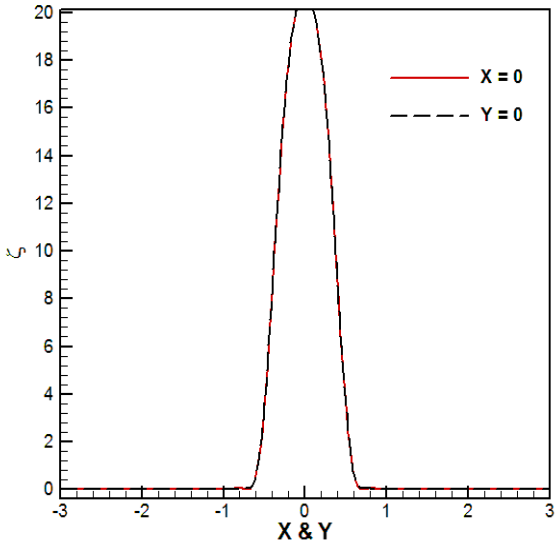

(f)

Figure 5.16.- Continued

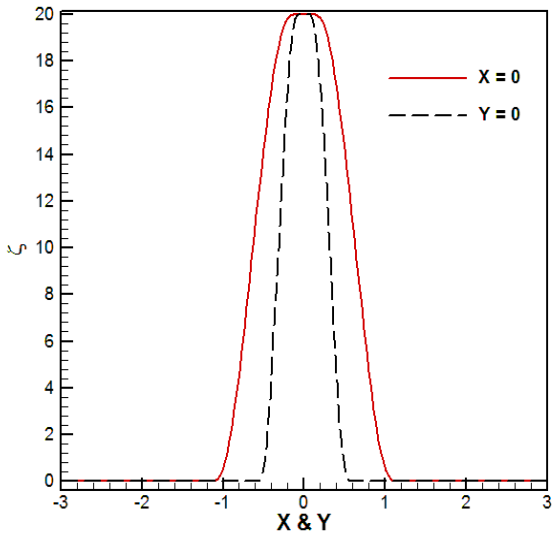

(a)

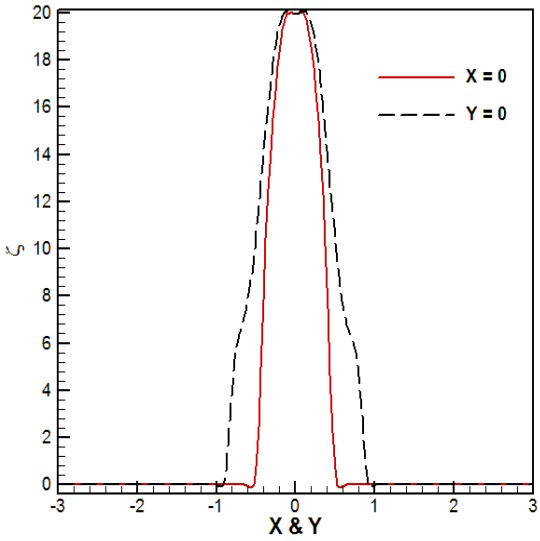

(b)

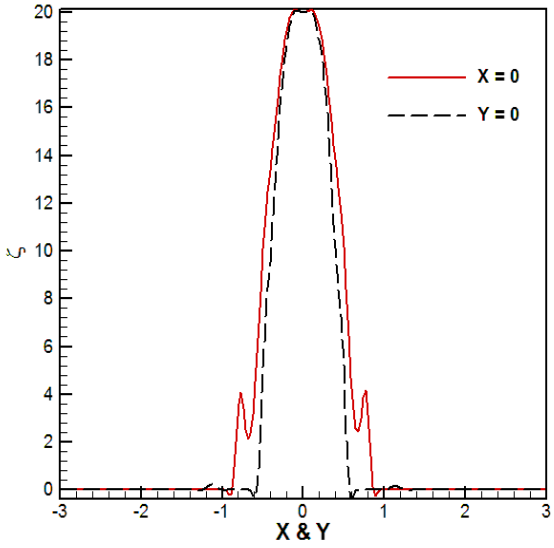

(c)

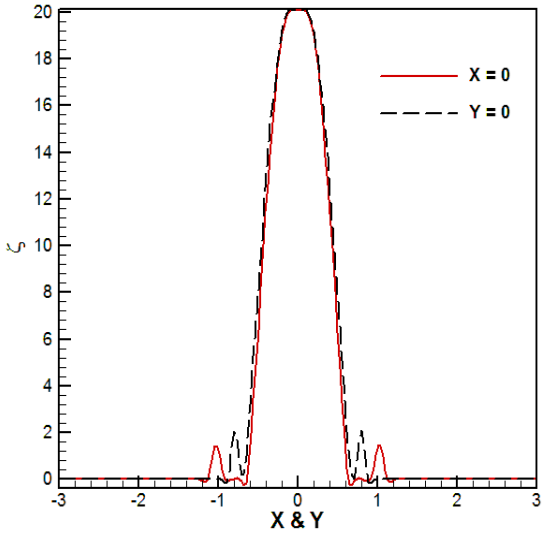

(d)

Figure 5.17 Vorticity along the x and y axis for the evolution of an initially elliptical vortex aspect ratio = 2.00, shown in Figure 5.13, remeshing frequency, $N_{rem} = 5$, 200x200 grid, $\Delta x = \Delta y = 0.03$ and $\Delta t = 3.0 \times 10^{-3}$ at times, (a) T = 0.0, (b) T = 0.5, (c) T = 1.0, (d) T = 1.5, (e) T = 2.0 and (f) T = 4.0 using VIC method.

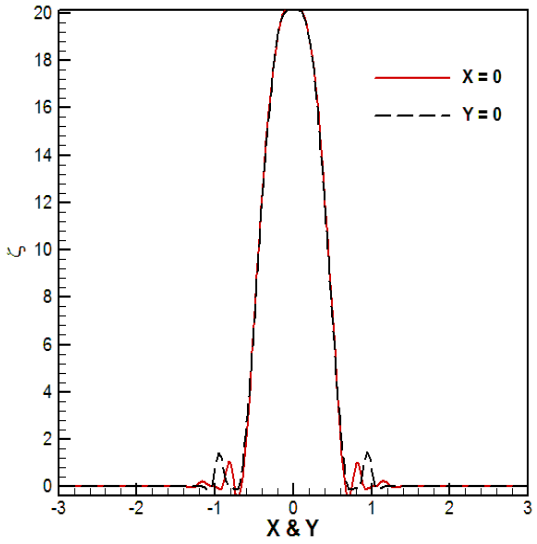

(e)

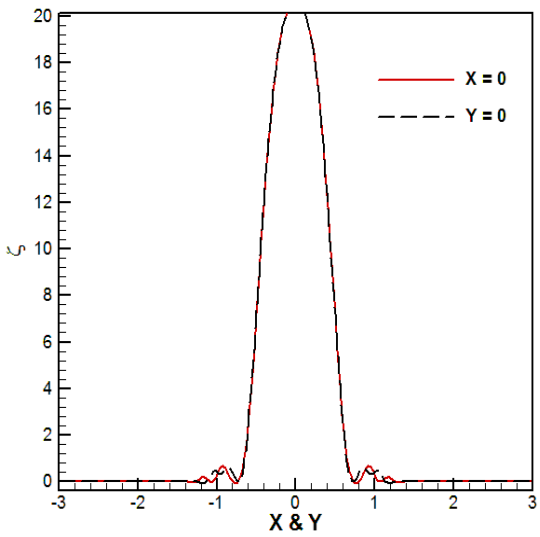

(f)

Figure 5.17.- Continued

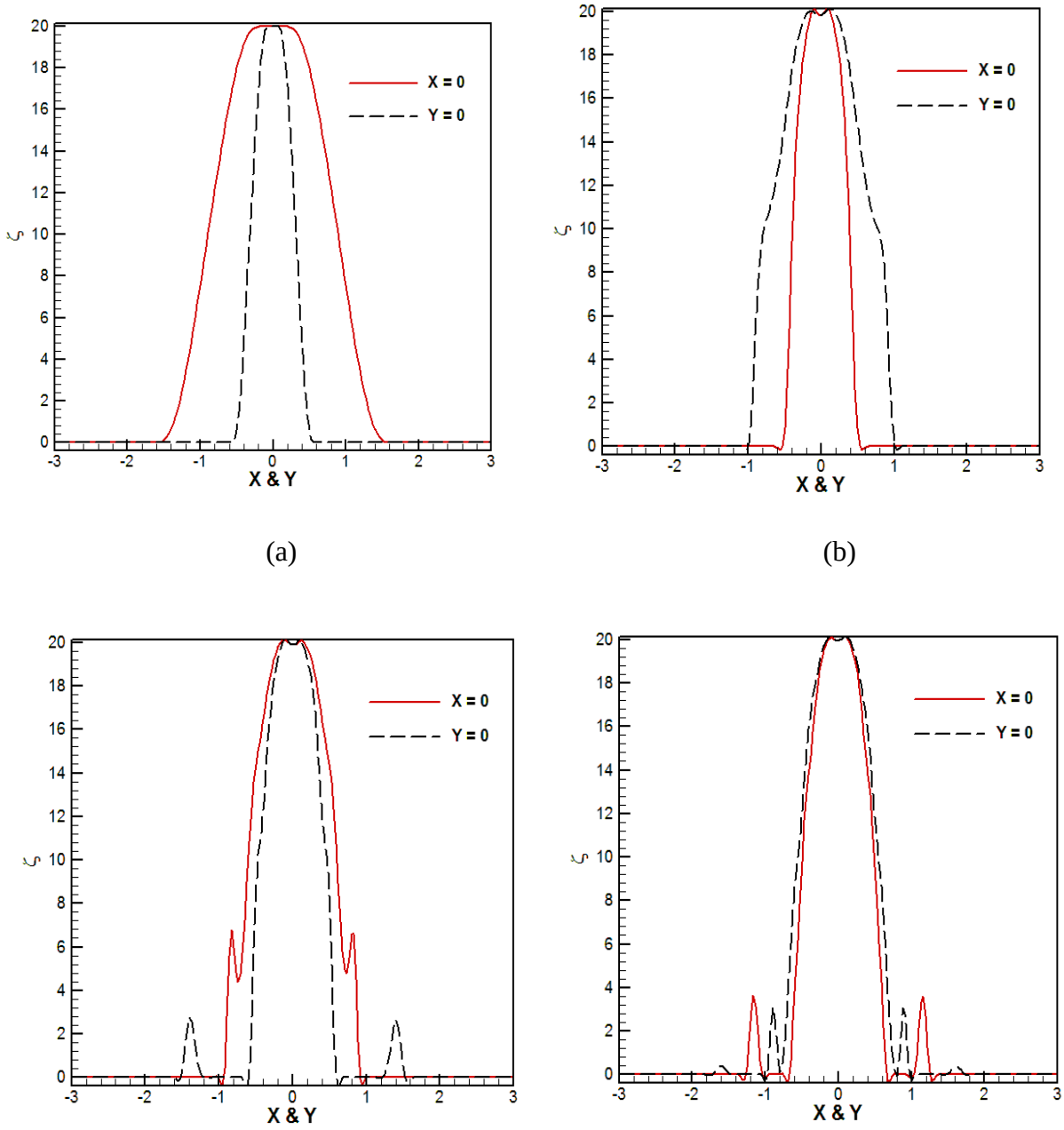

(a) (b)

(c) (d)

Figure 5.18 Vorticity along the x and y axis for the evolution of an initially elliptical vortex aspect ratio = 2.86, shown in Figure 5.14, remeshing frequency, $N_{rem} = 5$, 200x200 grid, $\Delta x = \Delta y = 0.03$ and $\Delta t = 3.0 \times 10^{-3}$ at times, (a) T = 0.0, (b) T = 0.5, (c) T = 1.0, (d) T = 1.5, (e) T = 2.0 and (f) T = 4.0 using VIC method.

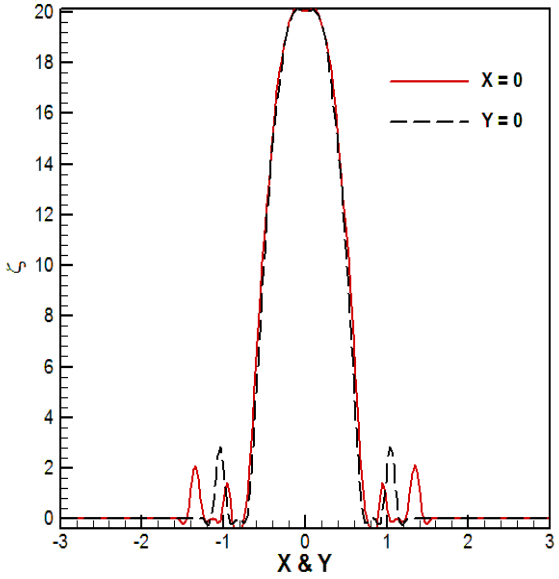

(e)

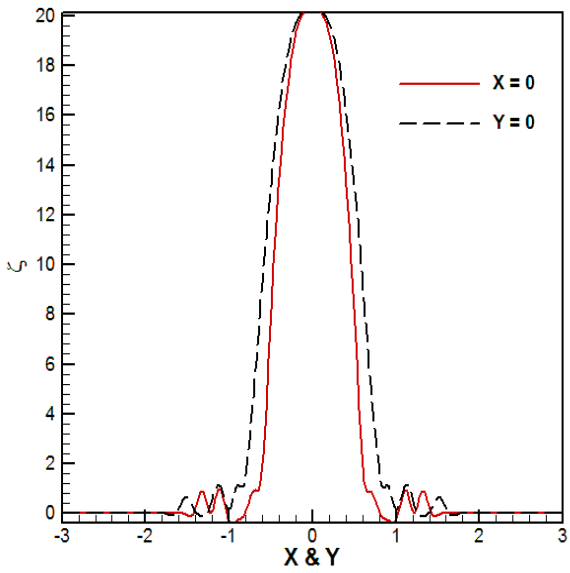

(f)

Figure 5.18- Continued

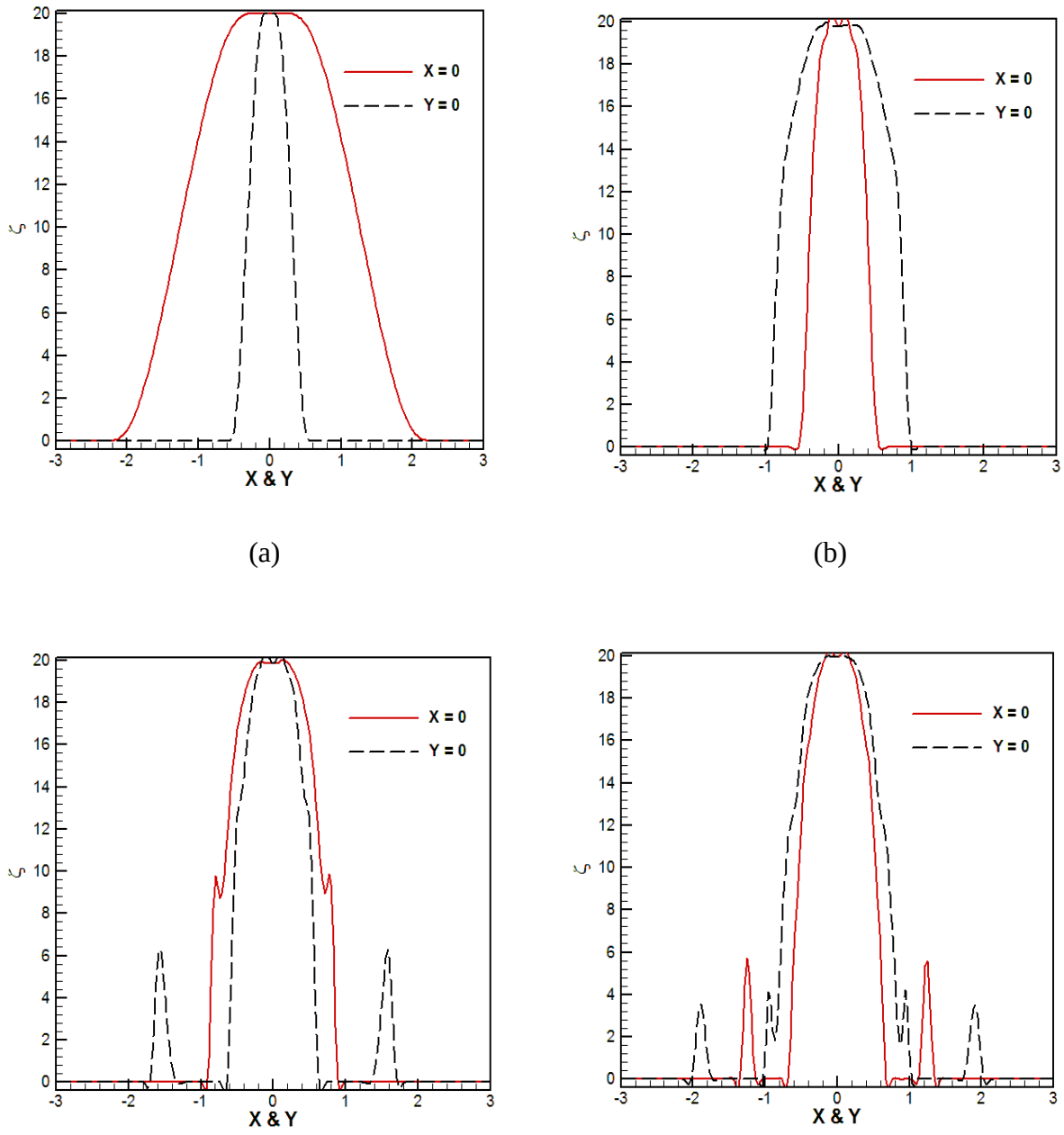

Figure 5.19 Vorticity along the x and y axis for the evolution of an initially elliptical vortex aspect ratio = 4.06, shown in Figure 5.15, remeshing frequency, $N_{rem} = 5$, 200x200 grid, $\Delta x = \Delta y = 0.03$ and $\Delta t = 3.0 \times 10^{-3}$ at times, (a) T = 0.0, (b) T = 0.5, (c) T = 1.0, (d) T = 1.5, (e) T = 2.0 and (f) T = 4.0 using VIC method.

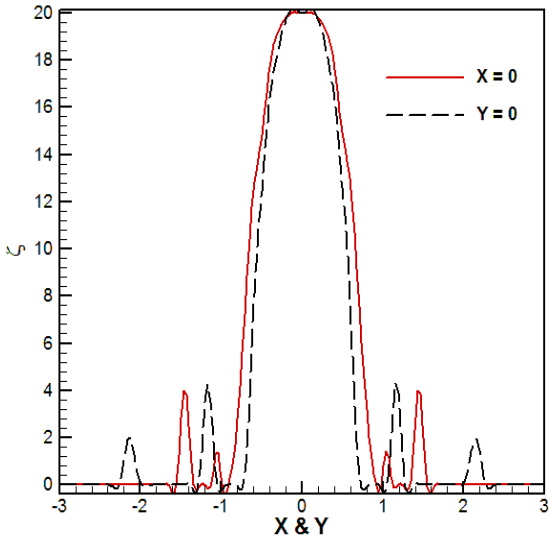

(e)

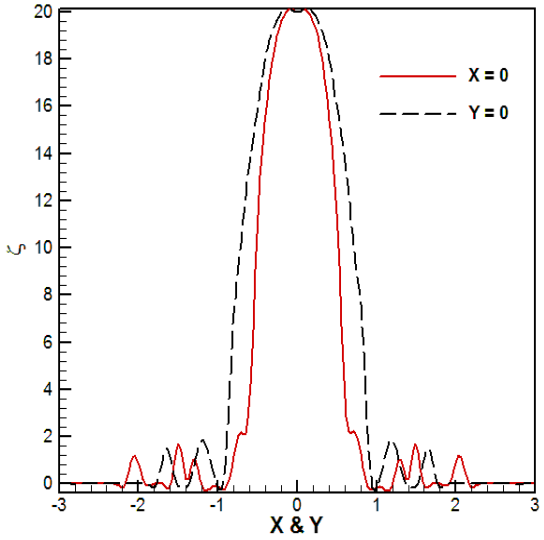

(f)

Figure 5.19- Continued

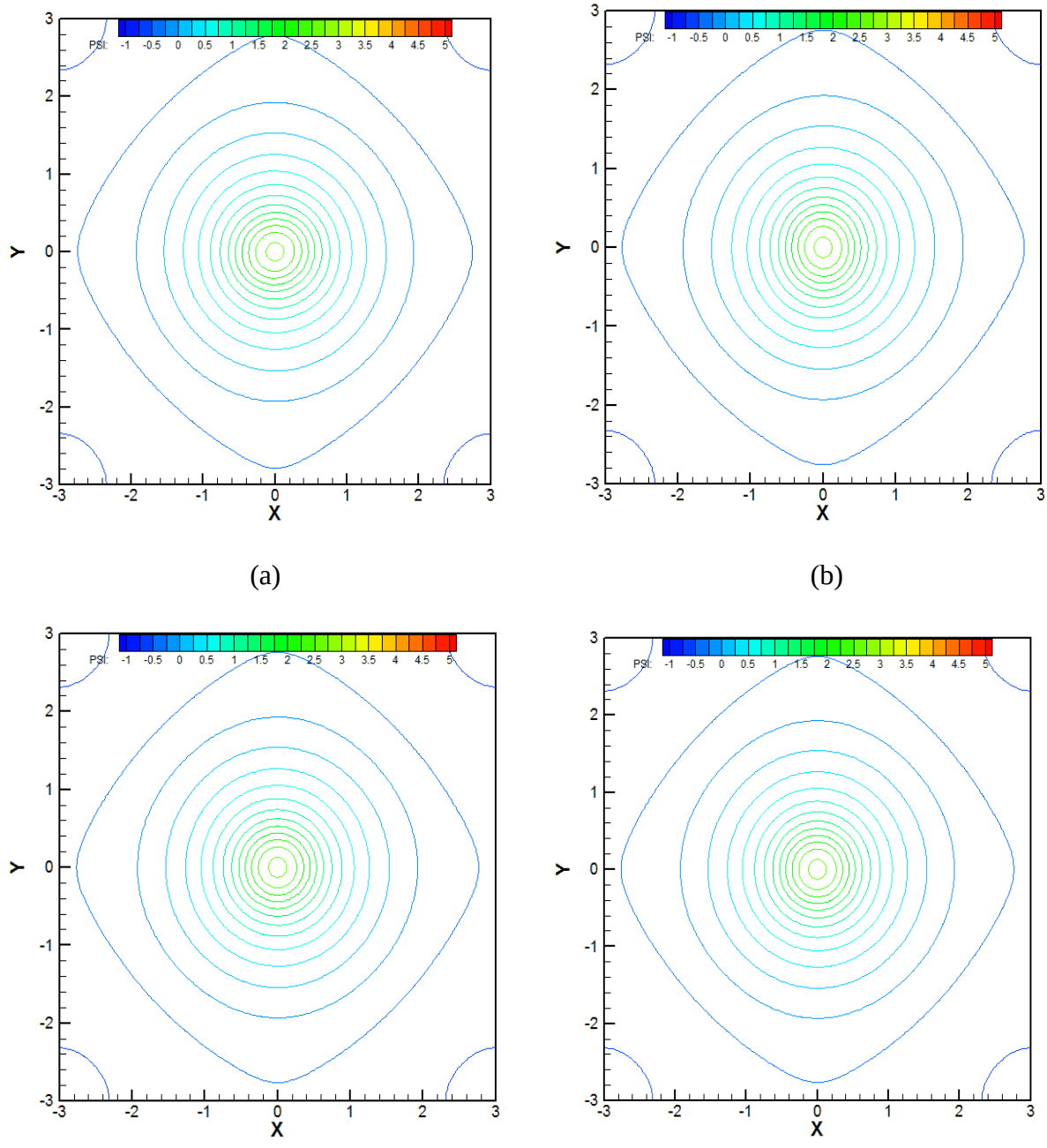

Figure 5.20 Stream function prediction for the evolution of an initially elliptical vortex with aspect ratio = 1.415, as shown in Figure 5.12, remeshing frequency, $N_{rem} = 5$, 200x200 grid, $\Delta x = \Delta y = 0.03$ and $\Delta t = 3.0 \times 10^{-3}$ at times, (a) T = 0.5, (b) T = 1.0, (c) T = 1.5, (d) T = 2.0 and (e) T = 4.0 using VIC method.

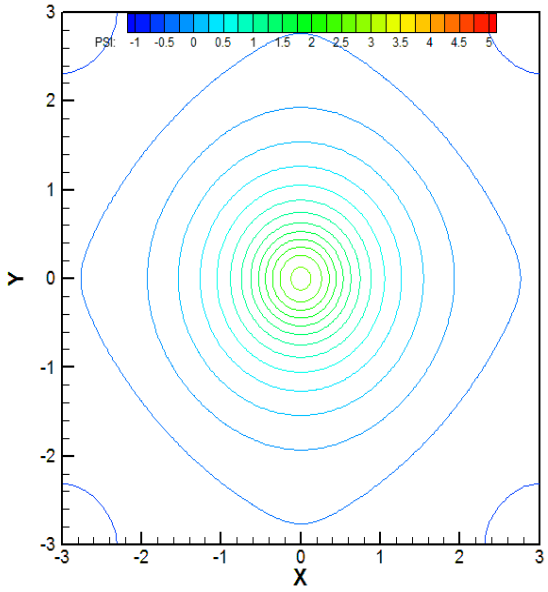

(e)

Figure 5.20- Continued

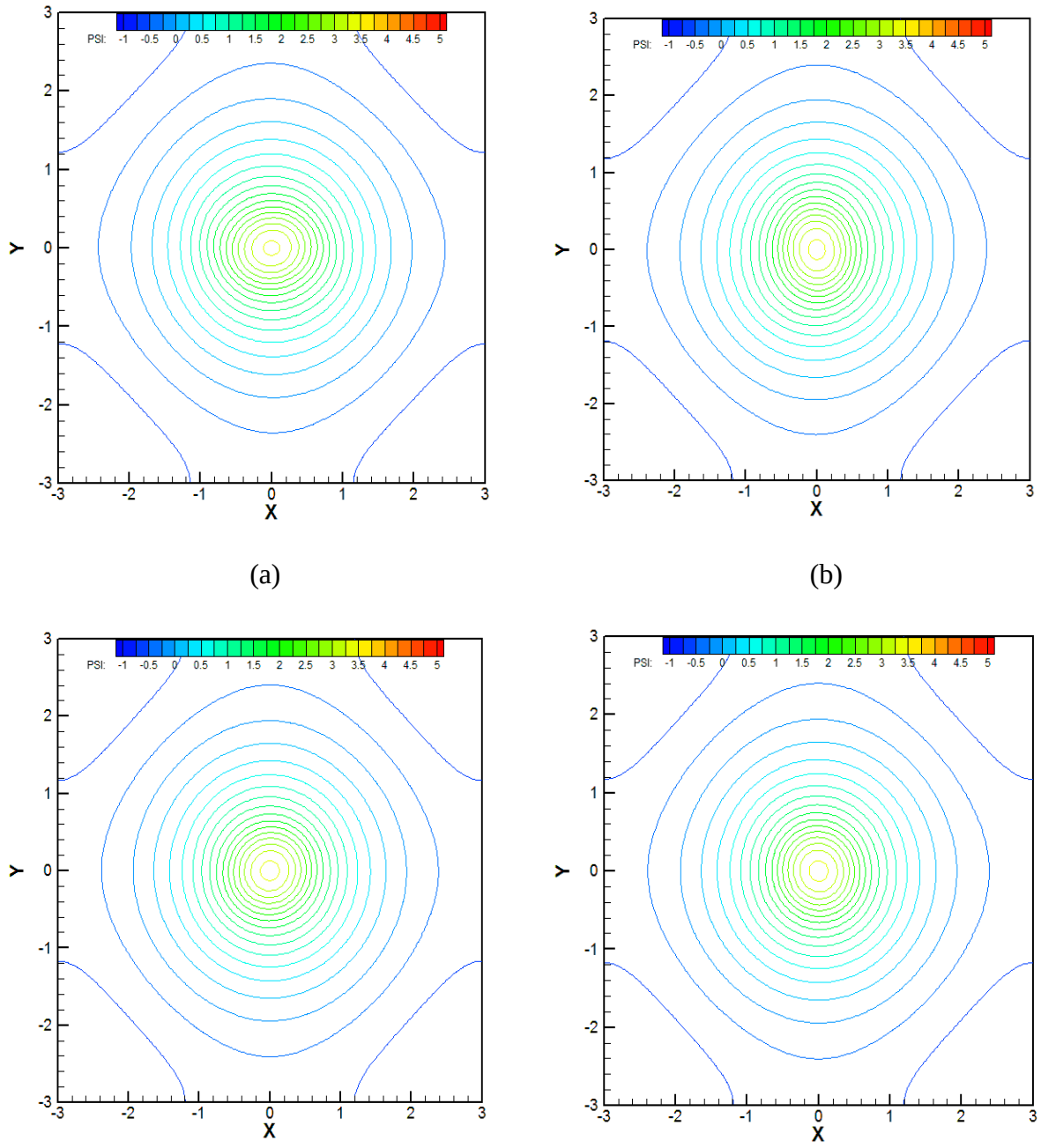

Figure 5.21 Stream function prediction for the evolution of an initially elliptical vortex with aspect ratio = 2.00, as shown in Figure 5.12, remeshing frequency, $N_{rem} = 5$, 200x200 grid, $\Delta x = \Delta y = 0.03$ and $\Delta t = 3.0 \times 10^{-3}$ at times, (a) T = 0.5, (b) T = 1.0, (c) T = 1.5, (d) T = 2.0 and (e) T = 4.0 using VIC method.

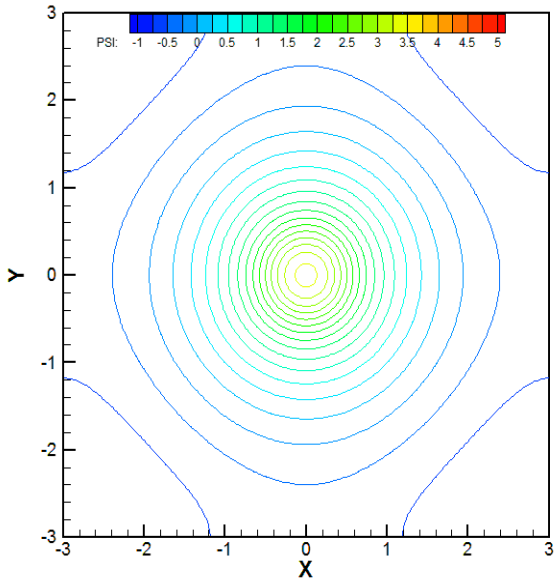

(e)

Figure 5.21- Continued

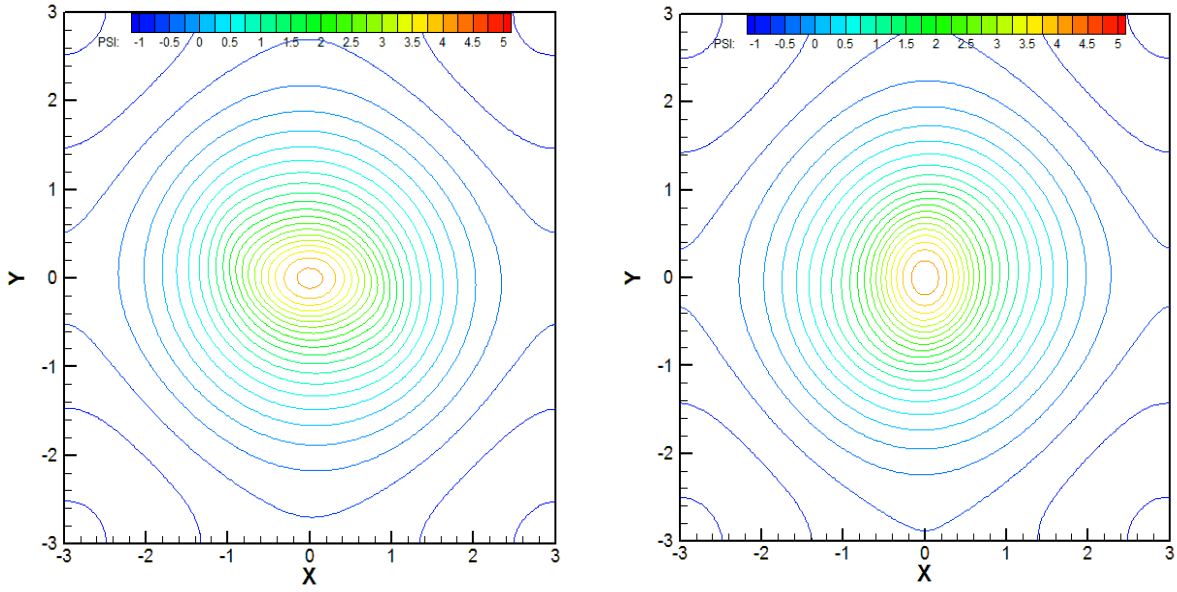

(a) (b)

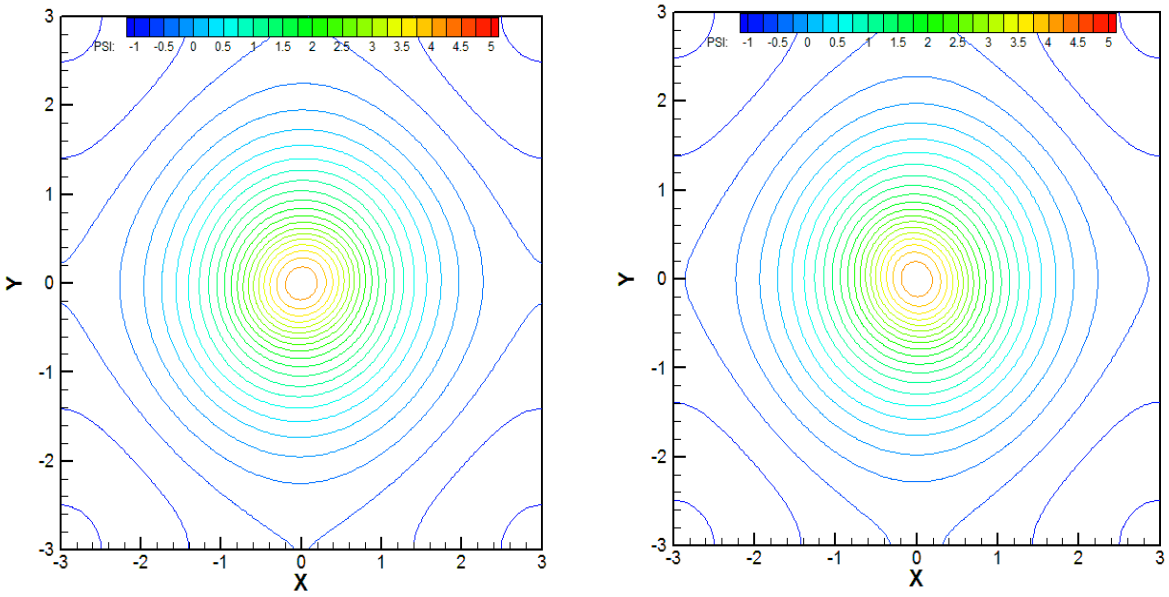

(c) (d)

Figure 5.22 Stream function prediction for the evolution of an initially elliptical vortex with aspect ratio = 2.86, as shown in Figure 5.12, remeshing frequency, $N_{rem} = 5$, 200x200 grid, $\Delta x = \Delta y = 0.03$ and $\Delta t = 3.0 \times 10^{-3}$ at times, (a) T = 0.5, (b) T = 1.0, (c) T = 1.5, (d) T = 2.0 and (e) T = 4.0 using VIC method.

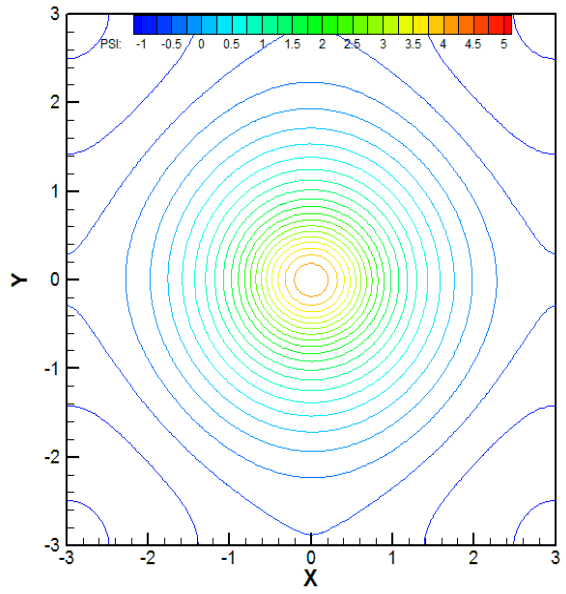

(e)

Figure 5.22- Continued

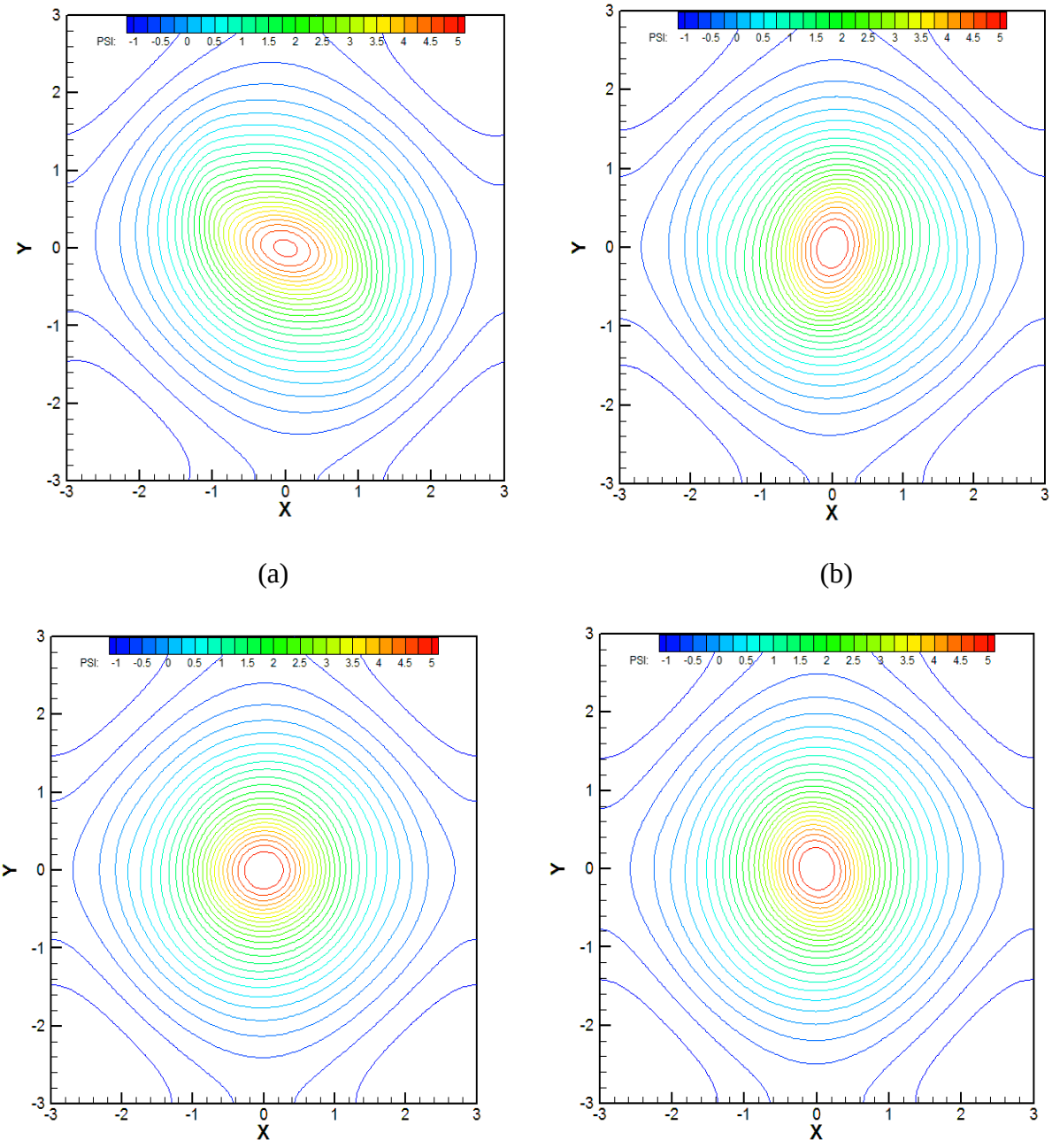

Figure 5.23 Stream function prediction for the evolution of an initially elliptical vortex with aspect ratio = 4.06, as shown in Figure 5.12, remeshing frequency, $N_{rem} = 5$, 200x200 grid, $\Delta x = \Delta y = 0.03$ and $\Delta t = 3.0 \times 10^{-3}$ at times, (a) T = 0.5, (b) T = 1.0, (c) T = 1.5, (d) T = 2.0 and (e) T = 4.0 using VIC method.

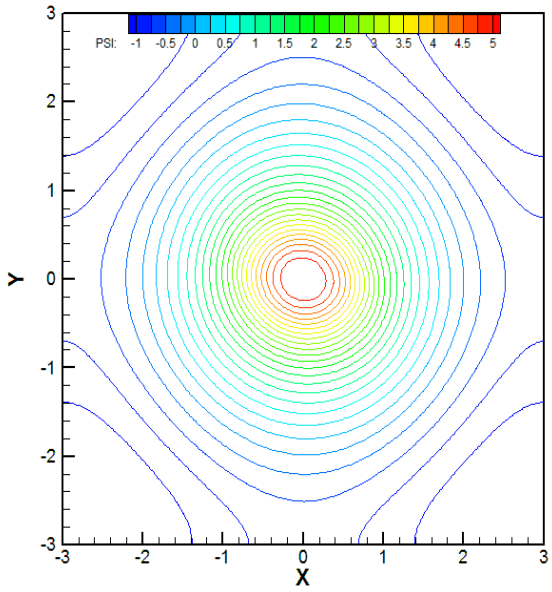

(e)

Figure 5.23- Continued

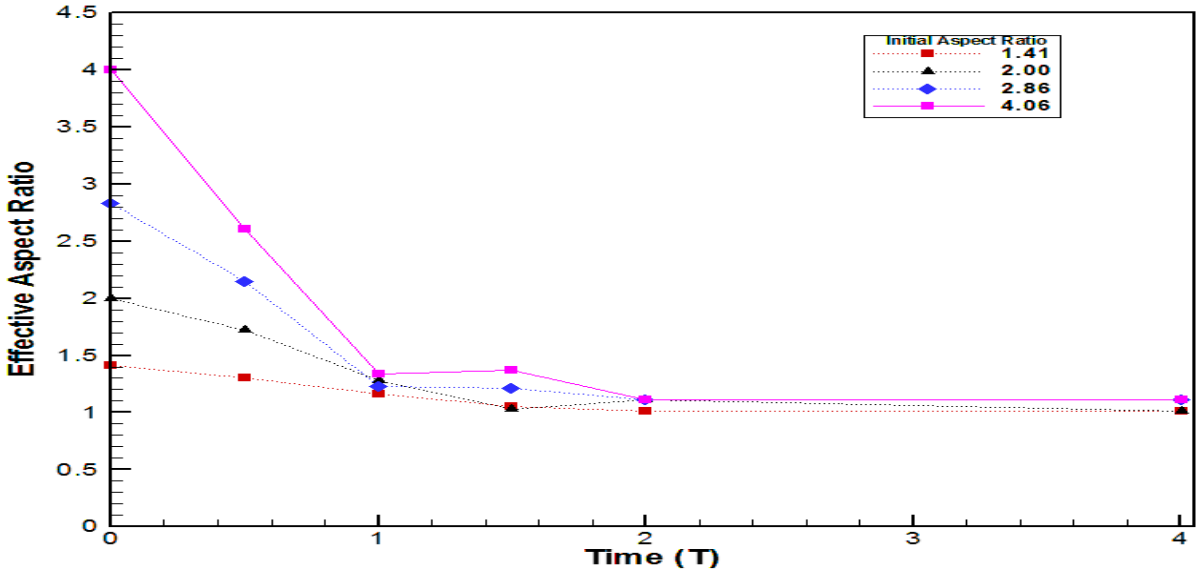

Figure 5.24 Effective aspect ratio in the conservation of vorticity for different initial aspect ratio, using 200x200 grid, $\Delta x = \Delta y = 0.03$, $\Delta t = 3.0 \times 10^{-3}$, at times, $T = 0.5,\ 1.0,\ 1.5,\ 2.0$ and 4.0 using VIC method.

Chapter 6

Conclusions and Recommendations

6.1 Conclusions

A vortex-in-cell numerical method for two-dimensional, incompressible, inviscid, flow has been successfully implemented and applied to a study of elliptical vortices with non-uniform vorticity distribution. A pseudo-spectral method is used as a benchmark to verify the vortex-in-cell implementation. In the vortex-in-cell method, vortex particles help to visualize the flow and provide useful tools for analysing flow in term of vorticity dynamics. The results of a convergence study as a function of each parameter of the scheme give confidence in the accuracy of the computed results.

In this work, the study of the evolution of the vorticity field helps one to understand the process of filamentation and axisymmetrization of initially elliptical vortices with non-uniform vorticity distribution. From the different simulation results, one can conclude that, in all cases, the vortex structure rotates in anti-clockwise direction, the spiral arms are ejected from the main core and re-approach, reattach, and merge as the vorticity aspect ratio reduces. It was noticed that, when

the aspect ratio is increased the lengths of the vertical arms that are ejected from the main core also increase significantly and the decay time of an initially elliptical vortex distribution also increases. In addition, axisymmetrization of a given initially elliptical vortex with non-uniform vorticity distribution profile occurred for all cases studied. Hence, the rate of axisymmetrization depends on the shape of the given initial vorticity field.

6.2 Recommendations for Future Studies

This study demonstrates that a hybrid Eulerian-Lagrangian method shows high accuracy with relatively low cost, hence these schemes are useful for practical applications. In addition, the following are recommendations for possible future developments and investigations related to the present work:

1. Similar studies could be done by extending the solver to three-dimensional domains; this can improve its applicability to more physically realistic situations. However more time would be required for the calculations. Parallel computation would no doubt be required.
2. The code implemented in this work uses predictor-corrector time integration, which is second-order accurate. In order to improve the efficiency and time to run the code, implementation of an alternative higher-order time-integration scheme should be considered.
3. Further improvement could be done in the existing work by placing more than one particle in each cell. This would increase the time of the computation, but would also increase the accuracy of the results. A thorough analysis of the trade-offs would be required.

4. Also, in the present vortex-in-cell simulation, the size of the grid element in both directions is assumed to be constant and equal to each other. This is appropriate for the present study, as flow parameters vary at similar rates in both directions. It is possible to modify the vortex-in-cell code such that grid elements have variable size in both directions. This may improve the simulation efficiency for other cases.
5. The code implemented in this work is for two-dimensional, incompressible, inviscid flow; it is possible to introduce viscosity and check its effect on the existing simulation results in order to study the effects of viscosity on similar vortex-evolution problems.

References

Abernathy, F. H. and Kronauer R. E. (1962) “The Formation of Vortex Sheets”, J. Fluid Mech., vol.13, pp. 1-20.

Anderson, C. R. and Greengrad, C. (1985) “On Vortex Methods”, J. Numer. Anal., vol. 22, pp. 413-440.

Aref, H and Siggia, E. D. (1980) “Vortex Dynamics of Two-Dimensional Turbulent Shear Layer”, J. Fluid Mech., vol. 100, pp. 705-737.

Aris, R. (1989)” Vectors, Tensors and Basic Equations of Fluid Mechanics”, Dover Publications, New York.

Barba, L. A., Leonard, A. and Allen, C. B (2005) ”Advances in Viscous Vortex Methods - Meshless Spatial Adaption Based on Radial Basis Function Interpolation”, Int. J. Num. Meth. Fluids, vol. 47, pp 387 – 421.

Batchelor, G. K. (1979) “An Introduction to Fluid Dynamics”, Cambridge University Press.
Birdsal, C. K., and D. Fuss. (1969) "Clouds-in-clouds, clouds-in-cells physics for many-body plasma simulations", Journal of Computational Physics 3, pp. 494-511.

Chang, C. C. and Chern, R. L. (1991) “A Numerical Study of Flow around an Impulsively Started Circular Cylinder”, J. Fluid Mech., vol. 233, pp. 243-263.

Chang, C. C. and Chern, R. L. (1991) “A Numerical Study of Flow around an Impulsively Started Circular Cylinder”, J. Fluid Mech., vol. 233, pp. 243-263.

Chatelain, P., Curioni, A., Bergdorf, M, Rossinelli, D. Andreoni, W. and Koumoutsakos, P. (2008) “Billion vortex particle direct numerical simulations of aircraft wakes”, Comput. Methods Appl. Mech. Engrg., vol. 197, pp1296–1304.

Chorin, A. J. (1973) “Numerical Study of Slightly Viscous Flow”, J. Fluid. Mech., vol. 57, pp 785-796.

Chorin, A. J. (1996) “Vortex Methods”, In Computational Fluid Dynamics, Lesieur, M., Comte, P. and Zinn-Justin J. Elsevier Science.

Christiansen, J. P. (1973) “Numerical Solution of Hydrodynamics by the Method of Point Vortices”, J. Comput. Phys., vol. 13, pp 363-379.

Cottet G. H., Koumoutsakos, P. D. (2000) “Vortex methods: theory and practice”, Cambridge university press, Cambridge.

Cottet, G. H. and Poncet, P. (2003) “Advances in Direct Numerical Simulations of 3D Wall-Bounded Flows by Vortex-in-Cell Methods”, J. Comp. Phys., vol. 193, pp136–158.

Cottet, G., Michaux, B., Ossia, S. and VandeLinden, G., (2002) "A Comparison of Spectral and Vortex Methods in Three-Dimensional Incompressible Flows", J. Comp. Phys. vol. 175, pp 702-712.

Couet, B., Buneman, O. and Leonard, A. (1981) "Simulation of Three-Dimensional Incompressible Flows with Vortex-in-Cell method", J. Comp. Phys., vol. 39, pp. 305- 328.

Drazin, P. G. (2002) "Introduction to Hydrodynamic Stability", Cambridge University Press.

Dritschel, D. G. (1989) "Contour dynamics and contour surgery: numerical algorithms for extended, high resolution modelling of vortex dynamics in two dimensional, inviscid, incompressible flows", Comp. Phys. Rep. 10, 77.

Dritschel, D. G. (1989) "Strain-induced vortex stripping," in Mathematical Aspects of Vortex Dynamics, edited by R. Caflisch (Society of Industrial and Applied Mathematics, Philadelphia), PA, pp 107.

Dritschel, D. G. and B. Legras (1989) "Modeling oceanic and atmospheric vortices," Phys. Today 46, 44.

Fine K. S., Cass A. C., Flynn W. G., and Driscoll C. F. "Relaxation of 2D turbulence to vortex crystals".

Fornberg, B. (1975) "On a Fourier method for the integration of hyperbolic equations", Sot. Industr. Appl. Math., J. Numer. Anal., 12, 509-528.

G. Winckelmans (2004) "Vortex methods", in: E. Stein, R. De Borst, T.J. Hughes (Eds.), Encyclopedia of Computational Mechanics, vol. 3, John Wiley and Sons.

Ghoneim AF and Givi P. (1987) "Vortex-Scalar Element Calculations of a Diffusion Flame Stabilized on a Plane Mixing Layer", NASA Tech. Memo. 100133 ICOMP-87-4.

Giovannini, A. and Gagnon, Y. (2006)" Validation of a Three-Dimensional Vortex Particle Method for Fluid Flows", AMRX Applied Mathematics Research Express vol. 2006, Article ID 17027, 1–31

Gottlieb, D., and Orszag, S. A. (1977) "Numerical analysis of spectral methods, Theory and Application", Sot. Industr. Appl. Math. Monograph.

Green, S. I. (1995) "Fluid Vortices", Kluwer Academic Press
Greengrad, C. and Rokhlin, V. (1987) "A Fast Algorithm for Particle Simulation". J Comp. Phys., vol. 73, pp 325-348.

Harlow, F. H. (1956) "The Particel-in-Cell method for two dimensional hydrodynamic problems", Los Alamos Scientific Laboratory.

Helmholtz H. von (1858) “Uber Integrale der hydrodynamics hen Gleichungen, welche derWirbelbewegung entsprechen”, J. f¨ur die reine und angewandte Mathematik, 55, 25–55.
Hockney R. W. and Eastwood J. W. (1981) “Computer Simulation Using Particles”, McGraw–Hill, New York.

Inoue, O., Leonard A. (1987) “ Vortex simulation of forced/unforced mixing layers”, AIAA. J., vol. 26, pp. 1417-1418.

Koumoutsakos P. (1993) “Direct Numerical Simulations of Unsteady Separated Flows Using Vortex Methods”, Ph.D. thesis, California Institute of Technology.

Koumoutsakos, P. (1997) “Inviscid axisymmetrization of an elliptical vortex”, J. Comput. Phys. 138, 821–857.

Kreiss, H.-O. and Oliger, J. (1972) “Comparison of accurate methods for the integration of hyperbolic equations:, Tellus , 24, 199-215.

Leonard, A., (1980) “Vortex Methods for Flow Simulation”, J. comp. phys., vol. 37, pp. 289-335.

Leonard, A., (1985) “Computing Three-Dimensional Incompressible Flows with Vortex Elements”, Ann. Rev. Fluid Mech., vol. 17, 523-559.

Liu, H. C. and Doorly, D. J. (2000) “Vortex Particle-in-Cell Method for Three-Dimensional Viscous Unbounded Flow Computations”, Int. J. Numer. Meth. Fluids.

Lui, C. H. (2002) “Vortex Simulation of Unsteady Shear Flow Induced by a Vortex Ring”, Computers and fluids, vol. 31, pp. 183-207.

Mariotti, A., Legras, B., Dritschel, D.G. (1994) “Vortex stripping and the erosion of coherent structures in two-dimensional flows”, Phys. Fluids 6, 3954–3962.

Marshall, J. S. (2001) “Inviscid Incompressible Flow”, John Wiley & Sons, Inc.

Marshall, J. S. and Grant, J. R. (1995) “A Lagrangian Collocation Method for Vorticity Transport in Viscous Fluid Flows,. Proceedings of the Forum on Vortex Methods for Engineering Applications. Sandia National Labs. Albuquerque, NM.

Marshall, J. S. and Grant, J. R. (1997) “A Lagrangian Vorticity Collocation Method for Viscous, Axisymmetric Flows with and without Swirl”, J Comp. Phys., vol. 138, pp 302-330.

Marshall, J. S., Grant, J. R. , Gossler, A. A. and Huyer, S. A. (2000), “Vorticity Transport on a Lagrangian Tetrahedral Mesh”, J Comp. Phys., vol. 161, pp 85-113.

McWilliams, J.C. (1984) “The emergence of isolated vortices in turbulent flow”, J . Fluid Mech. 146, 21-43.

Melander, M.V., McWilliams, J.C., Zabusky, N.J. (1987) "Axisymmetrization and vorticity-gradient intensification of an isolated two-dimensional vortex through filamentation", J. Fluid Mech. 178, 137–159.

Melander, M.V., Zabusky, N.J., McWilliams, J.C. (1988) "Symmetric vortex merger in two dimensions: causes and conditions", J. Fluid Mech. 195, 303–340.

Micheal, J., Graham, R. and Arkell, R. H. (2000) "A Hybrid Vortex Method", in Vortex Methods , Editors: Kamemoto, K and Tsutahara, M., Word Scientific, pp. 16-25.

Milane, R. E. and Abdolhoseini, R. (2004) "Development of Three_Dimensional Vortex-in-Cell Method for a Spatially Growing Uniformly Sheared Flow", Int. J. Comp. Fluid Dyn., vol. 18. pp. 47-69.

Monaghan, J. J. (1985) "Extrapolating B-Splines for Interpolation", J. Comput. Phys., vol. 60, pp. 253-262.

Oliver A. McBryan (Professor Emeritus, University of Colorado Boulder, 1045 Regent Drive 430 UCB Boulder CO, 80309-0430 USA)
(http://www.cs.colorado.edu/~mcbryan/3656.04/mail/95.htm) (04th February 2014)

Orszag, S. A. (1972) "Comparison of pseudo-spectral and spectral approximation", Stud. Appl. Math., 51,253%259.

Ould-Salihi, M. L., Cottet G.-H., and Hamraoui M. E. (2000) "Blending finite-difference and vortex methods for incompressible flow computations", SIAM J. Sci. Comput. 22, no. 5 (2000): 1655-1674.

Pope, S. B. (2000) "Turbulent Flows", Cambridge University Press.

Puckett, E. G., (1993) "Vortex methods: An Introduction and Survey of Selected Research Topics", In Incompressible Fluid Dynamics: Trends and Advances, Gunzburger, M.D., Nicolaides, R.A. (eds). Cambridge University Press, pp 335-408.

Rosenhead, L. (1932) "The Point Vortex Approximation of a Vortex Sheet", Proc. R. Soc. London, Ser. A, v. 134, pp170-181.

Rossi, L. F. (1996) "Resurrecting core spreading vortex methods: A new scheme that is both deterministic and convergent", SIAM J. Sci. Comput., vol.17, pp 370-397.

Sadek, N. and Milane, R.E. (2007) "Viscous Vortex Particle Simulation of Three Dimensional Mixing Layer", 15th Annual Conference of the CFD Society of Canada, Toronto-Canada
Saffman, P. G. (1992) "Vortex Dynamics", Cambridge University Press.

Sadek, N. (2012) "Comparison of Two Vortex-In-Cell Schemes Implemented to a Three Dimensional Temporal Mixing Layer", PhD Thesis, University of Ottawa, Canada.

Saffman, P. G. (1992) “Vortex Dynamics”, Cambridge University Press.

Spencer, B. W. and Jones, B. G. (1971) “Statistical Investigation of Pressure and Velocity Fields in the Turbulent Two-Stream Mixing Layer”, AIAA paper No. 71-613, AIAA 4th Fluid and Plasma Dynamics Conference, Palo Alto CA, June 21-23, 1971.

Van Rees, W. M.; Leonard, A., Pullin, D.I.; Koumoutsakos, P. (2011) “A comparison of vortex and pseudo-spectral methods for the simulation of periodic vortical flows at high Reynolds numbers”, J. Comp. Phys., vol. 230, pp 2794–2805.

Wang, J.K., and Milane R.E. (2006) "Large Eddy simulation (2D) of a spatially developping Mixing Layer using Vortex-In-Cell for flow field and probability density function for scalar field”, International Journal For Numerical Methods in Fluids 50 (2006): 27-61.

Winckelmans, G. and Capart, R. (May 2004) “Wake Vortex induced rolling moment on a follower aircraft”, Technical Note AW-UCL-114-001.

Yanenko, N. N. (1971) “The Method of Fractional Steps”, Springer Verlag.

Zabusky, N. J., Hughes, M. H. and Roberts, K. V. (1979) “Contour dynamics for the Euler equations”.

Appendix A1 (Flow Chart)

The present work uses one main program (**vic200_200.f**) for the vortex-in-cell predictions of the evolution of the vorticity for initially elliptical vortices of different aspect ratio, as described below.

Vic200_200.f: This program calculates the instantaneous velocity and vorticity field at various times using the VIC method. Data files for flow fields contain the stream function and the vorticity at the grid nodes and the vorticity profile along the axes when $x = 0$ and $y = 0$.

vic200_200.f :
The main program is a numerical computation of vorticity field.

START

Initializing

1.) Initialize by placing the vortex particles at the centre of each grid cell;
2.) Calculate vorticity at particles location through Eqn. (4.21);
3.) Assume arbitrary values for stream function, ψ, at the internal nodes;
4.) Periodic boundary condition in both directions;

Start main loop at each time- step

Predictor:

Distribute the vorticity from the vortex elements to the nodes using $M_4^{'}$ interpolation scheme. [Eqn.(4.5)]

Solve the Poisson Equation for $\psi(i, j)$ using the Jacobi method for iteration with a left-to-right sweep of the nodes and bottom-to-top sweep of the lines. Iteration convergence is obtained when the difference between consecutive ψ is less than 0.1. [Eqn.(4.15)]

From Page 107

Compute velocities $u(i, j)$ and $v(i, j)$ at nodes using Eqn.(4.16)

Compute the velocities at the location of each vortex particle $(u_p\ ,\ v_p)$ using interpolation scheme. [Eqs.(4.17a) and (4.17b)]

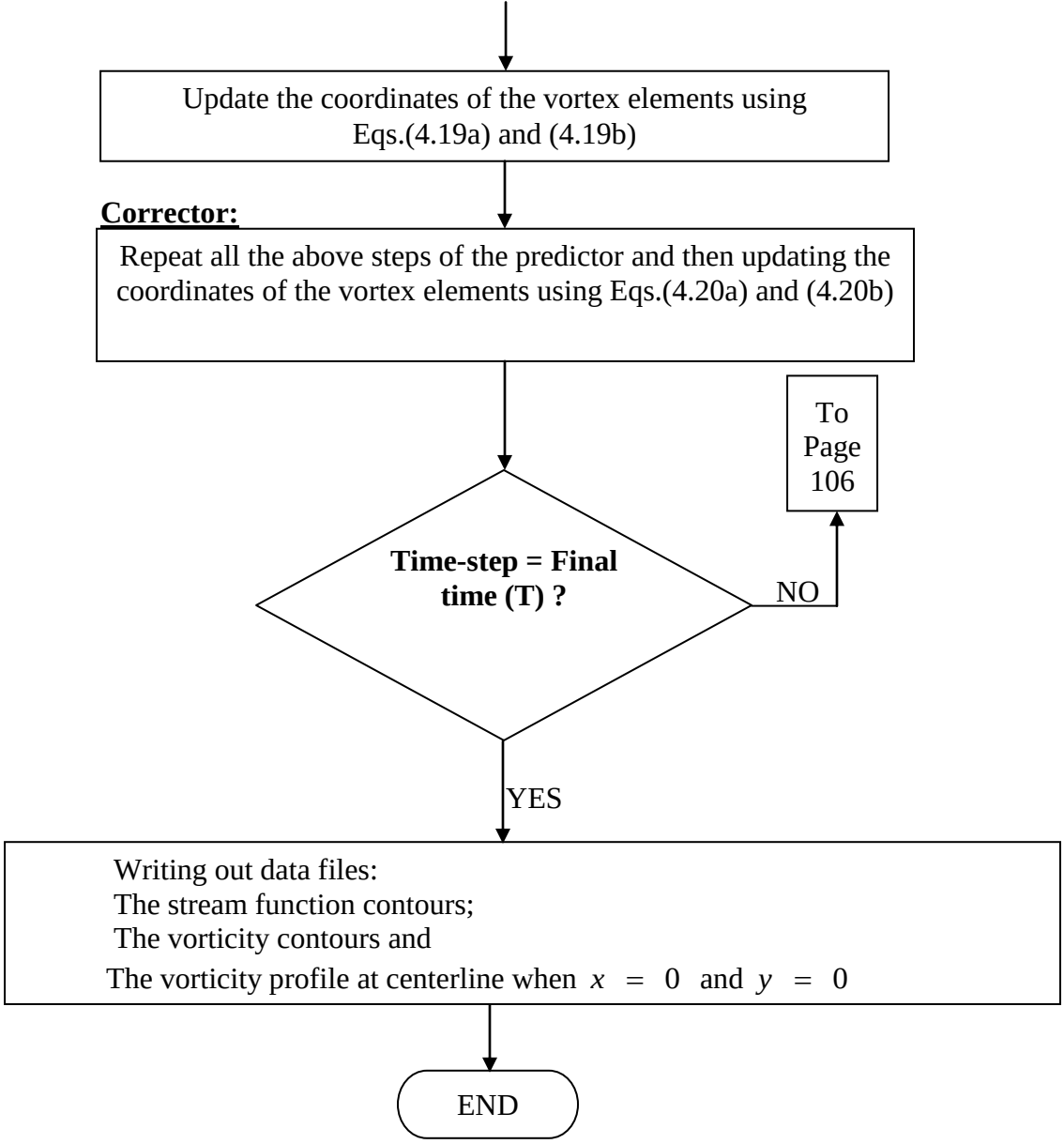
Update the coordinates of the vortex elements using Eqs.(4.19a) and (4.19b)
Corrector:
Repeat all the above steps of the predictor and then updating the coordinates of the vortex elements using Eqs.(4.20a) and (4.20b)
To Page 106
Time-step = Final time (T) ?
NO
YES
Writing out data files:
The stream function contours;
The vorticity contours and
The vorticity profile at centerline when x = 0 and y = 0
END

Appendix A2 (Tabulated Results)

The following is the complete numerical results of the present simulations using both VIC and pseudo-spectral methods, which are tabulated in Table A2.1. Alphabetic or numeric symbols used in this table are abbreviated as follows:

C = Case number

M = Numerical method: VIC = Vortex-In-cell, PS = Pseudo-Spectral

a = Major axis of an ellipse

b = Minor axis of an ellipse

AR = Aspect ratio

N / M = Number of nodes / Number of modes

Δx and Δy = Grid size in x and y direction

c = Timestep Constant

Δt = Timestep = $c \times \Delta x$

N_{rem} = Remeshing frequency, N/A = Not applicable

T = Final time

Cal. $\zeta_{\max}$ = Numerically calculated maximum vorticity.

(The exact value of maximum vorticity, $\zeta_{\max}$, is 20.)

Table A2.1: Complete Simulation Results

C	M	a	b	AR	N/ M	Δx and Δy	c	Δt (10^{-3})	N_{rem}	T	Cal. ζ_{max}	Error % ζ_{max}
The Effect of Grid Resolution (Section 5.2.1)												
1	VIC	1.26	0.44	2.864	50	0.120	0.1	12.00	5	1.008	22.277	11.385
2	VIC	1.26	0.44	2.864	100	0.060	0.1	6.00	5	1.002	20.354	1.770
3	VIC	1.26	0.44	2.864	200	0.030	0.1	3.00	5	1.002	20.199	0.995
4	VIC	1.26	0.44	2.864	300	0.020	0.1	2.00	5	1.000	20.145	0.725
5	VIC	1.26	0.44	2.864	400	0.015	0.1	1.50	5	1.0005	20.092	0.460
The Effect of Remeshing Frequency (Section 5.2.2)												
6	VIC	1.26	0.44	2.864	200	0.030	0.1	3.00	5	0.501	20.258	1.290
7	VIC	1.26	0.44	2.864	200	0.030	0.1	3.00	5	1.002	20.199	0.995
8	VIC	1.26	0.44	2.864	200	0.030	0.1	3.00	5	1.500	20.165	0.825
9	VIC	1.26	0.44	2.864	200	0.030	0.1	3.00	5	2.001	20.163	0.815
10	VIC	1.26	0.44	2.864	200	0.030	0.1	3.00	5	4.002	20.195	0.975
11	VIC	1.26	0.44	2.864	200	0.030	0.1	3.00	10	0.501	20.242	1.210
12	VIC	1.26	0.44	2.864	200	0.030	0.1	3.00	10	1.002	20.100	0.500
13	VIC	1.26	0.44	2.864	200	0.030	0.1	3.00	10	1.500	20.092	0.460
14	VIC	1.26	0.44	2.864	200	0.030	0.1	3.00	10	2.001	20.121	0.605
15	VIC	1.26	0.44	2.864	200	0.030	0.1	3.00	10	4.002	20.206	1.030
16	VIC	1.26	0.44	2.864	200	0.030	0.1	3.00	15	0.501	20.290	1.450
17	VIC	1.26	0.44	2.864	200	0.030	0.1	3.00	15	1.002	20.193	0.965
18	VIC	1.26	0.44	2.864	200	0.030	0.1	3.00	15	1.500	20.183	0.915
19	VIC	1.26	0.44	2.864	200	0.030	0.1	3.00	15	2.001	20.192	0.960
20	VIC	1.26	0.44	2.864	200	0.030	0.1	3.00	15	4.002	20.322	1.610
21	VIC	1.26	0.44	2.864	200	0.030	0.1	3.00	25	0.501	20.652	3.260
22	VIC	1.26	0.44	2.864	200	0.030	0.1	3.00	25	1.002	20.420	2.100
23	VIC	1.26	0.44	2.864	200	0.030	0.1	3.00	25	1.500	20.309	1.545
24	VIC	1.26	0.44	2.864	200	0.030	0.1	3.00	25	2.001	20.666	3.330

C	M	a	b	AR	N/ M	Δx and Δy	c	Δt (10^{-3})	N_{rem}	T	Cal. $\zeta_{\max}$	Error % $\zeta_{\max}$
The Effect of Remeshing Frequency (Section 5.2.2)												
25	VIC	1.26	0.44	2.864	200	0.030	0.1	3.00	25	4.002	20.484	2.420
The Effect of Time Step (Section 5.2.3)												
26	VIC	1.26	0.44	2.864	200	0.030	0.15	4.50	5	0.504	20.188	0.940
27	VIC	1.26	0.44	2.864	200	0.030	0.15	4.50	5	1.0035	20.117	0.585
28	VIC	1.26	0.44	2.864	200	0.030	0.15	4.50	5	1.503	20.086	0.430
29	VIC	1.26	0.44	2.864	200	0.030	0.15	4.50	5	2.0025	20.074	0.370
30	VIC	1.26	0.44	2.864	200	0.030	0.15	4.50	5	4.0005	20.160	0.800
31	VIC	1.26	0.44	2.864	200	0.030	0.2	6.00	5	0.504	20.179	0.895
32	VIC	1.26	0.44	2.864	200	0.030	0.2	6.00	5	1.002	20.046	0.230
33	VIC	1.26	0.44	2.864	200	0.030	0.2	6.00	5	1.500	20.029	0.145
34	VIC	1.26	0.44	2.864	200	0.030	0.2	6.00	5	2.004	20.122	0.610
35	VIC	1.26	0.44	2.864	200	0.030	0.2	6.00	5	4.002	20.106	0.530
36	VIC	1.26	0.44	2.864	200	0.030	0.4	12.00	5	0.504	20.261	1.305
37	VIC	1.26	0.44	2.864	200	0.030	0.4	12.00	5	1.008	20.371	1.855
38	VIC	1.26	0.44	2.864	200	0.030	0.4	12.00	5	1.500	19.852	-0.740
39	VIC	1.26	0.44	2.864	200	0.030	0.4	12.00	5	2.004	19.958	-0.210
40	VIC	1.26	0.44	2.864	200	0.030	0.4	12.00	5	4.008	20.055	0.275
41	VIC	1.26	0.44	2.864	200	0.030	0.55	16.50	5	0.5115	19.735	-1.325
42	VIC	1.26	0.44	2.864	200	0.030	0.55	16.50	5	1.0065	19.950	-0.250
43	VIC	1.26	0.44	2.864	200	0.030	0.55	16.50	5	1.5015	19.950	-0.250
44	VIC	1.26	0.44	2.864	200	0.030	0.55	16.50	5	2.013	19.863	-0.685
45	VIC	1.26	0.44	2.864	200	0.030	0.55	16.50	5	4.0095	19.984	-0.080
The Effect of Number of Fourier Modes (Section 5.3.1)												
46	PS	1.26	0.44	2.864	50	0.120	0.1	12.00	N/A	0.500	20.381	1.905
47	PS	1.26	0.44	2.864	50	0.120	0.1	12.00	N/A	1.000	20.598	2.990
48	PS	1.26	0.44	2.864	50	0.120	0.1	12.00	N/A	1.500	20.570	2.850

C	M	a	b	AR	N/ M	Δx and Δy	c	Δt (10^{-3})	N_{rem}	T	Cal. $\zeta_{\max}$	Error % $\zeta_{\max}$
The Effect of Number of Fourier Modes (Section 5.3.1)												
49	PS	1.26	0.44	2.864	50	0.120	0.1	12.00	N/A	2.000	20.658	3.290
50	PS	1.26	0.44	2.864	50	0.120	0.1	12.00	N/A	4.000	20.937	4.685
51	PS	1.26	0.44	2.864	80	0.075	0.1	7.50	N/A	0.500	20.115	0.575
52	PS	1.26	0.44	2.864	80	0.075	0.1	7.50	N/A	1.000	20.243	1.215
53	PS	1.26	0.44	2.864	80	0.075	0.1	7.50	N/A	1.500	20.230	1.150
54	PS	1.26	0.44	2.864	80	0.075	0.1	7.50	N/A	2.000	20.276	1.380
55	PS	1.26	0.44	2.864	80	0.075	0.1	7.50	N/A	4.000	20.430	2.150
56	PS	1.26	0.44	2.864	100	0.060	0.1	6.00	N/A	0.500	20.064	0.320
57	PS	1.26	0.44	2.864	100	0.060	0.1	6.00	N/A	1.000	20.110	0.550
58	PS	1.26	0.44	2.864	100	0.060	0.1	6.00	N/A	1.500	20.135	0.675
59	PS	1.26	0.44	2.864	100	0.060	0.1	6.00	N/A	2.000	20.149	0.745
60	PS	1.26	0.44	2.864	100	0.060	0.1	6.00	N/A	4.000	20.247	1.235
61	PS	1.26	0.44	2.864	120	0.050	0.1	5.00	N/A	0.500	20.035	0.175
62	PS	1.26	0.44	2.864	120	0.050	0.1	5.00	N/A	1.000	20.089	0.445
63	PS	1.26	0.44	2.864	120	0.050	0.1	5.00	N/A	1.500	20.121	0.605
64	PS	1.26	0.44	2.864	120	0.050	0.1	5.00	N/A	2.000	20.089	0.445
65	PS	1.26	0.44	2.864	120	0.050	0.1	5.00	N/A	4.000	20.146	0.730
66	PS	1.26	0.44	2.864	150	0.040	0.1	4.00	N/A	0.500	20.021	0.105
67	PS	1.26	0.44	2.864	150	0.040	0.1	4.00	N/A	1.000	20.048	0.240
68	PS	1.26	0.44	2.864	150	0.040	0.1	4.00	N/A	1.500	20.058	0.290
69	PS	1.26	0.44	2.864	150	0.040	0.1	4.00	N/A	2.000	20.052	0.260
70	PS	1.26	0.44	2.864	150	0.040	0.1	4.00	N/A	4.000	20.083	0.415
71	PS	1.26	0.44	2.864	180	0.033	0.1	3.33	N/A	0.500	20.014	0.070
72	PS	1.26	0.44	2.864	180	0.033	0.1	3.33	N/A	1.000	20.022	0.110
73	PS	1.26	0.44	2.864	180	0.033	0.1	3.33	N/A	1.500	20.040	0.200
74	PS	1.26	0.44	2.864	180	0.033	0.1	3.33	N/A	2.000	20.031	0.155

C	M	a	b	AR	N/ M	Δx and Δy	c	Δt (10^{-3})	N_{rem}	T	Cal. $\zeta_{\max}$	Error % $\zeta_{\max}$
The Effect of Number of Fourier Modes (Section 5.3.1)												
75	PS	1.26	0.44	2.864	180	0.033	0.1	3.33	N/A	4.000	20.049	0.245
76	PS	1.26	0.44	2.864	200	0.030	0.1	3.00	N/A	0.500	20.010	0.050
77	PS	1.26	0.44	2.864	200	0.030	0.1	3.00	N/A	1.000	20.017	0.085
78	PS	1.26	0.44	2.864	200	0.030	0.1	3.00	N/A	1.500	20.029	0.145
79	PS	1.26	0.44	2.864	200	0.030	0.1	3.00	N/A	2.000	20.023	0.115
80	PS	1.26	0.44	2.864	200	0.030	0.1	3.00	N/A	4.000	20.036	0.180
81	PS	1.26	0.44	2.864	220	0.027	0.1	2.73	N/A	0.500	20.008	0.040
82	PS	1.26	0.44	2.864	220	0.027	0.1	2.73	N/A	1.000	20.013	0.065
83	PS	1.26	0.44	2.864	220	0.027	0.1	2.73	N/A	1.500	20.019	0.095
84	PS	1.26	0.44	2.864	220	0.027	0.1	2.73	N/A	2.000	20.018	0.090
85	PS	1.26	0.44	2.864	220	0.027	0.1	2.73	N/A	4.000	20.029	0.145
86	PS	1.26	0.44	2.864	240	0.025	0.1	2.50	N/A	0.500	20.006	0.030
87	PS	1.26	0.44	2.864	240	0.025	0.1	2.50	N/A	1.000	20.009	0.045
88	PS	1.26	0.44	2.864	240	0.025	0.1	2.50	N/A	1.500	20.014	0.070
89	PS	1.26	0.44	2.864	240	0.025	0.1	2.50	N/A	2.000	20.014	0.070
90	PS	1.26	0.44	2.864	240	0.025	0.1	2.50	N/A	4.000	20.024	0.120
Study of Different Aspect Ratio Results For Pseudo-Spectral Method												
91	PS	1.2	0.63	1.905	220	0.027	0.1	2.73	N/A	0.500	20.008	0.040
92	PS	1.2	0.63	1.905	220	0.027	0.1	2.73	N/A	1.000	20.015	0.075
93	PS	1.2	0.63	1.905	220	0.027	0.1	2.73	N/A	1.500	20.020	0.100
94	PS	1.2	0.63	1.905	220	0.027	0.1	2.73	N/A	2.000	20.024	0.120
95	PS	1.2	0.63	1.905	220	0.027	0.1	2.73	N/A	4.000	20.042	0.210
96	PS	1.26	0.89	1.416	220	0.027	0.1	2.73	N/A	0.500	20.013	0.065
97	PS	1.26	0.89	1.416	220	0.027	0.1	2.73	N/A	1.000	20.024	0.120
98	PS	1.26	0.89	1.416	220	0.027	0.1	2.73	N/A	1.500	20.033	0.165
99	PS	1.26	0.89	1.416	220	0.027	0.1	2.73	N/A	2.000	20.042	0.210
100	PS	1.26	0.89	1.416	220	0.027	0.1	2.73	N/A	4.000	20.078	0.390

C	M	a	b	AR	N/ M	Δx and Δy	c	Δt (10^{-3})	N_{rem}	T	Cal. $\zeta_{\max}$	Error % $\zeta_{\max}$
Study of Different Aspect Ratio Results For Pseudo-Spectral Method												
101	PS	1.26	0.31	4.065	220	0.027	0.1	2.73	N/A	0.500	20.008	0.040
102	PS	1.26	0.31	4.065	220	0.027	0.1	2.73	N/A	1.000	20.011	0.055
103	PS	1.26	0.31	4.065	220	0.027	0.1	2.73	N/A	1.500	20.023	0.115
104	PS	1.26	0.31	4.065	220	0.027	0.1	2.73	N/A	2.000	20.020	0.100
105	PS	1.26	0.31	4.065	220	0.027	0.1	2.73	N/A	4.000	20.022	0.110
Study of Results Without Remeshing For VIC Method												
106	VIC	1.26	0.44	2.864	200	0.030	0.1	3.00	N/A	0.501	61.221	206.10
107	VIC	1.26	0.44	2.864	200	0.030	0.1	3.00	N/A	1.002	66.953	234.76
108	VIC	1.26	0.44	2.864	200	0.030	0.1	3.00	N/A	1.500	61.195	205.97
109	VIC	1.26	0.44	2.864	200	0.030	0.1	3.00	N/A	2.001	50.324	151.62
110	VIC	1.26	0.44	2.864	200	0.030	0.1	3.00	N/A	4.002	67.925	239.62
Study of Different Aspect Ratio Results For VIC Method (Section 5.6)												
111	VIC	1.26	0.31	4.065	200	0.030	0.1	3.00	5	0.501	20.496	2.480
112	VIC	1.26	0.31	4.065	200	0.030	0.1	3.00	5	1.002	20.395	1.975
113	VIC	1.26	0.31	4.065	200	0.030	0.1	3.00	5	1.500	20.285	1.425
114	VIC	1.26	0.31	4.065	200	0.030	0.1	3.00	5	2.001	20.234	1.170
115	VIC	1.26	0.31	4.065	200	0.030	0.1	3.00	5	4.002	20.200	1.000
116	VIC	1.26	0.63	2.000	200	0.030	0.1	3.00	5	0.501	20.110	0.550
117	VIC	1.26	0.63	2.000	200	0.030	0.1	3.00	5	1.002	20.108	0.540
118	VIC	1.26	0.63	2.000	200	0.030	0.1	3.00	5	1.500	20.126	0.630
119	VIC	1.26	0.63	2.000	200	0.030	0.1	3.00	5	2.001	20.164	0.820
120	VIC	1.26	0.63	2.000	200	0.030	0.1	3.00	5	4.002	20.295	1.475
121	VIC	1.26	0.89	1.416	200	0.030	0.1	3.00	5	0.501	20.060	0.300
122	VIC	1.26	0.89	1.416	200	0.030	0.1	3.00	5	1.002	20.121	0.605
123	VIC	1.26	0.89	1.416	200	0.030	0.1	3.00	5	1.500	20.196	0.980
124	VIC	1.26	0.89	1.416	200	0.030	0.1	3.00	5	2.001	20.269	1.345

C	M	a	b	AR	N/ M	Δx and Δy	c	Δt (10^{-3})	N_{rem}	T	Cal. $\zeta_{\max}$	Error % $\zeta_{\max}$
Study of Different Aspect Ratio Results For VIC Method (Section 5.6)												
125	VIC	1.26	0.89	1.416	200	0.030	0.1	3.00	5	4.002	20.501	2.505
Study of Numerical Results For VIC Method (Section 5.5)												
126	VIC	1	0.5	2.000	200	0.030	0.1	3.00	5	0.000	20.000	0.000
127	VIC	1	0.5	2.000	200	0.030	0.1	3.00	5	0.501	20.096	0.480
128	VIC	1	0.5	2.000	200	0.030	0.1	3.00	5	1.002	20.092	0.458
129	VIC	1	0.5	2.000	200	0.030	0.1	3.00	5	1.500	20.079	0.395
130	VIC	1	0.5	2.000	200	0.030	0.1	3.00	5	2.001	20.085	0.425
131	VIC	1	0.5	2.000	200	0.030	0.1	3.00	5	4.002	20.134	0.670